

DOE/ET-53088-245

IFSR #245

---

**Stability of Ballooning Modes in Tokamaks  
with Energetic Particles**

*Nicolas Dominguez Vergara*

Institute for Fusion Studies  
The University of Texas at Austin  
Austin, Texas 78712-1060

August 1986

---

STABILITY OF BALLOONING MODES IN TOKAMAKS WITH ENERGETIC  
PARTICLES

APPROVED BY SUPERVISORY COMMITTEE:

Robert L. Berk

Marshall Rosenbluth

James W. Van Dam

Wendell Horton Jr.

Edward F. Power Jr.

H. Vernon Wong

STABILITY OF BALLOONING MODES IN TOKAMAKS WITH  
ENERGETIC PARTICLES

Publication No. \_\_\_\_\_

Nicolas Domínguez Vergara , Ph. D.  
The University of Texas at Austin, 1986

Supervising Professors: James W. Van Dam  
Herbert L. Berk

The effects of energetic particles are of interest since fast ions are present in neutral-beam and rf-heated tokamaks and will occur in ignition devices in the form of alpha particles. Moreover, it may be desirable to create such particles by auxiliary heating in order to exploit their stabilizing properties and thus attain a high beta plasma. Here a range of issues related to the stabilization of MHD ballooning mode in tokamaks by the use of energetic particles is investigated analytically and numerically.

The presence of a highly energetic plasma component can stabilize MHD ballooning modes in tokamaks and may allow direct access to the high-beta second stability regime. Here, an improved

estimate of such stability has been obtained, in the large-aspect-ratio circular limit, by means of a variational refinement of the lower bound for the energetic particle potential energy. We also investigate the effect of various profiles for the hot particle pressure on stability, and we explore the stability of off-angle modes.

Moderately energetic particles, however, can destabilize the plasma through resonant interaction at their curvature drift frequency. We study these so-called "balloon-bone" modes, using a delta function model for their resonant response. The complete forms of the Mercier solutions in the MHD region are obtained analytically and numerically. Matched onto the inertia layer, these solutions give a dispersion relation valid for finite shear and poloidal beta values, which then is analyzed by the Nyquist technique. Results are presented for the limit in which Alfvénic effects are negligible, namely,  $\bar{\omega}_{dh} \ll \omega_A$ , where  $\bar{\omega}_{dh}$  is the curvature drift frequency and  $\omega_A$  is the Alfvén frequency, and in which the energetic particles are modeled with a slowing-down distribution in energy.

Finally, we investigated the effect introduced by the presence of a nonresonant, highly energetic species on the stability of resistive ballooning modes, including parallel compressibility and

cross field transport. A dispersion relation is obtained by matching the solutions in the ideal, resistive, and deeply resistive regions. Compressional effects associated with the hot particles are found to be partially stabilizing.

Copyright, 1986

by

Nicolas Dominguez Vergara.

All rights reserved.

---

This thesis is dedicated to Hortencia.

---

**STABILITY OF BALLOONING MODES IN TOKAMAKS  
WITH ENERGETIC PARTICLES**

---

by

NICOLAS DOMINGUEZ VERGARA, B. Sc. , M. S.

---

DISSERTATION

Presented to the Faculty of the Graduate School of  
The University of Texas at Austin  
in Partial Fulfillment  
of the Requirements  
for the Degree of

DOCTOR OF PHILOSOPHY

THE UNIVERSITY OF TEXAS AT AUSTIN

August, 1986



## ACKNOWLEDGMENTS

No one has ever helped, advised, and encouraged me in my professional life as has Dr. James W. Van Dam. His knowledge, criticism, generosity, and personal kindness during our close collaboration have given me much more than I expected.

It was also a privilege to have worked with and learned from Prof. Herbert L. Berk during my stay at the IFS, particularly during the course of another research that I did with him on mirror machines. I especially thank him for having read and criticized the work in the present thesis.

It has been a great honor to have received substantial contributions and criticism from Prof. Marshall N. Rosenbluth. I am indebted to him for fruitful discussions and for having read the manuscript.

I would also like to thank Dr. C. W. Horton , Dr. V. Wong, and Dr. E. Powers for having served on my supervisory committee.

It is also a pleasure to thank several members of the plasma community for their advice and enlightening discussions, especially Dr. J. N. Leboeuf, Dr. S. T. Tsai, and Dr. P. H. Diamond.

I acknowledge the support and academic help of many friends at the University of Texas, especially to Jorge Ballester for his warm friendship, as well as Marcia Enquist, Richard Sydora, Rodolfo Carrera, and Elena Montalvo

On the other side of the border, in Mexico, I thank Dr. Julio Herrera and Dr. Marcos Rosenbaum for their encouragement. I am grateful to UNAM and CONACYT for their past economic support during my graduate studies in Mexico and in Austin.

I also acknowledge the Institute for Fusion Studies for its financial support during part of my research and for the help and support of the IFS staff and its efficient secretarial group.

Finally, I especially thank my wife, Hortensia for her great help during my research and for typing the thesis and preparing the figures.

# TABLE OF CONTENTS

CHAPTER	Page
<b>I. INTRODUCTION</b> .....	1
<b>II. NON-RESONANT STABILIZATION OF IDEAL BALLOONING</b>	
<b>MODES WITH HIGHLY ENERGETIC PARTICLES</b> .....	16
2.1 <u>INTRODUCTION</u> .....	16
2.2 <u>EQUILIBRIUM EQUATIONS AND ASSUMPTIONS</u> .....	20
2.2.a <u>MODEL EQUILIBRIUM</u> .....	22
2.2.b <u>CALCULATION OF THE EIKONAL</u> .....	31
2.2.c <u>DISTRIBUTION FUNCTION FOR THE HOT SPECIES</u> .....	37
2.2.d <u>DRIFT NONREVERSAL CONDITION</u> .....	38
2.3 <u>VARIATIONAL REFINEMENT OF THE SCHWARTZ</u>	
<u>INEQUALITY AND THE BALLOONING MODE EQUATION</u> .....	42
2.4 <u>NUMERICAL SCHEME FOR SOLVING THE BALLOONING</u>	
<u>EQUATION</u> .....	50
2.5 <u>COMPARISON OF RESULTS USING THE IMPROVED SCHWARTZ</u>	
<u>INEQUALITY WITH PREVIOUS RESULTS WITHOUT THE</u>	
<u>IMPROVEMENT</u> .....	59
2.6 <u>STABILITY BOUNDARIES FOR DIFFERENT POLOIDAL</u>	
<u>PROFILES OF THE HOT PARTICLE PRESSURE</u> .....	72
2.7 <u>OFF-ANGLE MODES</u> .....	72
2.8 <u>CONCLUSIONS</u> .....	76

<b>III. RESONANT DESTABILIZATION OF BALLOONING MODES BY</b>	
<b>ENERGETIC PARTICLES</b> .....	81
3.1 <u>INTRODUCTION</u> .....	81
3.2 <u>ASSUMPTIONS</u> .....	86
3.3 <u>BALLOONING MODE EQUATION</u> .....	87
3.3.a QUADRATIC FORM AND THE BALLOONING	
MODE EQUATION .....	87
3.3.b FORM OF THE RESONANT TERM FOR A	
SLOWING-DOWN ENERGY DISTRIBUTION FUNCTION .....	94
3.4 <u>SOLUTION OF THE RESONANT BALLOONING</u>	
<u>MODE EQUATION</u> .....	101
3.4.a SOLUTION IN THE INTERIOR MHD REGION .....	101
3.4.b SOLUTION IN THE EXTERIOR INERTIAL REGION .....	112
3.5 <u>DISPERSION AND RESULTS</u> .....	119
3.6 <u>APPROXIMATE ANALYTICAL STABILITY CONDITIONS</u> .....	127
3.7 <u>CONCLUSIONS</u> .....	131
<b>IV. RESISTIVE BALLOONING STABILITY WITH HIGHLY</b>	
<b>ENERGETIC PARTICLES</b> .....	133
4.1 <u>INTRODUCTION</u> .....	133
4.2 <u>DERIVATION OF RESISTIVE BALLOONING MODE EQUATIONS</u> .....	135
4.3 <u>SOLUTION IN THE IDEAL REGION</u> .....	150
4.2.a NUMERICAL SOLUTION FOR $\Delta'$ .....	151
4.2.b ANALYTICAL SOLUTIONS FOR $\Delta'$ .....	152

4.4 <u>SOLUTION IN THE RESISTIVE REGION</u> .....	167
4.5 <u>STABILITY ANALYSIS</u> .....	175
4.6 <u>CONCLUSIONS</u> .....	178
<hr/>	
<b>V. SUMMARY AND DISCUSSION</b> .....	180
<b>APPENDIX A</b> .....	190
<b>APPENDIX B</b> .....	198
<b>REFERENCES</b> .....	220

---

## LIST OF FIGURES

Figure	Page
2.1 Tokamak equilibrium .....	23
2.2 Picture of hot particles confined on the outside of a tokamak .....	24
2.3 Trapped and untrapped particle regions in ballooning space .....	51
2.4 Stability regions for $\theta_0 = \pi/4$ , $3\pi/8$ , and $\pi/2$ without the Schwartz inequality improvement .....	60
2.5 Stability regions for $\theta_0 = \pi/4$ , $3\pi/8$ , and $\pi/2$ with the improved Schwartz inequality; $\zeta = 1/2$ was used in all the curves (compare with Fig. 2.4) .....	62
2.6 Comparison of stability boundaries for various inequality weighting functions ( $\theta_0 = \pi/2$ ) .....	63

2.7	Enlargement of the region inside of the small box in Fig. 2.6 .....	64
2.8	The same as Fig. 2.6 for $\theta_0 = 3\pi/8$ .....	65
2.9	The same as Fig. 2.6 for $\theta_0 = \pi/4$ .....	66
2.10	Analytic prediction of discrepancy for $\theta_0 = \pi/8$ .....	70
2.11	Marginal stability for various profiles with $\alpha_n$ set equal to the maximum value allowed by drift non-reversal .....	73
2.12	Stability boundaries for $\theta_k = 0$ and $\theta_k = 3\pi/8$ , with and without energetic particles .....	75
2.13	The same as Fig. 2.12, for $\theta_k = 3\pi/8$ and $\theta_k = \pi/2$ .....	77
3.1	Observations of MHD modes excited by energetic particles by K. Mc Guirre, et al. <sup>47</sup> in the PDX tokamak .....	83

3.2	Real and imaginary parts of $T(W)$ versus $W = \omega / \bar{\omega}_{dm}$ for $\alpha_c = \alpha_h = 0.05$ , $\epsilon = 0.3$ , $\bar{\omega}_{dm} / \omega_A = 0.2$ , and $S = 0.5$ .....	102
3.3	Ideal MHD and inertial regions in ballooning space .....	103
3.4	Piecewise constant $\Lambda^{(n)}$ and slowly continuous function $(S\theta)^\mu$ .....	107
3.5	Mercier exponent $\mu$ as a function of $\alpha_c$ for various values of $\alpha_h$ .....	110
3.6	Mercier coefficients as functions of $\alpha_c$ for $\alpha_h = 0$ , with $\theta_0 = \pi/4$ , $q = 1.5$ , and $S = 0.5$ .....	113
3.7	Mercier coefficients as functions of $\alpha_c$ for $\alpha_h = 1$ , with $\theta_0 = \pi/4$ , $q = 1.5$ , and $S = 0.5$ .....	114



3.8	Mercier coefficient $M_e$ as a function of $\alpha_c$ , for various values of $\alpha_h$ , with $\theta_0 = \pi/4$ , $q = 1.5$ , and $S = 0.5$ .....	115
3.9	Imaginary part of $G(w)$ versus real part of $G(w)$ , with $\epsilon = 0.3$ , $\alpha_h = \alpha_c = 0.05$ , $q = 1.5$ , $S = 0.5$ , and $\theta_0 = \pi/4$ .....	123
3.10	Marginal stability boundaries in $\alpha_c$ and $\alpha_h$ parameter space for the MHD and trapped- particle-induced ballooning mode branches for $\bar{\omega}_{dm}/\omega_A = 0.2$ , $\epsilon = 3$ , $S = 0.5$ , and $\theta_0 = \pi/4$ .....	124
3.11	The same as Fig. 3.10, except $\bar{\omega}_{dm}/\omega_A = 0.6$ .....	126
4.1	Numerical results for $\Delta'_e = N_e/M_e$ for various values of $\alpha_h$ .....	153
4.2	Numerical results for $\Delta'_0 = N_0/M_0$ for various values of $\alpha_h$ .....	154

4.3	Resistive parameter $\Delta'_e$ in the limit of small $\alpha_c$ , $\alpha_h$ , and $S$ .....	158
4.4	Resistive parameter $\Delta'_0$ in the limit of small $\alpha_c$ , $\alpha_h$ , and $S$ .....	159
4.5	Mercier coefficients for $S = 0.5$ , $\theta_0 = \pi/4$ , $q = 1.5$ , $\theta_k = 0$ and $\alpha_c = 0$ .....	163
4.6	A universal curve for the stability of resistive ballooning modes below the ideal threshold. The critical value of the driving energy, $\Delta'_c$ , is plotted versus $\hat{D}_h$ . [From Drake and Antonsen paper, Ref. 54] .....	176
5.1	Regimes for various theoretical descriptions .....	181
5.2	Simple sketch of stability boundaries for resonant and nonresonant ballooning modes .....	186

# CHAPTER I.

## INTRODUCTION

Ballooning modes in a tokamak plasma are magnetohydrodynamic (MHD) pressure gradient-driven perturbations localized in the unfavorable curvature region of the torus. The linear stability analysis of these perturbations in the high-toroidal-mode-number limit is reduced to the study of a perturbation on a single flux surface and its variation along a field line. It is known that if the shear (associated with the change in helical pitch of the magnetic field from one flux surface to another) is fixed while the plasma beta (defined as the dimensionless ratio of the pressure to the magnetic field energy density) is varied, the mode is stable for small beta values, but becomes unstable as the beta value is increased. However, if the beta is increased even more, the mode is predicted to become stable again. This high-beta stable regime is called the second stable region for ballooning modes.<sup>1,2</sup>

The existence of the unstable zone between the low-beta first and high-beta second stability regions constrains the maximum value of the plasma beta. It would be quite advantageous to provide a bridge between the low-beta regime of first stability and the high-beta

second stable regime, because then there would be no constraint on the maximum power, proportional to beta, that can be obtained from a fusion reactor. Thus, accessing the second stable regime for ballooning modes, and thereby attaining a stable high-beta plasma, is a problem of fundamental importance.

One effort toward stabilizing these modes in tokamaks is to shape the plasma by indenting its cross section, to produce D and bean-shape cross sections.<sup>3-4</sup> In this work we will not employ this approach for stabilizing ballooning modes; instead we will focus theoretical study on another approach, which attempts to stabilize these modes by means of the introduction of a very energetic species into the tokamak. The tokamak plasma then consists of two populations, one being the core plasma or thermal plasma, which in an ignited tokamak would be the fusion plasma, and another being the energetic particle population. The study of the role of hot particles in stability is by itself an important problem because suprathreshold alpha particles will be present as a product of fusion reactions in the upcoming generation of ignited tokamaks. This is a major reason for the increased interest in this topic in the last few years. Moreover, during the process of supplying auxiliary heating to the plasma by neutral beams or rf-waves in present-day tokamaks, the stability role of the energetic population has to be well understood. In fact,

experimental evidence of the excitation of MHD modes by beam-injected hot ions has been observed in the Princeton PDX tokamak.<sup>5</sup> These reasons constitute the motivation for the theoretical work presented here.

Plasma stabilization by energetic particles has been previously proposed and analyzed in the Astron<sup>6</sup> and ion ring devices<sup>7-9</sup> and in the ELMO bumpy torus.<sup>10</sup> More recently it has also been proposed that the intentional introduction of a superhot component into a tokamak could enhance MHD stability.<sup>11</sup> Although there are significant differences between mirrors and tokamaks — *e.g.*, tokamaks have rotational transform and shear, and their magnetic field lines are not closed except at rational surfaces — , nevertheless the stabilizing mechanism of energetic particles for MHD modes in both systems is similar. In order to act essentially as a passive current and thus provide stabilization, the energy of these particles must be high enough that their magnetic drift frequency,  $\omega_{dh}$ , is larger than approximately the growth rate,  $\gamma_{int}$ , for MHD interchange instability. In the mirror literature, the ratio  $\omega_{dh}/\gamma_{int}$  has been referred to as the "decoupling" coefficient,<sup>12</sup> where  $\omega_{dh}$  is the curvature drift frequency of the hot particles. If the value of this ratio is larger than about unity, the energetic particles may be

considered to be noninteracting. We shall see later that this condition is roughly the condition for the energetic particles to be nonresonant:  $\omega_{dh} \gg \omega$ , where  $\omega$  is the frequency of the MHD mode under consideration.

Historically, however, there has been a difference in how the behavior of the energetic particles was interpreted in mirror-type systems as compared to tokamaks. For instance, in the Elmo Bumpy Torus experiment, which consisted of 24 simple mirrors linked toroidally, it was traditionally thought that hot electrons created by microwave heating were digging a deep enough magnetic well to reverse the average gradient-B drift and thereby stabilize the background plasma against interchange instability.<sup>13</sup> When the non-MHD kinetic response of the hot electrons was accounted for,<sup>14</sup> it was found that although the fluid response of drift-reversed energetic particles was favorable for stability, their non-fluid compressional response still allowed for a negative energy perturbation, which could lead to instability, for example above the Lee-Van Dam threshold or due to interactions with positive energy waves or with dissipative response.<sup>15-17</sup> When the idea of using energetic particle stabilization was transplanted to tokamaks, it was natural to consider the non-drift-reversed limit, tokamaks being relatively low in beta compared to mirror plasmas. In this case the

negative energy perturbation theorem of Ref. 15 does not apply and it may be possible in principle to obtain absolute stability.

In the non-reversed case the hot particles' fluid contribution is destabilizing, whereas their compressional non-fluid response is stabilizing for the MHD mode. Moreover, theoretical calculations showed that the compressional terms stabilized the fluid behavior, at least for not too large values of the global shear.<sup>11</sup> Subsequently, the ballooning stability for EBT was redone, in the non-drift-reversed limit; however, no significant stabilization was obtained.<sup>18</sup> We may possibly attribute the difference between this unsuccessful attempt and the successful enhancement predicted in a tokamak to the nature of the two machines. That is, a tokamak, by virtue of its sheared magnetic field, already possesses first and second stability regimes and a relatively small intermediate unstable zone. The presence of energetic particles then tends to shrink the instability zone. In contrast, an EBT device is unstable without hot electrons to begin with, and therefore it is more difficult to achieve parameters for stable operation.

At this point, it may be helpful to give a simplified picture<sup>19</sup> of the special dynamics of highly energetic particles, which can contribute to the stabilization of MHD modes. Let us first describe

their behavior from a single-particle point of view, in which individual particles execute motion around, along, and across a magnetic field line. The gyromotion around a field line is characterized by the cyclotron frequency  $\Omega_h = e_h B / M_h c$ , where  $e_h$  and  $M_h$  are the charge and mass of an energetic particle,  $B$  is the magnetic field strength, and  $c$  is the speed of light; the longitudinal motion along a field line is characterized by a bounce frequency  $\omega_{bh} \cong V_h / L_{\parallel}$ , where the velocity  $V_h \cong \sqrt{T_h / M_h}$  is related to their energy  $T_h$  and where the typical parallel scale length in a tokamak is  $L_{\parallel} \cong qR$ , with  $R$  the major radius of the tokamak and  $q \cong rB_T / RB_p \sim O(1)$  the safety factor, with  $B_T$  and  $B_p$  the toroidal and poloidal magnetic fields; and the transverse motion across field lines is characterized by the guiding center magnetic curvature-gradient-B drift frequency  $\omega_{dh} \cong (k_{\perp} \rho_h) (V_h / R)$ , where  $k_{\perp} \cong nq / r$  is the perpendicular wave number, with  $n$  the toroidal mode number and  $r$  the minor radius, and  $\rho_h = V_h / \Omega_h$  is the Larmor radius, of a hot particle. Note that the various frequencies are related to each other as  $\omega_{dh} / \omega_{bh} \sim k_{\perp} \rho_h$  and  $\omega_{bh} / \Omega_h \sim \rho_h / L_{\parallel}$ . Thus, if we take the finite Larmor radius effects of the hot particles to be negligible (as we will throughout this work), we have the ordering  $\omega_{dh} \ll \omega_{bh} \ll \Omega_h$ .



The interesting and unusual feature of highly energetic particles is that their magnetic drift frequency  $\omega_{dh}$  can be comparable to or larger than the characteristic frequency,  $\omega$ , of MHD modes like ballooning and kink modes. This is unusual since in the normal fluid and fluid-like kinetic guiding center descriptions, the opposite limit of  $\omega_{dh} \ll \omega$  is assumed. These fluid descriptions are generally based on the idea that the plasma is "frozen in" with the magnetic field and, therefore, that particle drift off a field line is negligible in the time scale of interest. Highly energetic particles that satisfy the opposite limit of  $\omega_{dh} \gg \omega$ , however, are rapidly drifting across field lines; for such particles, the usual fluid description is inadequate. It has been shown<sup>14</sup> that in this limit the behavior of very hot particles is now governed by the conservation of the third, or flux, adiabatic invariant, in addition to the usual first two invariants of magnetic moment and longitudinal action. The situation becomes even more interesting when  $\omega_{dh} \cong \omega$ , since then the particle motion can interact resonantly with that of MHD waves.

Now let us move from a guiding center particle picture to a fluid/kinetic picture. For the sake of simplicity, we will focus on the highly energetic, nonresonant limit of  $\omega_{dh} \gg \omega$ . It is well known that

the low frequency MHD ballooning modes with small transverse wavelength are described by the vorticity equation <sup>20</sup>

$$\mathbf{B} \cdot \nabla \left[ \frac{|\mathbf{k}_\perp|^2}{B^2} \mathbf{B} \cdot \nabla \Phi \right] + \left[ \frac{\omega^2 |\mathbf{k}_\perp|^2}{V_A^2} \right] \Phi - (4\pi\omega/B^2 c^2) (\mathbf{B} \times \boldsymbol{\kappa}) \cdot \mathbf{k}_\perp (\tilde{\beta}_i + \tilde{\beta}_\perp) = 0. \quad (1.1)$$

This equation is equivalent to quasi-charge neutrality. Here  $\Phi$  is the perturbed electrostatic potential, related to the electric field by  $\mathbf{E}_\perp \cong -i\mathbf{k}_\perp \Phi$ ; the parallel component of the electric field is zero for MHD modes;  $V_A = B/\sqrt{4\pi N_i M_i}$  is the Alfvén velocity, with  $N_i$  and  $M_i$  the density and mass of the background plasma ions;  $\boldsymbol{\kappa} = (\mathbf{b} \cdot \nabla) \mathbf{b}$ , with  $\mathbf{b} = \mathbf{B}/B$ , is the magnetic field line curvature; and  $\tilde{\beta}_i + \tilde{\beta}_\perp \cong 2\tilde{\beta}_c + \tilde{\beta}_\perp$  is the sum of the perturbed total pressure components, where the core plasma is assumed to be isotropic and the hot particle species is assumed to be trapped and anisotropic ( $P_{\parallel h}/P_{\perp h} \ll 1$ ). The first term in Eq. (1.1) describes the bending of a field line as shear Alfvén waves propagate along it; the second term arises from the ion polarization drift motion; and the third term represents the free energy of interchange motion. To obtain the perturbed pressures in this third term, we note that the core plasma behaves like a warm fluid, whose basic response is that of  $\mathbf{E} \times \mathbf{B}$  convection: thus,  $-i\omega \tilde{\beta}_c + \tilde{\mathbf{V}} \cdot \nabla P_c = 0$ , with  $\tilde{\mathbf{V}} = c(\tilde{\mathbf{E}}_\perp \times \mathbf{B})/B^2$ , gives

$$\tilde{\beta}_c \cong - \left[ \frac{c(\mathbf{B} \times \nabla P_c) \cdot \mathbf{k}_\perp}{\omega B^2} \right] \tilde{\phi} \quad (1.2)$$

The energetic particles, on the other hand, respond poorly to the  $\mathbf{E} \times \mathbf{B}$  motion. Their response is nonhydrodynamic and requires a kinetic treatment. For the low frequency ( $\omega \ll \omega_{dh}$ ) fluctuations considered here, the drift kinetic equation for the hot particle distribution function  $f_h$  is dominated by their grad-B drift term:

$$\frac{v_\perp^2 \mathbf{B} \times \nabla B}{B^2} \cdot \nabla f_h \cong 0. \quad (1.3)$$

(Here, for simplicity we ignore the fact that Eq. (1.3) should be bounce averaged.) By linearizing Eq. (1.3) and integrating it over all velocities, we obtain an expression for the hot electron perturbed transverse pressure:

$$(\mathbf{b} \times \nabla B) \cdot \mathbf{k}_\perp \tilde{\beta}_{\perp h} \cong (\mathbf{b} \times \nabla P_{\perp h}) \cdot \mathbf{k}_\perp \tilde{\beta}_\perp \quad (1.4)$$

or

$$\tilde{\beta}_{\perp h} \cong \frac{\beta_{\perp h}}{8\pi} \left[ \frac{\omega_{*h}}{\omega_{dh}} \right] B \tilde{\beta}_\perp. \quad (1.5)$$

Here,  $\omega_{dh} = (cT_{\perp h}/e_h B^2) (\mathbf{b} \times \nabla B) \cdot \mathbf{k}_{\perp}$  is the grad-B drift frequency of the hot particles,  $\omega_{*h} = (cT_{\perp h}/e_h B) (\mathbf{b} \times \nabla \ln P_{\perp h}) \cdot \mathbf{k}_{\perp}$  is their diamagnetic frequency, and  $\beta_{\perp h} = 8\pi P_{\perp h}/B^2$  is their beta value. Equation (1.4) or (1.5) shows that the very energetic electrons respond not to displacements of the field line, but to changes in the field strength, in such a way as to preserve the magnetic flux through their magnetic drift precessional orbits.

We can relate the parallel perturbed magnetic field  $\tilde{B}_{\parallel}$  to  $\tilde{\Phi}$  by the use of the quasi-static condition for transverse perturbed pressure balance:

$$B \tilde{B}_{\parallel} + 4\pi (\tilde{P}_{\perp h} + \tilde{P}_c) = 0 \quad (1.6)$$

This relationship holds for low frequency modes whose perpendicular wavelength is much smaller than both the parallel wavelength and any equilibrium scale length. Equation (1.6) can be understood as the condition for annihilating the fast compressional Alfvén wave. Combining Eqs. (1.4)-(1.6), and introducing equilibrium pressure balance

$$\nabla_{\perp} \left[ \frac{B^2}{8\pi} + P_{\perp} \right] = \frac{B^2 \kappa}{4\pi} \quad (1.7)$$

we find that the hot particle pressure can be expressed as

$$\beta_{1h} = \left[ \frac{4\pi c}{\omega B^3} \right] (\mathbf{b} \times \nabla P_{1h}) \cdot \mathbf{k}_\perp$$

$$\left[ \frac{(\mathbf{b} \times \nabla P_c) \cdot \mathbf{k}_\perp \tilde{\Phi}}{(\mathbf{b} \times \boldsymbol{\kappa}) \cdot \mathbf{k}_\perp - 4\pi (\mathbf{b} \times \nabla P_c) \cdot \mathbf{k}_\perp / B^2} \right] \quad (1.8)$$

Finally, we use local approximations such that  $(\mathbf{b} \times \nabla P_c) \cdot \mathbf{k}_\perp / k_\perp \rightarrow dP_c/dr$ ,  $(\mathbf{b} \times \boldsymbol{\kappa}) \cdot \mathbf{k}_\perp / k_\perp \rightarrow -1/R$ ,  $(\mathbf{B} \cdot \nabla)^2 \rightarrow -B_T^2 / (qR)^2$ , and we define the Alfvén frequency  $\omega_A = V_A / qR$  and a normalized pressure gradient  $\alpha = -q^2 R (d\beta_T/dr) > 0$ . This yields the following dispersion relation:

$$\left[ \frac{\omega}{\omega_A} \right]^2 = 1 - \alpha_c \left[ 1 - \frac{\alpha_h/2}{2q^2 - \alpha_c} \right]. \quad (1.9)$$

Note that if we replace  $d/dr \rightarrow r^{-1}$ , with  $r$  the minor radius, we find that  $\alpha \cong \varepsilon \beta_p$ , where the poloidal beta value is related to the toroidal beta by  $\beta_p = \beta_T (q/\varepsilon)^2 \gg \beta_T$ , since the inverse aspect ratio,  $\varepsilon = r/R$ , is small. Typically, the beta threshold for ideal ballooning instability is  $\alpha_c \cong O(1)$ , as can be seen from Eq. (1.9)

without any hot particles. The presence of the super energetic species tends to reduce the effect of the destabilizing free energy represented by  $\alpha_c$ . In particular, if  $\alpha_c$  is near its threshold value, the hot particle term is enhanced and can effectively stabilize the mode. However, when  $\alpha_h$  and  $\alpha_c$  become too large such that  $\alpha_c + \alpha_h/2 \gtrsim 2q^2$ , the stabilizing effect is lost; this corresponds to drift reversal, *i.e.*  $(\mathbf{b} \times \nabla B) \cdot \mathbf{k}_\perp$  changes sign due to high beta. Interestingly, this simple analysis shows that hot particles trapped in a region of unfavorable curvature contribute a stabilizing effect; although counterintuitive to what would be expected from a fluid stability description, this stabilization results from the nonhydromagnetic response of the very energetic component. Finally, Eq. (1.9) indicates the existence of another core beta limit,  $\alpha_c \simeq 2q^2$ , which has been previously examined in the bumpy torus context.<sup>21,22</sup> This limit, which occurs for  $\alpha_c$  values above drift reversal, indicates that the mode becomes primarily magnetic. Other studies have shown that a magnetic compressional instability can occur here.<sup>23</sup>

The first clear indication that energetic particles could play a stabilizing role in tokamaks came from a study by Connor *et al.*<sup>24</sup> of the effect of beam ions on ballooning modes. This study was done

in the low bounce frequency limit,  $\omega_{bh} \ll \omega \lesssim \omega_{dh}$ , in which trapped particles cannot be distinguished from circulating ones. A window of stability was found when the beam ion energy was sufficiently high.

A subsequent study by Rosenbluth *et al.*<sup>11</sup> of low-frequency modes in the high bounce frequency limit,  $\omega \ll \omega_{dh} \ll \omega_{bh}$ , clearly showed the enhancement of ballooning stability when highly energetic particles are present. Their results indicated the possibility of stable access into the high-beta regime of second stability with respect to ballooning modes.

About the same time, experimental observations on the PDX tokamak indicated that moderately energetic beam ions, *i.e.*, not energetic enough to satisfy the nonresonant condition, could resonantly excite MHD instabilities.<sup>5</sup> These so-called "fishbone" oscillations were theoretically interpreted in this way by Chen *et al.* as beam ion-induced internal kink modes.<sup>25,26</sup> An analogous explanation was also given for the high-frequency precursor oscillations in terms of resonantly excited ballooning modes.<sup>27-31</sup> Recently, these resonant theories have been extended to include the effects of finite resistivity.<sup>32-34</sup>

In the present work, we will first examine in detail the stabilizing effect of highly energetic particles. Finite Larmor radius<sup>35</sup> and banana width effects<sup>34,36</sup> will be neglected here. We extend the work of Rosenbluth *et al.*<sup>11</sup> by introducing a more accurate bound for the trapped particle potential energy, which yields a better estimate of stability. We also compare the relative merit for stability of various hot particle pressure profiles, and we examine the stability of modes that peak off the tokamak midplane. This work will be described in Chap. II .

Next, we investigate the resonant destabilization of ballooning modes by moderately energetic trapped particles. By means of an asymptotic matching procedure valid when  $\omega \simeq \omega_{dh} \ll \omega_A$ , *i.e.*, when the high frequency Alfvén spectrum is unmodified, we obtain an analytical dispersion relation. The stability properties are given in terms of the resonant response function and the Mercier information for the ideal solution. The parameter regime of stability is found to be significantly reduced by the resonant "balloon bone" instability. This study will be described in Chap. III .

Finally, we generalize the nonresonant theory to include the effect of resistivity. By successively averaging over the rapid variation of the ballooning mode equation and matching the solutions



from the ideal to the resistive to the deeply resistive region, in which sonic compressibility and cross-field transport are included, we obtain the dispersion relation for resistive ballooning modes. This analysis will be presented in Chap. IV.

We note here, incidentally, that in Chaps. II and III, the starting equations that govern the dynamics of the core plasma and the energetic species will not be derived, inasmuch as these equations are available in the published literature. These equations will be initially presented here as a quadratic form, from which the equations of motion can be recovered variationally. In the case of nonresonant ideal ballooning modes the quadratic form will constitute an energy principle for stability. Even in other cases, it is convenient to use quadratic forms since they provide insight as to which unstable perturbations might be most dangerous. Also, in quadratic form, the various terms in the equations can be readily identified and also manipulated into or approximated by expressions that are analytically tractable. Occasionally we will make use of trial functions to estimate stability from a quadratic form. In our study of resistive ballooning modes in Chap. IV, however, we will present a detailed derivation of the fundamental equations.

A concluding summary of our work, with some discussion of various implications, will be given in Chap. V.

## CHAPTER II

### NON-RESONANT STABILIZATION OF BALLOONING MODES WITH HIGHLY ENERGETIC PARTICLES

#### 2.1 INTRODUCTION

Rosenbluth *et al.*<sup>11</sup> have predicted the stabilization of ideal ballooning modes when hot particles are introduced on the outer side of a tokamak. They considered a large-aspect-ratio tokamak described by a model equilibrium with circular flux surfaces and radially localized pressure gradients. They also considered highly energetic particles whose magnetic curvature drift frequency,  $\bar{\omega}_{dh}$ , is much larger than the frequency or growth rate,  $|\omega|$ , of the mode under consideration; *i.e.*,  $\bar{\omega}_{dh} \gg |\omega|$ . This condition will, in fact, be our definition for a superhot species, and it implies that the hot particles are drifting in the toroidal direction of the tokamak and oscillating up and down in the poloidal direction, on the outer side of the tokamak. The length of the excursions of the hot particles in the poloidal direction depends on the ratio of their energy  $E$  to their magnetic moment  $\mu$ . Rosenbluth *et al.* used a model in which all the hot particles were trapped and therefore had an anisotropic

pressure. Working with the low frequency energy principle,<sup>14,38</sup> they found that the superhot component makes a negative (*i.e.*, destabilizing) contribution to the fluid potential of the energy because the hot particles are localized on the outer side of the tokamak where the magnetic curvature is unfavorable, but that it makes an even larger positive (stabilizing) contribution to the kinetic part of the energy through an enhancement of the magnetic field compressional response. This constitutes the mechanism for stabilization.

In their treatment, the core plasma was described with MHD fluid equations, whereas the non-MHD hot species was described with the gyrokinetic equation to obtain its contribution to the perturbed dynamics. When the condition  $\bar{\omega}_{dh} \gg |\omega|$  is satisfied, resonant interaction of the hot particles with the core plasma is avoided, and a positive contribution to the energy is obtained from the non-local kinetic potential. The energy principle dictates that if the sum of the local fluid potential energy,  $\delta W_F$ , and the non-local kinetic potential energy,  $\delta W_k$ , is positive, then the mode will be stable. This is both a sufficient and a necessary condition for stability. The kinetic term is very difficult to handle, inasmuch as it involves multiple integrals of equilibrium quantities and the

perturbed fields. However, the analysis can be nontrivially simplified by working with a lower bound,  $\delta W_1$ , for the kinetic potential energy: *i.e.*,  $\delta W_1 \leq \delta W_k$ . This lower bound is derived by an application of the Schwartz inequality in the integral over velocity space. Unfortunately, the use of the Schwartz inequality imposes a maximum value on the hot particle pressure, since it requires that the hot particles not be drift reversed. Thus, the stability condition given by  $\delta W_k + \delta W_1 \geq 0$  in the non-resonant limit becomes only a sufficient, but not necessary, condition for stability. Therefore working with a lower bound for the kinetic potential, Rosenbluth *et al.* obtained a pessimistic estimate of stability. By solving the integro-differential equation for the ballooning mode perturbation, they found that direct access to the high-beta second stable regime for ballooning modes can be provided by the presence of the energetic particles.

In their treatment, however, an unexpectedly pessimistic result for the first stability boundary is obtained at large values of the global shear. This result was a consequence of using a pessimistic estimate of the total energy, which apparently is not very realistic at moderately large values of  $S$ . In the present work, we adopt their same assumptions and equilibrium model, but

we invent a better lower bound for the kinetic potential by using a weighted Schwartz inequality. The difference with respect to the results of Rosenbluth *et al.* becomes remarkable for large values of the global shear  $S$ . In this region the method used previously predicts an unexpected shape for the first stability boundary; this result was the main motivation for improving the lower bound. With it, we have now been able to obtain more realistic results.

In addition, we study the effect on stability of varying the poloidal profile of the hot particle pressure, while maintaining the constraint of drift nonreversal. We find that a hot particle pressure profile whose maximum is on the very outside of the tokamak is the most effective for stabilization.

We also have investigated the stability of modes which peak off the midplane, with and without the presence of hot particles. Without hot particles, the first stability region is improved whereas the second regime is reduced, due to the effect of the geodesic curvature at high beta values. In the presence of hot particles, stabilization results are obtained that are similar to those for modes that peak in the bad curvature region of a tokamak.

This chapter is divided into eight parts. In Section 2.2, the equilibrium model and assumptions are explained. In Section 2.3, the theoretical method for the variational refinement of the Schwartz inequality is explained, and the ballooning mode equation is derived. In Section 2.4 the numerical scheme for solving the ballooning equation is explained. In Sections 2.5, 2.6, and 2.7, the results are presented, and in Section 2.8 we give our conclusions.

## 2.2 EQUILIBRIUM EQUATIONS AND ASSUMPTIONS

We investigate the MHD stability of high-mode number modes, using an eikonal treatment in which the rapid variation across field lines is given by an eikonal  $S(\alpha, \beta)$ . In other words, if  $\tilde{\Phi}(\alpha, \beta, \ell, t)$  is a perturbed quantity where  $\alpha$  and  $\beta$  are transverse spatial coordinates and  $\ell$  is the arc length coordinate along a field line, we assume that it varies as

$$\Phi[\alpha, \beta, \ell, t] = \Phi(\ell) \exp \left\{ i \left[ S(\alpha, \beta) - \omega t \right] \right\} \quad (2.1)$$

where

$$\mathbf{b} \cdot \nabla S = 0 \quad (2.2)$$

$$\mathbf{b} = \frac{\mathbf{B}}{B} \quad (2.3)$$

Here,

$$\mathbf{B} = \nabla \alpha \times \nabla \beta \quad (2.4)$$

is the magnetic field in the Clebsch representation;  $\alpha$  and  $\beta$  are coordinates in directions perpendicular to the magnetic field;  $\mathbf{b}$  is a unit vector along the direction  $\mathbf{B}$ ;  $B$  is the strength of the magnetic field;  $\ell$  is the coordinate along the magnetic field; and  $\omega$  is the frequency of the linearly perturbed mode. In Eq. (2.1),  $\Phi(\ell)$  gives the slow variation of the mode with  $\ell$  and satisfies

$$|\mathbf{b} \cdot \nabla \ln \Phi(\ell)| \ll |\nabla_{\perp} S| \quad (2.5)$$

which means that the variation of the perturbation across the magnetic field line is large compared to its variation along  $\mathbf{b}$ . In our analysis of stability we will derive an integro-differential equation for the variation of the perturbation along the field line,  $\Phi(\ell)$ , thus reducing the analysis to a single rational surface. That is possible because we will be treating high-mode-number perturbations. One of the first calculations to be done in this chapter will be for  $\nabla S$ . As the preliminary for its calculation, we first discuss the model equilibrium.

### 2.2.a MODEL EQUILIBRIUM

We consider a large aspect ratio tokamak, such that the inverse aspect ratio  $\epsilon$ , is very small, *i. e.*,

$$\epsilon \equiv \frac{a}{R_0} \ll 1 \quad (2.6)$$

Here,  $R_0$  and  $a$  are the major and minor radii of the tokamak, respectively; see Fig. 2.1. The energetic particles are assumed to be trapped on the outer side of the tokamak between the poloidal angles  $\pm\theta_0$ ; see Fig. 2.2. Thus, they will be moving along a magnetic field line, bouncing between the poloidal angles  $\pm\theta_0$  and drifting toroidally across the field line. The hot particles' drift is due to their magnetic gradient-B and curvature drifts, which will be specified later. We will not consider any effects due to an equilibrium electric field;<sup>39</sup> banana width effects will also be neglected. The hot particles' motion is such that they will fill a toroidal ribbon on the outer side, limited by the poloidal angles  $\pm\theta_0$ . The condition that all of the hot particles are trapped leads to the ordering

$$\frac{P_{\parallel h}}{P_{\perp h}} \sim \epsilon \quad (2.7)$$



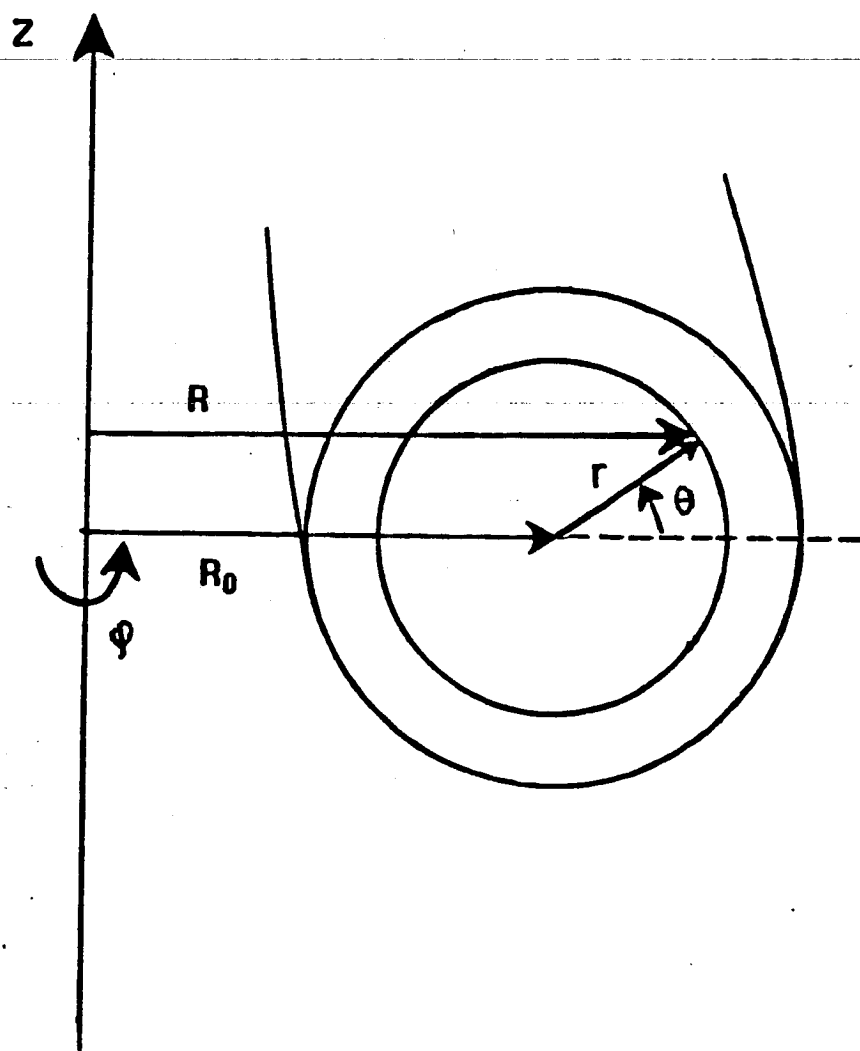


Fig. 2.1 Tokamak equilibrium

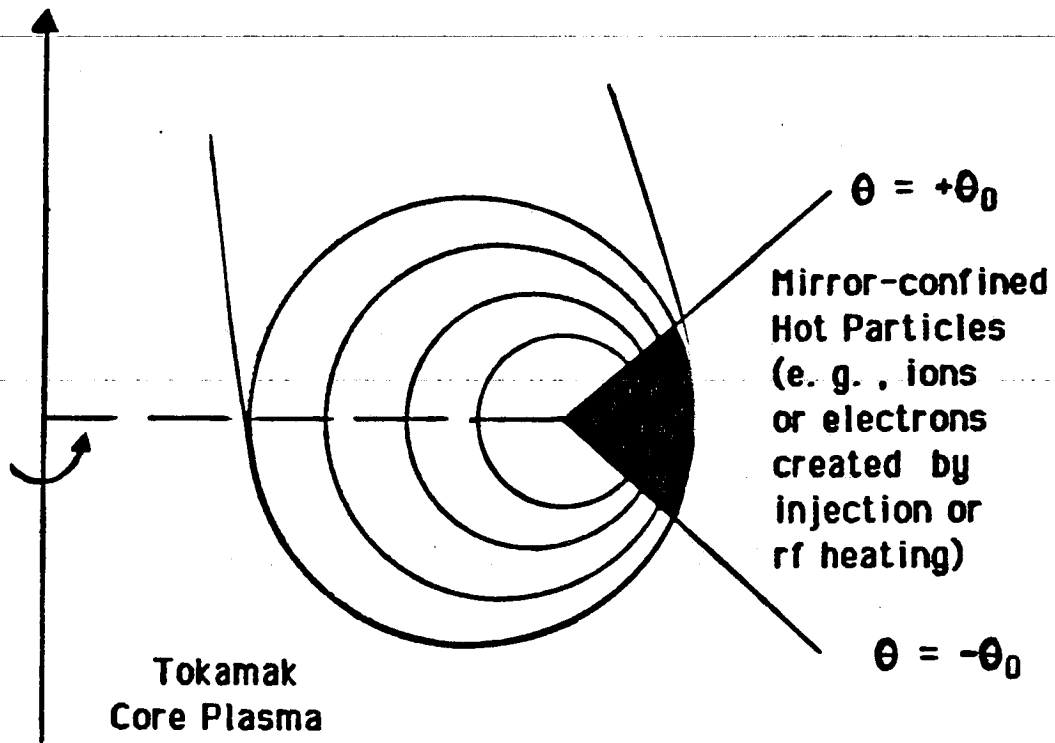


Fig. 2.2 Picture of hot particles confined on the outside of the tokamak.

where  $P_{\parallel h}$  and  $P_{\perp h}$  are the parallel and perpendicular components of the hot particle anisotropic pressure. The ordering given in Eq. (2.7) is a consequence of the shallowness of the magnetic poloidal well of a tokamak. The core plasma pressure,  $P_c$ , however, will be considered to be isotropic.

The beta values for the core plasma and for the hot particle component are defined as

$$\beta_c = \frac{8\pi P_c}{B^2} \quad (2.8)$$

and

$$\beta_{\perp h} = \frac{8\pi P_{\perp h}}{B^2} \quad (2.9)$$

We shall take the core plasma and hot particle beta values to be of the same order, with both being small compared to unity:

$$\beta_c \sim \beta_h \ll 1. \quad (2.10)$$

Thus, the usual firehose and mirror coefficients of anisotropy are given approximately by

$$\sigma = 1 + \frac{P_{\perp} - P_{\parallel}}{B^2} \approx 1 \quad (2.11)$$

and

$$\tau = 1 + \frac{1}{B} \frac{\partial P_{\perp}}{\partial B} \approx 1 \quad (2.12)$$

where  $P_{\perp} = P_c + P_{\perp h}$  and  $P_{\parallel} = P_c + P_{\parallel h}$  are the perpendicular and parallel components of the total pressure.

We assume that the flux surfaces are circular and that, although the beta values are low, the pressure gradients are locally steepened at the flux surface under consideration:

$$R \frac{d\beta}{dr} \sim O(1) \quad (2.13)$$

The distance,  $R$ , from the axis of symmetry can be written in terms of the radius,  $r$ , of the flux surface and the poloidal angle  $\theta$  as

$$R = R_0 + r \cos\theta \quad (2.14)$$

For an axisymmetric toroidal equilibrium, we can use the following representation for the magnetic field:

$$\mathbf{B} = \nabla\phi \times \nabla\Psi + I\nabla\phi . \quad (2.15)$$

Here  $\phi$  is the toroidal angle,  $\Psi$  is the poloidal flux, and  $I = RB_T$ . The condition of parallel pressure balance requires

$$\mathbf{b} \cdot \nabla \frac{P_{\parallel}}{B} = - \left[ \frac{(P_{\perp} - P_{\parallel})}{B^2} \right] \mathbf{b} \cdot \nabla B . \quad (2.16)$$

Thus,  $P_{\perp h}$  and  $P_{\parallel h}$  must satisfy the equilibrium force balance condition along a field line:

$$\mathbf{b} \cdot \nabla \frac{P_{\parallel h}}{B} = - \frac{P_{\perp h}}{B^2} \mathbf{b} \cdot \nabla B \quad (2.17)$$

By virtue of the axisymmetry, if we use the coordinates  $\Psi$ ,  $\theta$ , and  $u = \phi - q\theta$ , we find that  $\mathbf{b} \cdot \nabla = (\mathbf{b} \cdot \nabla\theta) \partial/\partial\theta$ . Note that since the  $\theta$  variation of  $B$  is of order  $\epsilon$ , then  $P_{\parallel h}/P_{\perp h} \sim 0(\epsilon)$  from Eq. (2.17), consistent with Eq. (2.7).

As a tractable pressure profile in poloidal angle, we take

$$P_{\perp h} = P_{\perp h0} \left\{ A + \eta(\cos\theta - \cos\theta_0) \right\} H \left[ \theta_0 - |\theta| \right] \quad (2.18)$$

with

$$P_{\perp hsq} = P_{\perp h0} H(|\theta| - \theta_0) \quad (2.19)$$

and

$$P_{\perp hsm} = P_{\perp h0} (\cos\theta - \cos\theta_0) H(|\theta| - \theta_0) \quad (2.20)$$

Thus,  $\theta_0$  gives the angle of localization of the hot particles: *i.e.*, all the particles are localized between the poloidal angles  $-\theta_0$  and  $\theta_0$ ; see Fig. (2.2). In Eq. (2.18),  $A$  and  $\eta$  are parameters that allow us to vary the hot particle pressure profile. For  $\eta = 0$ , we obtain the profile used by Rosenbluth *et al.*<sup>11</sup> For positive  $A$  and  $\eta > 0$  ( $\eta < 0$ ), a profile with a maximum (minimum) at  $\theta = 0$  is obtained. The  $A = 0$ ,  $\eta > 0$  profile avoids the problem of having  $\tau$  be singular at  $\theta = \pm \theta_0$  (although the stability results are not much changed from those for  $\eta = 0$ ). We solve for  $P_{\parallel h}$  using the parallel pressure balance equation (2.17). Thus,

$$P_{\parallel h}(\theta) = \varepsilon P_{\perp h0} H[\theta_0 - |\theta|] \left\{ A [\cos\theta - \cos\theta_0] + \left[ \frac{\eta}{2} \right] [\cos\theta - \cos\theta_0]^2 \right\} \quad (2.21)$$

Here,  $\phi$  is the toroidal angle (see Fig. 2.1) and

$$I = RB_T, \quad (2.22)$$

with  $B_T$  the toroidal magnetic field strength. The poloidal magnetic flux,  $\Psi$ , satisfies the anisotropic Grad equation: <sup>40</sup>

$$\nabla \cdot \left[ \sigma \frac{\nabla \Psi}{R^2} \right] = - (\sigma R^2)^{-1} \left[ \frac{dG}{d\Psi} \right] - \frac{\partial P_i}{\partial \Psi}. \quad (2.23)$$

Here,  $G = G(\Psi) = (1/2) (\sigma RB_T)^2$  is a flux function; the partial derivative is  $\partial/\partial\Psi = (\partial/\partial\Psi)|_B$ . At this point, we invoke our radially steepened pressure gradient model in order to retain only radial gradients in the Grad equation. We propose that  $\Psi = \Psi_0(r) + \Psi_1(r, \theta)$ , where  $\Psi_1/\Psi_0 \sim O(\varepsilon)$ ; the  $\theta$  dependence of  $\Psi_1$  will be determined algebraically from the form of the reduced Grad equation, viz:

$$\frac{1}{r} \frac{\partial}{\partial r} \left[ r \frac{\partial \Psi}{\partial r} \right] + \frac{d}{d\Psi} (G + R_0^2 P_c) = 2r R_0 \cos \frac{\partial P_c}{\partial \Psi} - \frac{R_0^2 \partial P_{lh}}{\partial \Psi} \quad (2.24)$$

Note that in our sharp gradient model, we have neglected partial derivatives with respect to  $\theta$  in comparison with partial derivatives with respect to  $r$ . However, to be consistent with the requirement that  $\Psi_1$  be periodic in  $\theta$  with period  $2\pi$ , we subtract from Eq. (2.24) its  $\theta$ -average. Using the expression for  $P_{\text{th}}$  given in Eq. (2.21), we obtain its average as

$$\begin{aligned} \langle P_{\text{th}}/P_{\perp\text{ho}} \rangle &= \frac{1}{2} \int_{-\pi}^{\pi} d\theta H(\theta_0 - |\theta|) \left\{ A(\cos\theta - \cos\theta_0) + \eta \left(\frac{1}{2}\right) (\cos\theta - \cos\theta_0)^2 \right\} \\ &= \left(\frac{1}{\pi}\right) \left\{ A(\sin\theta_0 - \theta_0 \cos\theta_0) + \eta \left[ \left(\frac{1}{8}\right) [\sin(2\theta_0) - 2\theta_0 \cos 2\theta_0] \right. \right. \\ &\quad \left. \left. - (\sin\theta_0 - \theta_0 \cos\theta_0) \cos\theta_0 \right] \right\} \end{aligned} \quad (2.25)$$

Then the lowest-order equation for  $\Psi_0$  is

$$\frac{1}{r} \frac{\partial}{\partial r} \left[ \frac{r \partial \Psi_0}{\partial r} \right] + \frac{d}{d\Psi_0} (G + R_0^2 P_c) + \langle P_{\text{th}}/P_{\perp\text{ho}} \rangle r R_0 \frac{\partial P_{\perp\text{ho}}(\Psi)}{\partial \Psi} = 0, \quad (2.26)$$

and the next-order equation for  $\Psi_1$  is

$$\frac{1}{r} \frac{\partial}{\partial r} \left[ \frac{r \partial \Psi_1}{\partial r} \right] + \Psi_1 \frac{d^2(G + R_0^2 P_c)}{d\Psi_0^2} = -2 r R_0 \cos\theta \left[ \frac{\partial P_c}{\partial \Psi_0} \right]$$



$$- r R_0 \left[ H(\theta_0 - |\theta|) \left\{ A(\cos\theta - \cos\theta_0) + \frac{\eta}{2} (\cos\theta - \cos\theta_0)^2 \right\} - \langle P_{\perp h} / P_{\perp h 0} \rangle \right] \left[ \frac{\partial P_{\perp h}}{\partial \Psi} \right] \quad (2.27)$$

To lowest order, Eq. (2.26) gives  $d\Psi_0/dr \cong RB_p$ . Also, in Eq. (2.26), the  $\Psi_1^2 (G + R_0^2 P_c) / d\Psi_0^2$  term is small (of order  $\Delta/r$ , where  $\Delta = (d \ln P_{\perp h} / dr) - 1$ ) and may be dropped.

## 2.2.b CALCULATION OF THE EIKONAL

In general  $S = S(\alpha, \beta)$ , and we can write the perpendicular wavenumber as

$$\mathbf{k}_{\perp} = \nabla S(\alpha, \beta) = \left[ \frac{\partial S}{\partial \alpha} \right] \nabla \alpha + \left[ \frac{\partial S}{\partial \beta} \right] \nabla \beta. \quad (2.28)$$

We may take  $\alpha = \Psi$ , the poloidal flux function, since  $\Psi$  has the property that  $\mathbf{b} \cdot \nabla \Psi = 0$ . We also note that for high-mode-number ballooning modes, we can ignore the radial variation of the mode, at least to lowest order in a  $1/n \ll 1$  expansion, where  $n$  is the toroidal wave number. Thus,

$$\nabla S \approx \left[ \frac{\partial S}{\partial \beta} \right] \nabla \beta. \quad (2.29)$$

However, the magnitude of  $\nabla S$  cancels out of the ballooning equation, being a factor common to all terms. Hence, the problem of obtaining the eikonal reduces to that of solving for  $\nabla\beta$ .

We solve for this quantity as follows. We take the cross product of Eq. (2.4) with  $\nabla\alpha$  to obtain

$$\mathbf{B} \times \nabla\alpha = - \left[ \nabla\alpha (\nabla\alpha \cdot \nabla\beta) - \nabla\beta |\nabla\alpha|^2 \right] \quad (2.30)$$

or

$$\nabla\beta = \mathbf{B} \times \frac{\nabla\alpha}{|\nabla\alpha|^2} + \lambda \nabla\alpha, \quad (2.31)$$

where

$$\lambda = \frac{\nabla\beta \cdot \nabla\alpha}{|\nabla\alpha|^2} \quad (2.32)$$

We obtain an equation for  $\lambda$  by using

$$\begin{aligned} \nabla \cdot (\nabla\phi \times \nabla\beta) &= 0 = \nabla \cdot \left[ \frac{\nabla\phi \times (\mathbf{B} \times \nabla\alpha)}{|\nabla\alpha|^2} \right] + \nabla \cdot \left[ \nabla\phi \times \lambda \nabla\alpha \right] \\ &= \nabla \cdot \left[ \mathbf{B} (\nabla\phi \cdot \nabla\alpha) - \nabla\alpha (\mathbf{B} \cdot \nabla\phi) \right] + (\nabla\phi \times \nabla\alpha) \cdot \nabla\lambda. \end{aligned} \quad (2.33)$$

Using the fact that  $\nabla\psi \cdot \nabla\alpha = 0$ , due to the toroidal symmetry, we obtain

$$(\nabla\psi \times \nabla\alpha) \cdot \nabla\lambda = \nabla \cdot \left[ (\mathbf{B} \cdot \nabla\psi) \frac{\nabla\alpha}{|\nabla\alpha|^2} \right]. \quad (2.34)$$

With the choice of poloidal flux  $\Psi$  for  $\alpha$ , we note that  $\nabla\psi \times \nabla\Psi = B_p$  is the poloidal magnetic field; also  $\mathbf{B} \cdot \nabla\psi = B_T/R$ . Therefore,

$$B_p \cdot \nabla\lambda = \nabla \cdot \left[ \frac{B_T \nabla\Psi}{R |\nabla\Psi|^2} \right]. \quad (2.35)$$

We now use  $B_p \cdot \nabla\lambda \rightarrow (B_p/r) (\partial\lambda/\partial\theta)$  to obtain

$$\left( \frac{B_p}{r} \right) \left( \frac{\partial\lambda}{\partial\theta} \right) \cong \frac{1}{r} \frac{\partial}{\partial r} \left[ r \left( \frac{B_T}{R} \right) \left( \frac{1}{RB_p} \right) \times \left\{ \left[ 1 - \frac{1}{RB_p} \frac{d\Psi_1}{dr} \right] \right\} \right] = \frac{1}{rR} \frac{\partial q}{\partial r} - \frac{1}{r} \frac{\partial}{\partial r} \left[ r \frac{\partial\Psi_1}{\partial r} \right] \frac{q}{R^2 B_p} \quad (2.36)$$

To obtain  $\lambda$ , it is not actually necessary to solve Eq. (2.27) for  $\Psi_1$ . We need merely substitute Eq. (2.27) directly into Eq. (2.36) for  $\lambda$ :

$$\frac{\partial\lambda}{\partial\theta} = \left[ \frac{1}{RB_p} \right] \left[ \frac{\partial q}{\partial r} \right] + \left[ \frac{q^2 r}{RB_T B_p^2} \right] \left\{ 2 \cos\theta \left[ \frac{dP_c}{dr} \right] \right.$$

$$+ \left[ \frac{dP_{\perp h0}}{dr} \right] \left[ H(\theta_0 - |\theta|) \left\{ A(\cos\theta - \cos\theta_0) + \left(\frac{\eta}{2}\right) (\cos\theta - \cos\theta_0)^2 \right\} - \langle P_{th}/P_{\perp h0} \rangle \right] \}. \quad (2.37)$$

Integrating this expression, we obtain

$$\lambda(\theta) = \left[ \frac{dq/dr}{RB_p} \right] (\theta - \theta_k) + \left[ \frac{rq^2}{RB_T B_p^2} \right] \times \left\{ 2 \left[ \frac{dP_c}{dr} \right] (\sin\theta - \sin\theta_k) + \left[ \frac{dP_{\perp h0}}{dr} \right] [g(\theta) - g(\theta_k)] \right\}. \quad (2.38)$$

The function  $g(\theta)$  is given by

$$g(\theta) = Ag_{sq}(\theta) + \eta g_{sm}(\theta). \quad (2.39)$$

Where

$$g_{sq}(\theta) = \begin{cases} \sin\theta - \left(\frac{\tilde{\theta}}{\pi}\right) [\pi \cos\theta_0 + t_0] & , 0 \leq \tilde{\theta} < \theta_0 \\ \left[1 - \left(\frac{\tilde{\theta}}{\pi}\right)\right] t_0 & , \theta_0 \leq \tilde{\theta} < 2\pi - \theta_0 \\ \sin\theta - \left[\left(\frac{\tilde{\theta}}{\pi}\right) - 2\right] [\pi \cos\theta_0 + t_0] & , 2\pi - \theta_0 \leq \tilde{\theta} < 2\pi. \end{cases} \quad (2.40)$$

$$g_{sm}(\theta) = \begin{cases} \left( \frac{1}{8} \right) \sin(2\theta) - \cos\theta_0 \sin\theta + \tilde{\theta} \left[ (\cos\theta_0)^2 \right. \\ \left. - \left( \frac{1}{4} \right) \cos(2\theta_0) - \left( \frac{t_1}{\pi} \right) \right], & 0 \leq \tilde{\theta} < \theta_0 \\ \left[ 1 - \left( \frac{\tilde{\theta}}{\pi} \right) \right] t_1, & \theta_0 \leq \tilde{\theta} < 2\pi - \theta_0 \\ \left( \frac{1}{8} \right) \sin(2\theta) - \cos\theta_0 \sin\theta + (\tilde{\theta} - 2\pi) \left[ (\cos\theta_0)^2 \right. \\ \left. - \left( \frac{1}{4} \right) \cos(2\theta_0) - \left( \frac{t_1}{\pi} \right) \right], & 2\pi - \theta_0 \leq \tilde{\theta} < 2\pi. \end{cases} \quad (2.41)$$

Here,  $\tilde{\theta} = \theta$  modulo  $2\pi$  and

$$t_0 = \sin\theta_0 - \theta_0 \cos\theta_0 \quad (2.42)$$

and

$$t_1 = \left( \frac{1}{8} \right) \left[ \sin(2\theta_0) - 2\theta_0 \cos\theta_0 \right] - t_0 \cos\theta_0 \quad (2.43)$$

We anticipate that in the ballooning representation  $\theta$  will become the "extended" poloidal coordinate along a field line, such that  $-\infty < \theta < \infty$ .

In the same way,  $\theta_k$  is the zero of the eikonal; this quantity approximately indicates where the mode prefers to peak.

Therefore, we obtain

$$\nabla\beta \cong \left[ \frac{q}{r} \right] \left\{ \hat{\theta} + \hat{r} \left[ S(\theta - \theta_k) - \alpha_c (\sin\theta - \sin\theta_k) - \frac{\alpha_h}{2} [g(\theta) - g(\theta_k)] \right] \right\} \quad (2.44)$$

where

$$S = d(\ln q)/d(\ln r) \quad (2.45)$$

is the global shear, and

$$\alpha_c = -2q^2 \left[ \frac{R}{B_T^2} \right] \left[ \frac{dP_c}{dr} \right] \quad (2.46)$$

$$\alpha_h = -2q^2 \left[ \frac{R}{B_T^2} \right] \left[ \frac{dP_{\perp h0}}{dr} \right] \quad (2.47)$$

Finally,

$$\nabla S \left[ \frac{\partial S}{\partial \beta} \right]^{-1} = \nabla \beta = \frac{q}{r} \left\{ \hat{\theta} + \hat{r} h(\theta) \right\} \quad (2.48)$$

where

$$h(\theta) = S(\theta - \theta_k) - \alpha_c (\sin \theta - \sin \theta_k) - \left[ \frac{\alpha_h}{2} \right] \left[ g(\tilde{\theta}) - g(\theta_k) \right] \quad (2.49)$$

is the integrated local shear. Using the definition for  $h(\theta)$ , we can finally write

$$|\nabla S|^2 \left[ \frac{\partial S}{\partial \beta} \right]^{-2} = \left[ \frac{q^2}{r^2} \right] (1 + h^2) \quad (2.50)$$

### 2.2.c DISTRIBUTION FUNCTION FOR THE HOT SPECIES.

The hot particle population is described by a distribution function  $F_h(\Psi, E, \mu)$ , which we assume can be written in separable form: <sup>41</sup>

$$F_h(\Psi, E, \mu) = A(\Psi) F(E) G(\lambda), \quad (2.51)$$

where  $E$  is the energy,  $\mu = mV_{\perp}^2/2B$  is the magnetic moment,  $V_{\perp}$  is the perpendicular component of the velocity, and  $\lambda = E/\mu$  is a pitch angle type of variable. This expression is consistent with assuming that the hot particle pressure is an isorhopic function, *i.e.*,  $P_h(\Psi, B)$ , with all the  $\theta$ -dependence subsumed in the dependence on the field strength  $B = B(\Psi, \theta)$ . In fact, the function  $G(\lambda)$  can be obtained from the form taken for the pressure, given in Eq. (2.18), by use of an Abel transformation.<sup>41</sup> Thus, we obtain

$$G(\lambda) = \left[ \frac{P_{\perp h 0}}{\pi B_T^2} \right] H(B_0 - \lambda) \left\{ \frac{A}{\sqrt{B_0 - \lambda}} + \frac{2\eta\sqrt{B_0 - \lambda}}{\epsilon B_T} \right\} \quad (2.52)$$

In Eq. (2.52),  $H$  is again the Heaviside step function. For the nonresonant theory that we are treating in this chapter, it will not be necessary to specify  $F(E)$  explicitly.

#### 2.2.d DRIFT NONREVERSAL CONDITION

We consider that the hot particles drift across field lines very rapidly, such that their bounce-averaged drift frequency,  $\bar{\omega}_{dh}$ , is much larger than the frequency of the mode,  $\omega$ , *i.e.*,



$$\bar{\omega}_{dh} \gg |\omega| \sim \text{MHD growth rate} \quad (2.53)$$

Here,

$$\omega_{dh} = \frac{\mathbf{b} \times (M_h V_{\perp}^2 \boldsymbol{\kappa} + \mu \nabla B) \cdot \nabla S}{M_h \Omega_h} \quad (2.54)$$

is the magnetic drift frequency due to the curvature and the gradient of the field strength. The bounce-averaged drift frequency  $\bar{\omega}_{dh}$  is given by

$$\bar{\omega}_{dh}(E, \mu) = \frac{\oint \frac{d\ell}{V_{\parallel}} \omega_{dh}(E, \mu, \ell)}{\oint \frac{d\ell}{V_{\parallel}}} \quad (2.55)$$

Here  $\oint d\ell/V_{\parallel}$  represents integration along the field line between the points where the particle's parallel velocity vanishes. The bounce averaged quantity  $\bar{\omega}_{dh}(E, \mu)$  is clearly proportional to the energy  $E$  and is a function of the pitch angle variable  $\lambda = E/\mu$ . In Eq. (2.54),  $\Omega_h = e_h B/M_h c$  is the signed cyclotron frequency of the hot particles.

We will refer to any population of highly energetic particles as "superhot" if it satisfies the condition given in Eq. (2.53). Particles satisfying this condition are unable to interact resonantly with the plasma. This condition, for reactor parameters, would require energies on the order of few MeV. Let us make an estimate of the required energy by using the decoupling condition:  $\alpha_h / \bar{\omega}_{dh} < 0.5$ , where  $\alpha_h \approx 0.25 (N_h T_h / N_i m_i r R)^{1/2}$  is the hot electron interchange growth rate and  $\bar{\omega}_{dh} \approx (m/r) (c T_h / e B_T R)$  is the curvature drift frequency. In this expression,  $N_h$  is the hot particle density,  $T_h$  is the hot particle temperature,  $N_i$  is the plasma density,  $B_T$  is the toroidal field,  $e$  is the charge of a proton, and  $m$  is the poloidal mode number. Considering  $\beta_{dh} = \beta_i$ , the decoupling condition yields  $T_h / T_i > (rR)^{1/2} / 2m\rho_i$ , where  $\rho_i$  is the ion Larmor radius. For reactor-like parameters, let us say,  $r = 1.5$  m,  $R = 5$  m,  $B_T = 5$  T, and  $T_i = 10$  KeV, we obtain  $T_h \gtrsim 3$  MeV (for  $m = 3$ ).

We will now assume that all the hot particles are mirror confined on the unfavorable-curvature, outer side of the torus and that their bounce-averaged magnetic drift is not reversed: *i.e.*,

$$\frac{\bar{\omega}_{dh}(\lambda_0)}{\omega_{*h}} > 0, \quad (2.56)$$

where

$$\omega_{*h} = - \frac{(b \times \nabla F_h) \cdot \nabla S}{M_h \Omega_h (\partial F_h / \partial E)} \quad (2.57)$$

is their diamagnetic drift frequency. We choose to evaluate  $\bar{\omega}_{dh}$  at the pitch angle of those particles that have their turning point at  $\theta = \theta_0$ , when the pressure vanishes: thus,  $\bar{\omega}_{dh} = \bar{\omega}_{dh}(\lambda_0)$ , where  $\lambda_0 = B(\theta = \theta_0)$ . If these extremal particles are not drift reversed, none of the hot particles will be. Physically, condition (2.56) means that the energetic species' contribution to the fluid part of the potential energy is negative, whereas their contribution to the kinetic part is positive (stabilizing). The condition expressed by Eq. (2.56) is the drift reversal condition. This condition will limit the maximum value for the hot plasma  $\alpha_h$  for fixed values of the shear,  $S$ , and the core plasma beta,  $\alpha_c$ . Fortunately, it will be seen that this limitation on the validity of the lower bound is not severe for particles trapped in the bad curvature region. It would become a severe limitation if one wanted to use this approach to explore the effects of a population of hot particles that mirror on the inner

side of the tokamak (*i.e.*,  $\theta_0 > \pi/2$ ), analogous to "sloshing" ions in mirror devices.

The drift non-reversal condition can be expressed as

$$A_1 \alpha_h + A_2 \alpha_c < A_3 S + A_4 \quad (2.58)$$

The derivation of Eq. (2.58) will be given in Appendix A, as well as the expressions for the coefficients  $A_1$ ,  $A_2$ ,  $A_3$ , and  $A_4$ , which can be written in terms of complete elliptic integrals.

### 2.3 VARIATIONAL REFINEMENT OF THE SCHWARTZ INEQUALITY AND THE BALLOONING MODE EQUATION

In this section we obtain the ballooning mode equation by starting from the low frequency ( $\bar{\omega}_{dh} \gg \omega$ ) kinetic energy principle in the high bounce frequency limit ( $\omega_{\text{bounce}} \gg \omega_{\text{drift}}$ ), with no finite Larmor radius effects. The form of the low frequency potential energy,  $\delta W_{LF}$ , has been derived elsewhere,<sup>14,38</sup> and we quote it here:

$$\delta W_{LF} = \delta W_F + \delta W_k . \quad (2.59)$$

$\kappa = (\mathbf{b} \cdot \nabla) \mathbf{b}$  is the magnetic field curvature,  $\mathbf{e} = \nabla S \times \mathbf{b}/B$ , and  $\nabla = \nabla - \nabla B (\partial/\partial B)$ . The energy principle means that  $\delta W_{LF} > 0$  is a sufficient condition for stability. Since the energetic particles are taken to be trapped in the unfavorable curvature region where, as described earlier, their magnetic drift is not reversed  $\overline{\omega_{dh}(\lambda_0)}/\omega_{*h} > 0$ , then  $\delta W_k$  will be positive and stabilizing whereas the interchange free energy term in  $\delta W_f$  can give a negative, destabilizing contribution.

The exact form for the kinetic potential  $\delta W_k$ , given in Eq. (2.61), is very difficult to handle, since it involves bounce averages. Rosenbluth *et al.*<sup>11</sup> overcame this difficulty by employing, in place of  $\delta W_k$ , its non-trivial lower bound,  $\delta W_1$ , derived by means of the Schwartz inequality:  $\delta W \geq \delta W_1$ . This substitution allows one to convert from dealing with an energy distribution average of microscopic bounce-averaged quantities to dealing with line averages of macroscopic quantities (such as the pressure). The use of either  $\delta W_k$  or  $\delta W_1$  will lead to a ballooning mode equation of the integro-differential type; the latter, however, is much more tractable. Also, since  $\delta W_1$  is a lower bound, we are assured that if  $\delta W_f + \delta W_1$  is positive, then the actual system is indeed stable.

The fluid part,  $\delta W_F$ , of the potential energy is given by

$$\delta W_F = \frac{1}{2} \int \frac{ds}{B} \left[ \sigma |\nabla S|^2 (\mathbf{b} \cdot \nabla \phi)^2 + \tau \left( Q_{\parallel} - \frac{\sigma}{\tau} B \mathbf{e} \cdot \mathbf{x} \phi \right)^2 \right. \\ \left. - (\mathbf{e} \cdot \mathbf{x}) \left[ \mathbf{e} \cdot \tilde{\nabla} P_{\perp} + \frac{\sigma}{\tau} \mathbf{e} \cdot \tilde{\nabla} P_{\parallel} \right] \phi^2 \right] \quad (2.60)$$

The kinetic part,  $\delta W_k$ , describes only the non-MHD highly energetic species, assumed to be trapped. In the nonresonant limit,  $\bar{\omega}_{dh} \gg \omega$ , it is given by

$$\delta W_k = \frac{1}{2} \int dE d\mu (\mathbf{e} \cdot \nabla F_h) \frac{\left[ \int \frac{ds}{V_{\parallel}} \left[ \mu Q_{\parallel} + V_{\parallel}^2 \mathbf{e} \cdot \mathbf{x} \phi \right] \right]^2}{\int \frac{ds}{V_{\parallel}} \left[ \mu \mathbf{e} \cdot \nabla B + \mathbf{e} \cdot \mathbf{x} V_{\parallel}^2 \right]} \quad (2.61)$$

Here,  $Q_{\parallel} = \tilde{B}_{\parallel} + \mathbf{e} \cdot \nabla B$  is the Lagrangian magnetic field perturbation parallel to the equilibrium magnetic field (whereas  $\tilde{B}_{\perp}$  is the usual Eulerian perturbation),  $\phi$  is the perturbed electrostatic potential,  $P_{\perp, \parallel}$  are the components of the total equilibrium pressure,

The expression for  $\delta W_1$  is derived with the use of the Cauchy-Schwartz inequality  $\langle a^2/b \rangle \geq \langle a \rangle^2 / \langle b \rangle$  if  $b > 0$ , where in the case of the lower bound the angle brackets mean  $\int dE d\mu$ . From Eq. (2.61) one then finds the lower bound  $\delta W_1$  to be

$$\delta W_1 = \frac{1}{2} \frac{\left\{ \int dE d\mu \left[ \frac{ds}{V_{\parallel}} \right] (\mathbf{e} \cdot \nabla F_h) G(E, \mu) \left[ \mu Q_{\parallel} + V_{\parallel}^2 \mathbf{e} \cdot \mathbf{x} \phi \right] \right\}^2}{\int dE d\mu \int \frac{ds}{V_{\parallel}} (\mathbf{e} \cdot \nabla F_h) G^2(E, \mu) \left[ \mu \mathbf{e} \cdot \nabla B + V_{\parallel}^2 \mathbf{e} \cdot \mathbf{x} \right]} \quad (2.62)$$

When the function  $G(E, \mu)$  in Eq. (2.62) is set equal to unity, we obtain the lower bound that was used by Rosenbluth *et al.* In this case the energy space integrations can be done immediately to give

$$\delta W_1 = \frac{\left\{ \int \frac{ds}{B} \left[ \left( \frac{Q_{\perp}}{B} \right) \mathbf{e} \cdot \tilde{\nabla} P_{\perp h} + \mathbf{e} \cdot \mathbf{x} \phi (\mathbf{e} \cdot \tilde{\nabla} P_{\parallel h}) \right] \right\}^2}{\int \frac{ds}{B} \left[ \frac{(\mathbf{e} \cdot \tilde{\nabla} P_{\perp h}) (\mathbf{e} \cdot \nabla B)}{B} + (\mathbf{e} \cdot \tilde{\nabla} P_{\parallel h}) (\mathbf{e} \cdot \mathbf{x}) \right]} \quad (2.63)$$

However, as was pointed out earlier, we have found that using the simple lower bound of Eq. (2.63) leads to an overly pessimistic

estimate of marginal stability as the value of the global shear is increased.

This difficulty can be avoided by use of other forms for the function  $G$ . We note that the Schwartz inequality permits an arbitrary positive function of the energy variables,  $G(E, \mu)$ , to be included, as it was in obtaining Eq. (2.62). This degree of freedom can be exploited in order to obtain a better lower bound. In fact, it is straightforward to observe that if  $\delta W_1$  is varied with respect to its functional dependence on  $G$ , one finds  $\delta W_1$  is maximized when  $G = \text{const.} \times \int (ds/V_1) (\mu Q_1 + V_1^2 \mathbf{e} \cdot \mathbf{x} \Phi) / \int (ds/V_1) (\mu \mathbf{e} \cdot \nabla B + V_1^2 \mathbf{e} \cdot \mathbf{x})$  and its maximum value is the exact value:  $\delta W_{1, \text{max}} = \delta W_K$ . Since bounce averages do not depend on both  $E$  and  $\mu$  but only on their ratio, we propose to use a function of the form

$$G(\lambda) = 1 + \alpha \left[ 1 - \frac{\lambda}{B_0} \right]^\zeta, \quad (2.64)$$

where  $B_0 = B_T \llbracket 1 - (r/R) \cos \theta_0 \rrbracket$  is the field at  $\theta = \theta_0$ ,  $\lambda = E/\mu$  is related to the pitch angle, and  $\zeta$  is an exponent which will be changed as a free parameter, whereas the coefficient  $\alpha$  will be determined variationally so as to yield the *least* pessimistic estimate of stability. For  $\alpha = 0$  we reproduce the results in Ref. 11



For finite  $\alpha$ , we will obtain an improved estimate of stability, due to the pitch-angle weighting introduced by the function  $G$ .

We now obtain the ballooning equation by varying  $\delta W_F + \delta W_I$  with respect to  $Q_\perp$ ,  $\Phi$ , and  $\alpha$  in each trapped particle region. An integro-differential ballooning equation is thereby obtained:

$$\begin{aligned}
 & \mathbf{B} \cdot \nabla \left[ \frac{\sigma |\nabla S|^2}{B^2} (\mathbf{B} \cdot \nabla \Phi) \right] + \mathbf{e} \cdot \mathbf{x} \left[ \mathbf{e} \cdot \nabla P_{\parallel} + \frac{\sigma}{\tau} \mathbf{e} \cdot \nabla P_{\perp} \right] \Phi = \\
 & (\mathbf{e} \cdot \mathbf{x}) (\mathbf{e} \cdot \nabla P_{\perp h}) \left[ A + \eta (\cos \theta - \cos \theta_0) \right] \times \\
 & \frac{\left[ R_2 R_4 - R_1 R_5 - \epsilon_1 \left[ R_2 R_3 - R_1 R_4 \right] \right]}{\left[ R_4^2 - R_3 R_5 \right]} \quad (2.65)
 \end{aligned}$$

Where,

$$\epsilon_1 = G_{\zeta} \left[ \frac{B_0 - B}{B_0} \right]^{\zeta} \frac{\left\{ A + \eta F_{\zeta} (\cos \theta - \cos \theta_0) \right\}}{\left\{ A + \eta (\cos \theta - \cos \theta_0) \right\}}$$

$$R_1 = (\mathbf{e} \cdot \nabla P_{\perp h 0}) \int \frac{d\ell}{B} \left\{ A + \eta (\cos \theta - \cos \theta_0) (\mathbf{e} \cdot \mathbf{x}) \right\}$$

$$R_2 = (\mathbf{e} \cdot \nabla P_{\perp h0}) \int \frac{d\ell}{B} \left[ A + \eta F_{\zeta} (\cos\theta - \cos\theta_0) \right] \Phi(\mathbf{e} \cdot \mathbf{x}) G_{\zeta} \left[ \frac{B_0 - B}{B_0} \right]^{\zeta}$$

$$R_3 = (\mathbf{e} \cdot \nabla P_{\perp h0}) \int \frac{d\ell}{B} \left[ \frac{A}{B} + \frac{\eta}{B} (\cos\theta - \cos\theta_0) \right] \left[ B \mathbf{e} \cdot \mathbf{x} - \frac{\mathbf{e} \cdot \nabla P_{\perp c}}{B} \right]$$

$$R_4 = (\mathbf{e} \cdot \nabla P_{\perp h0}) \int \frac{ds}{B} \left[ \frac{B - B_0}{B_0} \right]^{\zeta} G_{\zeta} \left[ \frac{A}{B} - \frac{\eta F_{\zeta}}{B} (\cos\theta - \cos\theta_0) \right] \left[ B \mathbf{e} \cdot \mathbf{k} - \frac{\mathbf{e} \cdot \nabla P_{\perp h}}{B} \right]$$

$$R_5 = (\mathbf{e} \cdot \nabla P_{\perp h0}) \int \frac{ds}{B} G_{\zeta}^2 \left[ \frac{B_0 - B}{B_0} \right]^{2\zeta} \left\{ \frac{\eta^2}{B^2} (\cos\theta - \cos\theta_0)^2 \left\{ F_{\zeta}^2 - \frac{x_{\zeta}}{G_{\zeta}} \right\} \right.$$

$$\left. + \frac{A^2}{B^2} \left[ 1 - \frac{\Gamma \left[ 2\zeta + \frac{1}{2} \right]}{\sqrt{\pi} \Gamma(2\zeta + 1) G_{\zeta}^2} \right] \right\}$$

$$\left. + \frac{A\eta}{B^2} (\cos\theta - \cos\theta_0) \left[ 2F_{\zeta} - \frac{x_{\zeta}}{G_{\zeta}} - \frac{\Gamma \left[ 2\zeta + \frac{1}{2} \right]}{\sqrt{\pi} (2\zeta + 1) G_{\zeta}^2} \right] \right\}$$

$$+ \int \frac{d\ell}{B} \left[ \frac{B_0 - B}{B_0} \right]^{2\zeta} G_{\zeta}^2 (\mathbf{e} \cdot \nabla P_{\perp h}) \left\{ \frac{\eta}{B} (\cos\theta - \cos\theta_0) \frac{x_{\zeta}}{G_{\zeta}} \right.$$

$$\left. + \frac{A}{B} \frac{\Gamma\left[2\zeta + \frac{1}{2}\right]}{\sqrt{\pi} \Gamma(2\zeta + 1) G_\zeta^2} \right\} \left[ B \mathbf{e} \cdot \mathbf{x} - \frac{\mathbf{e} \cdot \nabla P_{1c}}{B} \right]$$

$$G_\zeta = \frac{\Gamma\left[\zeta + \frac{1}{2}\right]}{\sqrt{\pi} \Gamma(\zeta + 1)} \quad , \quad F_\zeta = \frac{2\Gamma\left[\zeta + \frac{3}{2}\right]}{\sqrt{\pi} \Gamma(\zeta + 2) G_\zeta} \quad , \quad \kappa_\zeta = \frac{2\Gamma\left[2\zeta + \frac{3}{2}\right]}{\sqrt{\pi} \Gamma(2\zeta + 2) G_\zeta}$$

In the expression (2.65), the first term on the left-hand side represents the bending stabilizing term, whereas the second one is the destabilizing interchange term. On the right-hand side is the stabilizing compressional term due only to the hot particles.

For regions without hot particles, the equation to be solved is simply given by

$$\mathbf{B} \cdot \nabla \left[ \frac{\sigma |\nabla S|^2 \mathbf{B} \cdot \nabla \phi}{B^2} \right] + (\mathbf{e} \cdot \mathbf{x}) \left[ \mathbf{e} \cdot \nabla P_{1c} + \mathbf{e} \cdot \nabla P_{1c} \right] \phi = 0, \quad (2.66)$$

using our model equilibrium and the ballooning representation we proceed to solve the ballooning equation.

## 2.4 NUMERICAL SCHEME FOR SOLVING THE BALLOONING EQUATION

The ballooning space in which we solve the ballooning equation is divided into trapped and untrapped particle regions. The centers of the trapped particle regions are at  $\theta_m = 2\pi m$ , where  $m$  is an integer. These regions have a width of  $2\theta_0$ . The untrapped particle regions are located in the intervals  $[2\pi m + \theta_0, 2\pi(m+1) - \theta_0]$ . In Fig. 2.3, we pictorially show in the ballooning space a few trapped and untrapped particle intervals.

We numerically solve the ballooning equation using a fourth-order Runge-Kutta method in each trapped region. When  $\theta_k = 0$ , the marginally stable mode corresponds to the one that has even parity about  $\theta = 0$ , is well behaved at infinity, does not change sign for  $|\theta| < \infty$ , and whose amplitude asymptotically approaches zero as  $\theta \rightarrow \infty$ .<sup>42-44</sup> To find an even solution we begin with the initial conditions:

$$\Phi(\theta = 0) = 1 ,$$

$$\frac{d}{d\theta} \Phi(\theta = 0) = 0 , \tag{2.67}$$

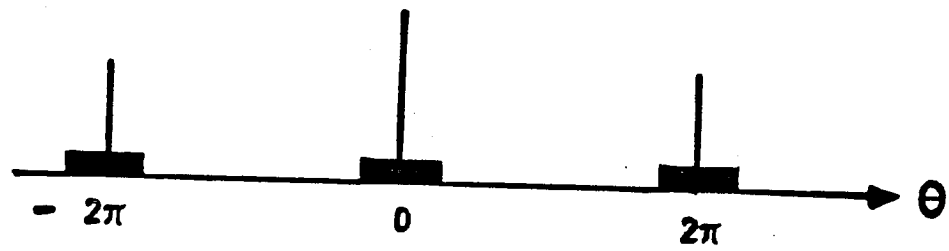


Fig. 2.3 Trapped and untrapped particle regions in ballooning space.

and solve for  $\Phi$  only for positive values of  $\theta$  because of the even symmetry of  $\Phi$ . We start solving for  $\Phi$  in the first trapped region,  $0 < \theta \leq \theta_0$ , and get  $\Phi(\theta_0)$  and  $\Phi'(\theta_0)$ , which are used as the initial conditions when solving the differential equation in the succeeding untrapped particle region,  $\theta_0 < \theta \leq 2\pi - \theta_0$ . Having solved the differential equation in this untrapped interval, we obtain  $\Phi(2\pi - \theta_0)$  and  $\Phi'(2\pi - \theta_0)$ , which are used as initial conditions for the next trapped particle region,  $2\pi - \theta_0 < \theta \leq 2\pi + \theta_0$ , and so on. Within the  $n^{\text{th}}$  trapped region,  $2\pi(n-1) - \theta_0 < \theta \leq 2\pi(n-1) + \theta_0$ , the solution of the ballooning equation can be written as<sup>45</sup>

$$\Phi = \Phi_0 + C_1 \Phi_1 + C_2 \Phi_2, \quad (2.68)$$

where  $\Phi_0$ ,  $\Phi_1$ , and  $\Phi_2$  satisfy the equations

$$\mathcal{L} \Phi_0(\theta) = 0 \quad (2.69)$$

$$\mathcal{L} \Phi_1(\theta) = \left(\frac{1}{2}\right) \alpha_h \left[ A + \eta (\cos\theta - \cos\theta_0) \right] D(\theta) \quad (2.70)$$

$$\mathcal{L} \Phi_2(\theta) = \left(\frac{1}{2}\right) \alpha_h \left[ A + \eta (\cos\theta - \cos\theta_0) \right] D(\theta) \mathcal{L}_1(\theta), \quad (2.71)$$

with the initial conditions

$$\Phi_0(\theta_-) = \Phi_{10}$$

$$\Phi'_0(\theta_-) = \Phi_{1p} \quad (2.72)$$

$$\Phi_1(\theta_-) = 0$$

$$\Phi'_1(\theta_-) = 0 \quad (2.73)$$

$$\Phi_2(\theta_-) = 0$$

$$\Phi'_2(\theta_-) = 0 \quad (2.74)$$

Here  $\theta_- = 2\pi(n-1) - \theta_0$ , and  $\Phi_{10}$  and  $\Phi_{1p}$  are the values of  $\Phi$  and  $\Phi'$  at  $\theta = \theta_-$ , obtained by solving the differential equation in the preceding interval. For the first trapped particle region  $\theta_- = 0$  and for the even mode  $\Phi_{10} = 1$  and  $\Phi_{1p} = 0$ . In Eqs. (2.69)-(2.71) for  $\Phi_0$ ,  $\Phi_1$ , and  $\Phi_2$ , the operator  $\mathcal{L}$  is given by

$$\mathbf{L} = \left[ \frac{d}{d\theta} \right] \left[ 1+h^2(\theta) \right] \left[ \frac{d}{d\theta} \right] + D(\theta) \\ \times \left\{ \alpha_c + \left[ \frac{\alpha_{h0}}{2} \right] \left[ A + \eta \left[ \cos\theta - \cos\theta_0 \right] \right] \right\}. \quad (2.75)$$

Other definitions are

$$l_1 = G_z \left[ \cos\theta - \cos\theta_0 \right]^z \\ D(\theta) = \cos\theta + h(\theta) \sin\theta \quad (2.76)$$

The quantity  $D(\theta)$  is proportional to the curvature, with the first and second terms being related to the normal and geodesic curvature, respectively. Other definitions are as follows:

$$C_1 = \left\{ \left[ J_2 I_2(0) - J_3 I_1(0) \right] \left[ -J_2^2 + J_1 J_3 - J_1 I_2(2) + J_2 I_1(2) \right] \right. \\ \left. - \left[ J_2 I_2(0) - J_3 I_1(0) \right] \left[ J_2 I_1(1) - J_1 I_2(1) \right] \right\} / \Delta$$



$$C_2 = \left\{ \begin{aligned} & \left[ J_2^2 - J_1 J_3 - J_2 l_2(1) + J_3 l_1(1) \right] \left[ J_1 l_2(0) - J_2 l_1(0) \right] \\ & - \left[ J_2 l_2(0) - J_3 l_1(0) \right] \left[ J_2 l_1(1) - J_1 l_2(1) \right] \end{aligned} \right\} / \Delta$$

$$\Delta = \left[ J_2^2 - J_1 J_3 - J_2 l_2(1) + J_3 l_1(1) \right] \left[ -J_2^2 + J_1 J_3 - J_1 l_2(2) + J_2 l_1(2) \right] \\ - \left[ J_3 l_1(2) - J_2 l_2(2) \right] \left[ J_2 l_1(1) - J_1 l_2(1) \right]$$

$$I_1(j) = \int d\theta D(\theta) \Phi_j(\theta) \left[ A + \eta (\cos\theta - \cos\theta_0) \right]$$

$$I_2(j) = \int d\theta D(\theta) \Phi_j(\theta) \mathcal{L}_1(\theta) \left[ A + \eta F_\zeta (\cos\theta - \cos\theta_0) \right]$$

$$J_1 = \int d\theta \left[ D - \frac{\alpha_c}{2q^2} \right] \left[ A + \eta (\cos\theta - \cos\theta_0) \right]$$

$$J_2 = \int d\theta \left[ D - \frac{\alpha_c}{2q^2} \right] \mathcal{L}_1 \left[ A + \eta F_\zeta (\cos\theta - \cos\theta_0) \right]$$

$$\begin{aligned}
J_3 = & \left[ \frac{\alpha_h}{2q^2} \right] \int d\theta \, l_1^2 \left[ \eta^2 (\cos\theta - \cos\theta_0)^2 \left[ F_\zeta^2 - \frac{X_\zeta}{G_\zeta} \right] \right. \\
& + A^2 h_{\epsilon\zeta} + A\eta (\cos\theta - \cos\theta_0) \left[ 2F_\zeta - \frac{X_\zeta}{G_\zeta} - (1-h_{\epsilon\zeta}) \right] \left. \right] \\
& + \int d\theta \left[ D - \frac{\alpha_c}{2q^2} \right] \left[ A(1-h_{\epsilon\zeta}) + \frac{\eta X_\zeta}{G_\zeta} (\cos\theta - \cos\theta_0) \right] l_1^2
\end{aligned}$$

Also, we let  $h_{\epsilon\zeta} = 1 - \Gamma(2\zeta + 1/2) / \sqrt{\pi} \Gamma(2\zeta + 1) G_\zeta^2$  where  $\Gamma$ , is the gamma function.

Note that without improvement ( $\zeta=0$ ), the ballooning equation in a trapped particle region reduces to that obtained by Rosenbluth *et al.* :

$$\frac{d}{d\theta} (1+h^2) \frac{d}{d\theta} \Phi + \left[ \alpha_c + H \frac{\alpha_h}{2} \right] D\Phi = H \left[ \frac{\alpha_h}{2} \right] D \frac{\int_t D\Phi d\theta}{\int_t \left[ D - \frac{\alpha_c}{2q^2} \right] d\theta}$$

(2.77)

The solution of Eq. (2.77) can be written as

$$\Phi = \Phi_0 + \Lambda \Phi_1, \quad (2.78)$$

where

$$\Lambda = \frac{\int d\theta D \Phi_0}{\int d\theta \left[ D - \frac{\alpha_c}{2q^2} - D\Phi_1 \right]}, \quad (2.79)$$

$\Phi_0$  is the solution of

$$\frac{d}{d\theta} (1 + h^2) \frac{d}{d\theta} \Phi_0 + \left[ \alpha_c + H \frac{\alpha_h}{2} \right] D \Phi_0 = 0, \quad (2.80)$$

and  $\Phi_1$  is the solution of

$$\frac{d}{d\theta} (1 + h^2) \frac{d}{d\theta} \Phi_1 + \left[ \alpha_c + H \frac{\alpha_h}{2} \right] D \Phi_1 = \frac{\alpha_h}{2} D \quad (2.81)$$

with initial conditions

$$\Phi_0(\theta_-) = \Phi_{l0} \quad \Phi'_0(\theta) = \Phi_{lp} \quad (2.82)$$

$$\Phi_1(\theta_-) = 0, \quad \Phi'_1(\theta_-) = 0. \quad (2.83)$$

In each untrapped region we have simply

$$\mathbf{L} \Phi(\theta) + \alpha_c D(\theta) \Phi(\theta) = 0 \quad (2.84)$$

When solving for  $\Phi$ , we fixed the values of  $q$ ,  $\theta_0$ , and  $S$  and varied  $\alpha_c$ . If  $\Phi$  had a zero crossing (i.e., became negative) at a finite value of  $\theta$ , the mode is unstable by the oscillation theorem.<sup>42</sup>

For  $\theta_k \neq 0$ , the marginal mode is no longer even in  $\theta$ . It can be easily seen that the new symmetry property of the eigenfunction is  $\Phi(-\theta, -\theta_k) = \Phi(\theta, \theta_k)$ . In this case we start the integration of the differential equation from  $\theta = -\theta_L$ , where  $\theta_L \gg 1$ , with initial conditions  $\Phi(-\theta_L) = 0$ , and  $\Phi'(-\theta_L) = 1$ . We shoot forward in the direction of increasing  $\theta$ , and the mode will be unstable according to the oscillation theorem if  $\Phi$  crosses zero.

## 2.5 COMPARISON OF RESULTS USING THE IMPROVED SCHWARTZ INEQUALITY WITH PREVIOUS RESULTS WITHOUT THE IMPROVEMENT

In Fig. 2.4 we plot the results for stability without improvement ( $\zeta = 0$ ). A square profile for the hot particle pressure profile was chosen, and modes peaking on the midplane were studied by choosing  $\theta_k = 0$ . The safety factor,  $q$ , was set equal to 2.

The dashed lines in Fig. 2.4 are the first and second stability boundaries for ballooning modes without hot particles. Also in Fig. 2.4 are plotted the stability boundaries when hot particles are included: the stability boundary for  $\theta_0 = \pi/4$  is shown with the dash-cross line, that for  $\theta_0 = 3\pi/8$  is shown with the dash-dot line and that for  $\theta_0 = \pi/2$  is shown with the solid line. The maximum value of  $\alpha_h$  allowed by the drift non-reversal condition has been used in our results. This condition is different for different values of  $\theta_0$ . Drift nonreversal for infinitesimal in all  $\alpha_h$  holds on the left-hand side of the dotted lines; thus, the dotted lines in the picture correspond to  $\alpha_h = 0$ .

Below the large dashed line at  $S = 2.0$  is the region explored previously by Rosenbluth *et al.* We can see in this region their

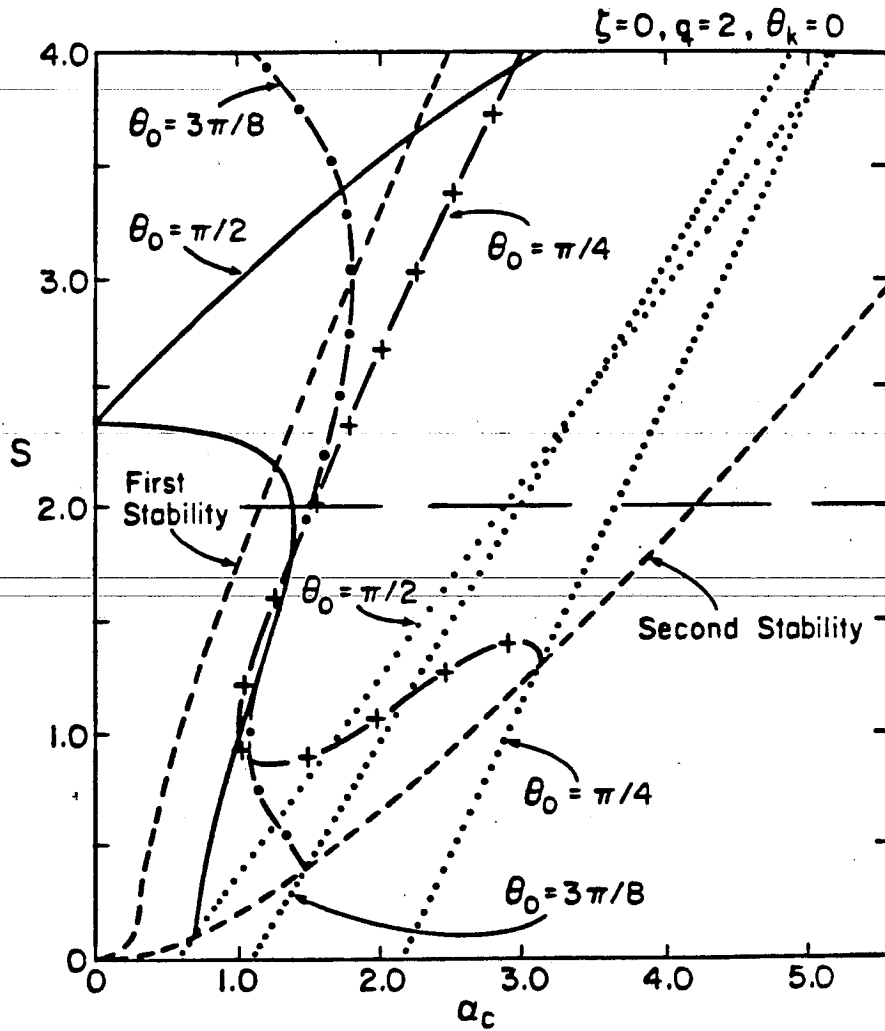


Fig. 2.4 Stability regions for  $\theta_0 = \pi/4, 3\pi/8, \text{ and } \pi/2$  without the Schwartz inequality improvement.

results for the stabilizing role of the hot particles: there is an improved first stable region, and a bridge between the first and the second stable regions. Above the line at  $S = 2.0$  we present the stability boundaries when larger values of  $S$  are considered. It appears that the introduction of the hot particles make the plasma becomes unstable in parameter regimes where it was stable in their absence. The most dramatic unexpected behavior occurs for  $\theta_0 = \pi/2$ . This apparent paradox is resolved when the better lower bound of  $\delta W_k$  is used. In Fig. 2.5, we present the results when the better lower bound is employed. As it can be seen, the boundaries now have a reasonable shape. This results from the fact that with the unimproved lower bound, parameter regimes that are not found to be stable are not thereby necessarily unstable. In Fig. 2.5,  $\zeta = 1/2$  was used: this value seems to give the best results for various values of  $\theta_0$ .

In Fig. 2.6, we show the dependence of the stability boundaries on  $\zeta$  for  $\theta_0 = \pi/2$ . In Fig. 2.7, an enlargement of the area shown boxed in Fig. 2.6 is presented in order to show a little more clearly the effect of changing the exponent  $\zeta$ . In fact the locus of the curves for different values of  $\zeta$  should be taken to obtain the best estimate for the true stability boundary. In Figs. 2.8 and 2.9, curves similar to those in Fig. 2.6 are presented for  $\theta_0 = 3\pi/8$  and  $\theta_0 = \pi/4$ , respectively. As can be seen, the results for  $\zeta = 0$  are the same as

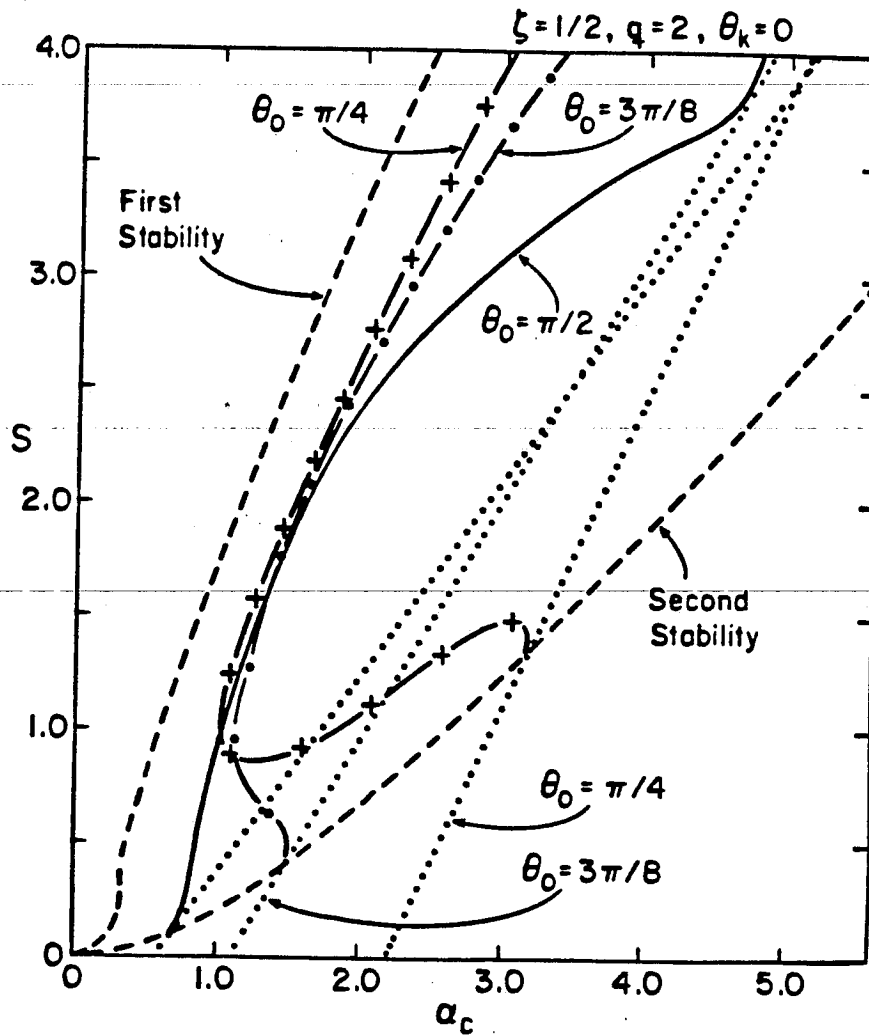


Fig. 2.5 Stability regions for  $\theta_0 = \pi/4, 3\pi/8,$  and  $\pi/2$  with the improved Schwartz inequality;  $\zeta = 1/2$  was used in all the curves (compare with Fig. 2.4)



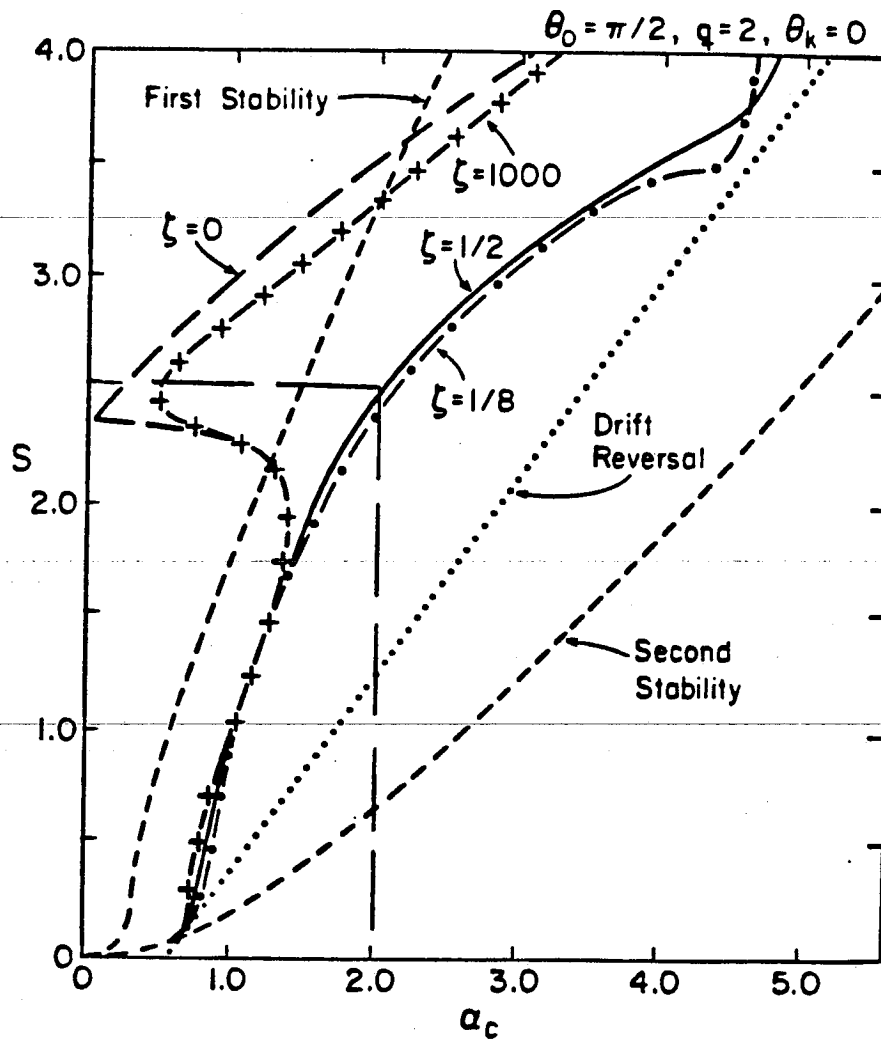


Fig. 2.6 Comparison of stability boundaries for various inequality weighting functions ( $\theta_0 = \pi/2$ ).

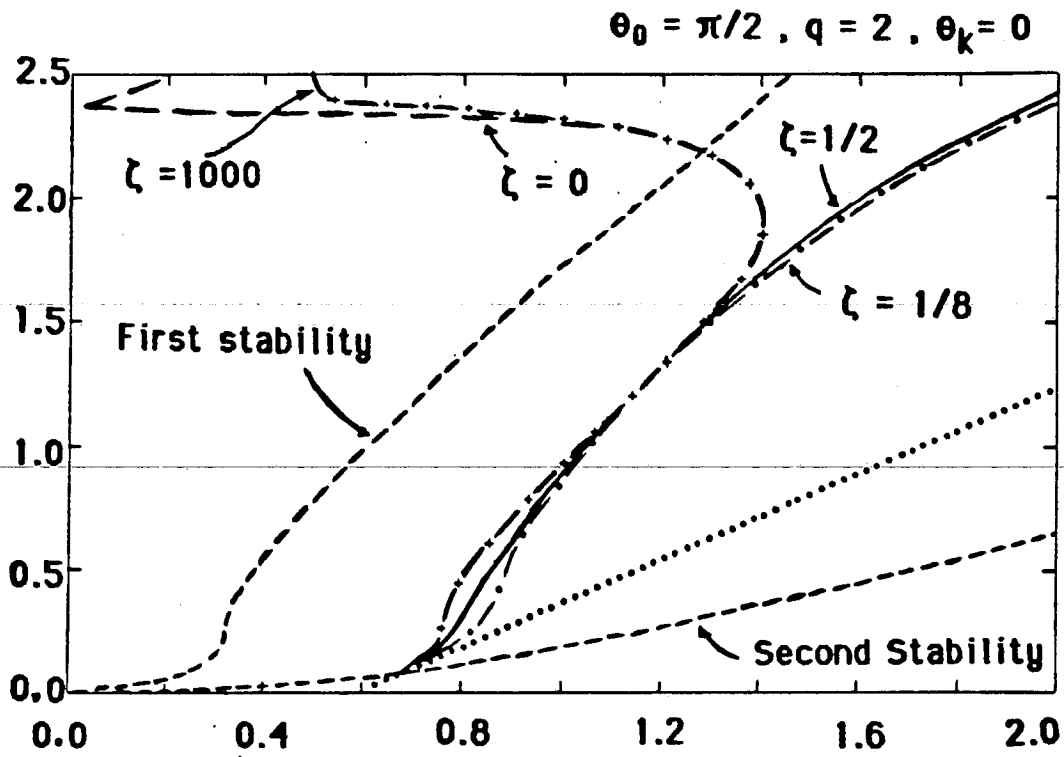


Fig. 2.7 Enlargement of the region inside the small box in Fig. 2.6

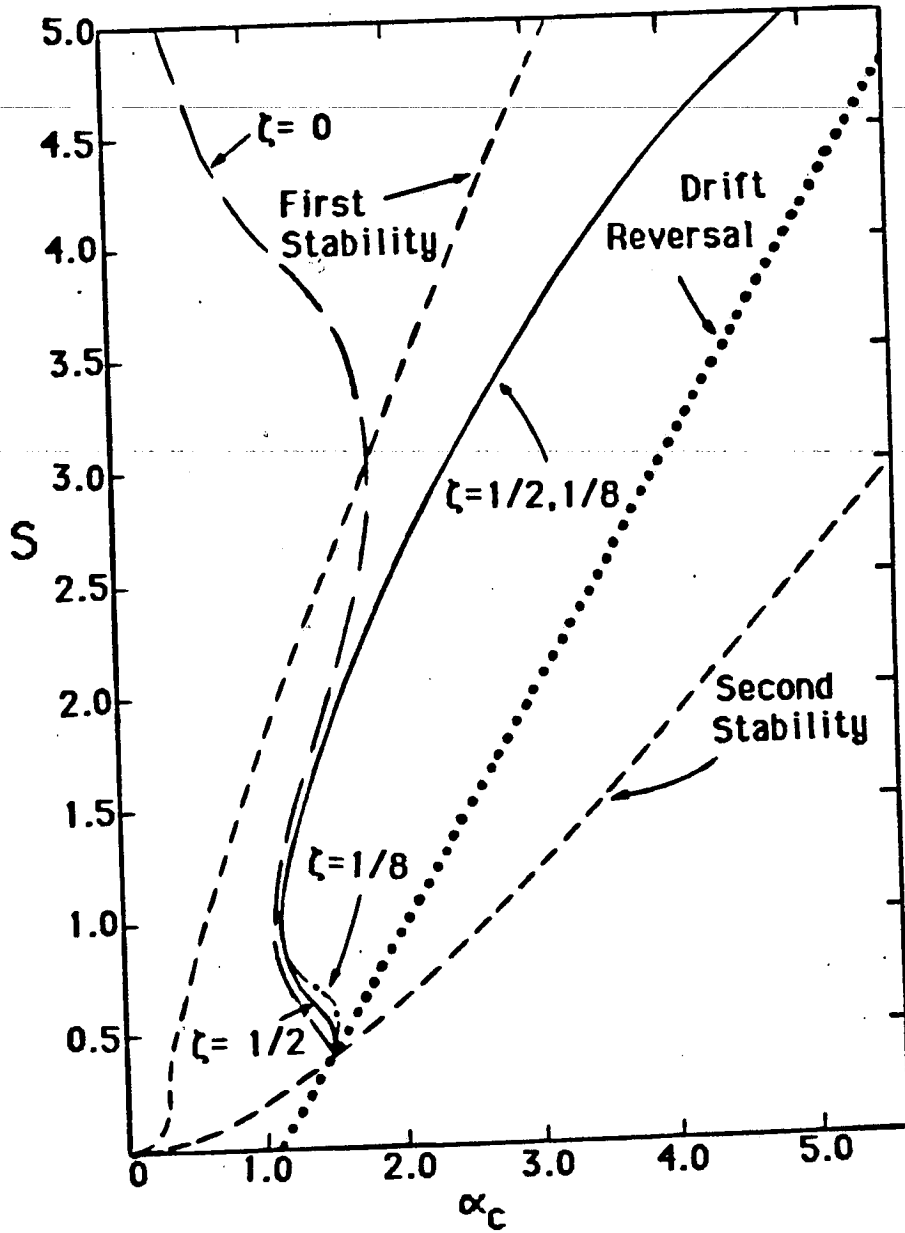


Fig. 2.8 The same as Fig. 2.6 for  $\theta_0 = 3\pi/8$ .

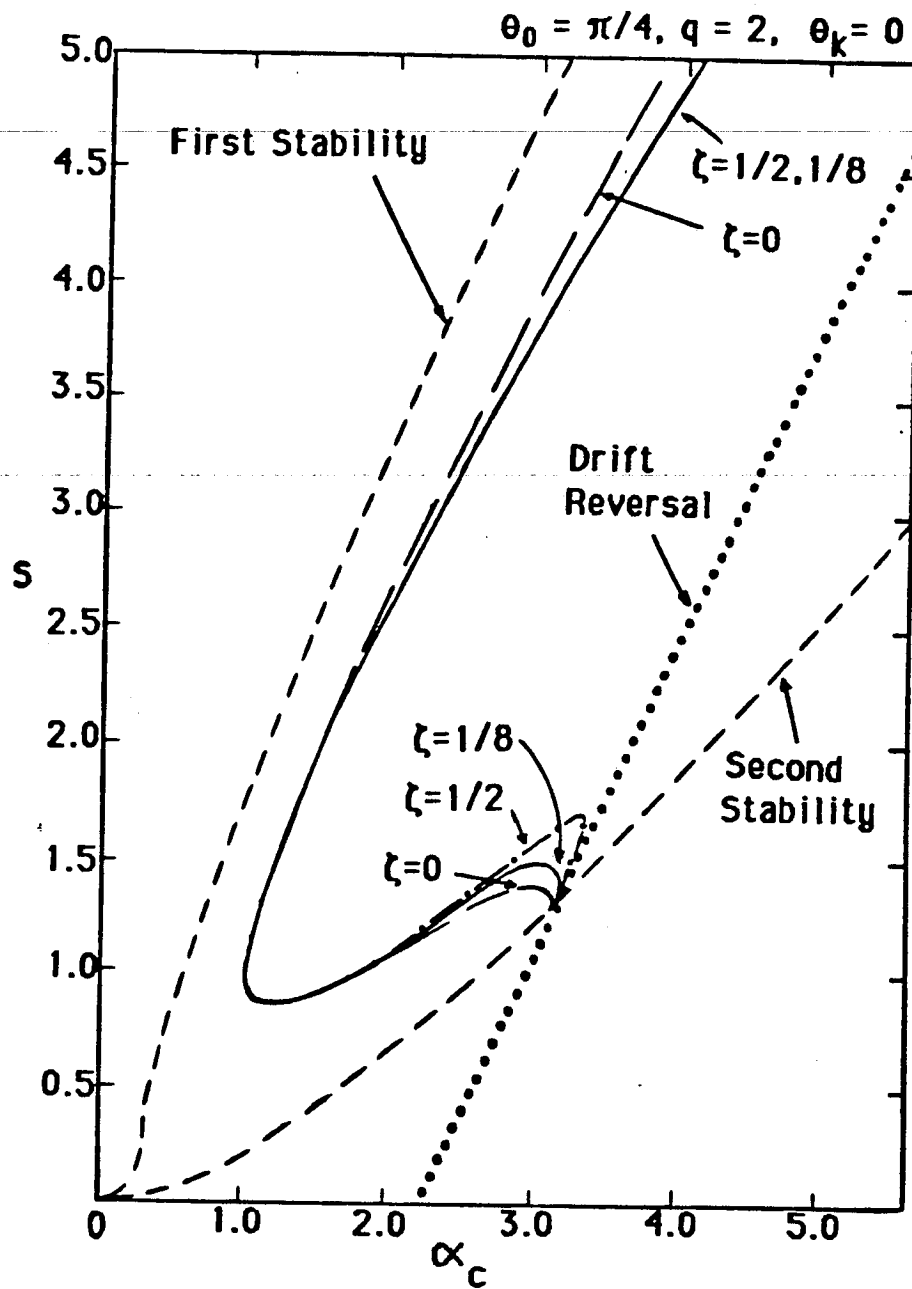


Fig. 2.9 The same as Fig. 2.6 for  $\theta_0 = \pi/4$

in Ref. 11. For large values of  $\zeta$  the weighting function approaches 1 and, thus, the same results as for  $\zeta = 0$  are obtained. The best values were obtained for values of  $\zeta$  around 1/2.

For all of the values of  $\theta_0$  that were considered, it was found that for values of the shear less than 2, the stability boundaries obtained with various values of  $\zeta$  are not much different from the one obtained with  $\zeta = 0$ . For larger values of  $S$ , however, different values of  $\zeta$  do give different stability boundaries.

We have been able to predict analytically the onset of the discrepancy at large  $S$  in the limit of small trapped particle width ( $\theta_0 \ll 1$ ). In this deeply trapped limit we can analytically obtain the even solution of the ballooning equation in the first trapped particle region,  $0 \leq \theta \leq \theta_0$ . The square-top hot particle pressure profile,  $\zeta = 0$ , and  $\theta_k = 0$ , were assumed in this calculation. We obtained  $\Phi$  by using a Taylor series, where the  $n^{\text{th}}$  derivative of  $\Phi$  at zero  $d^n \Phi(0)/d\theta^n$ , was calculated from Eqs. (2.78)-(2.81), as follows. For small  $\theta_0$  and  $\theta$ , we can write  $g(\theta) = \theta [1 - A(\theta_0)/\pi]$ ,  $h(\theta) = \theta u$ , and  $D(\theta) = 1 + \theta^2 d$ .

Here we defined

$$A(\theta_0) = \pi \left[ 1 - \frac{\theta_0^2}{2} \right].$$

$$u = S - \alpha_c - \frac{\alpha_h}{2} \left[ 1 - \frac{A(\theta_0)}{\pi} \right] \quad , \quad \text{and}$$

$$d = S - \alpha_c - \frac{1}{2} - \frac{\alpha_h}{2} \left[ 1 - \frac{A(\theta_0)}{\pi} \right] \quad .$$

Using Eq. (2.80) to obtain the value of  $d^2\Phi_0/d\theta^2$  and the initial conditions to obtain the value of  $\Phi_0$ , we find,

$$\Phi_0 = 1 - \psi_0 \theta^2 \quad ,$$

here

$$\psi_0 = \frac{\left[ \alpha_c + \frac{\alpha_h}{2} \right]}{2}$$

Likewise, from Eq. (2.81) and the initial conditions for  $\Phi_1$ , we obtain

$$\Phi_1 = \frac{\alpha_h}{4} \theta^2 \quad .$$

By using the expressions for  $\Phi_0$  and  $\Phi_1$ , we have

$$\Lambda = \frac{1 + (d - \psi_0) \frac{\theta_0^2}{3}}{\nu} \quad ,$$

With

$$V = 1 - \frac{\alpha_c}{2q^2} + \left[ d - \frac{\alpha_h}{4} \right] \frac{\theta_0^2}{3} .$$

The eigenfunction  $\Phi$  is singular when the denominator  $V$  vanishes. This is the onset for the discrepancy and corresponds to a known degeneracy for integral equations of the Fredholm type.<sup>45</sup> For small  $\theta_0$ , we can write the drift nonreversal condition (2.58) as

$$\alpha_h \leq 2q^2 \left[ 1 - \frac{\alpha_c}{2q^2} + \theta_0^2 \left[ -\frac{1}{4} + \frac{S}{2} - \frac{\alpha_c}{32q^2} - \frac{7\alpha_c}{16} \right] \right] . \quad (2.85)$$

Using the maximum value for  $\alpha_h$  allowed in the inequality (2.85) in the equation for  $V$  we find that  $V$  vanishes when

$$0.876 - 0.157 \alpha_c + 0.044 S = 0 . \quad (2.86)$$

where we used the parameters  $q = 2$  and  $\theta_0 = \pi/8$ . In Fig. (2.10) we have plotted the linear relationship given in Eq. (2.86) with a dotted line. In the same picture we have plotted the stability boundaries without hot particles (dashed lines) and the stability boundary obtained numerically (solid line). The dotted line representing Eq. (2.86) compares fairly well with the onset of the discrepancy at  $S \approx 12$  as displayed in the solid curve.

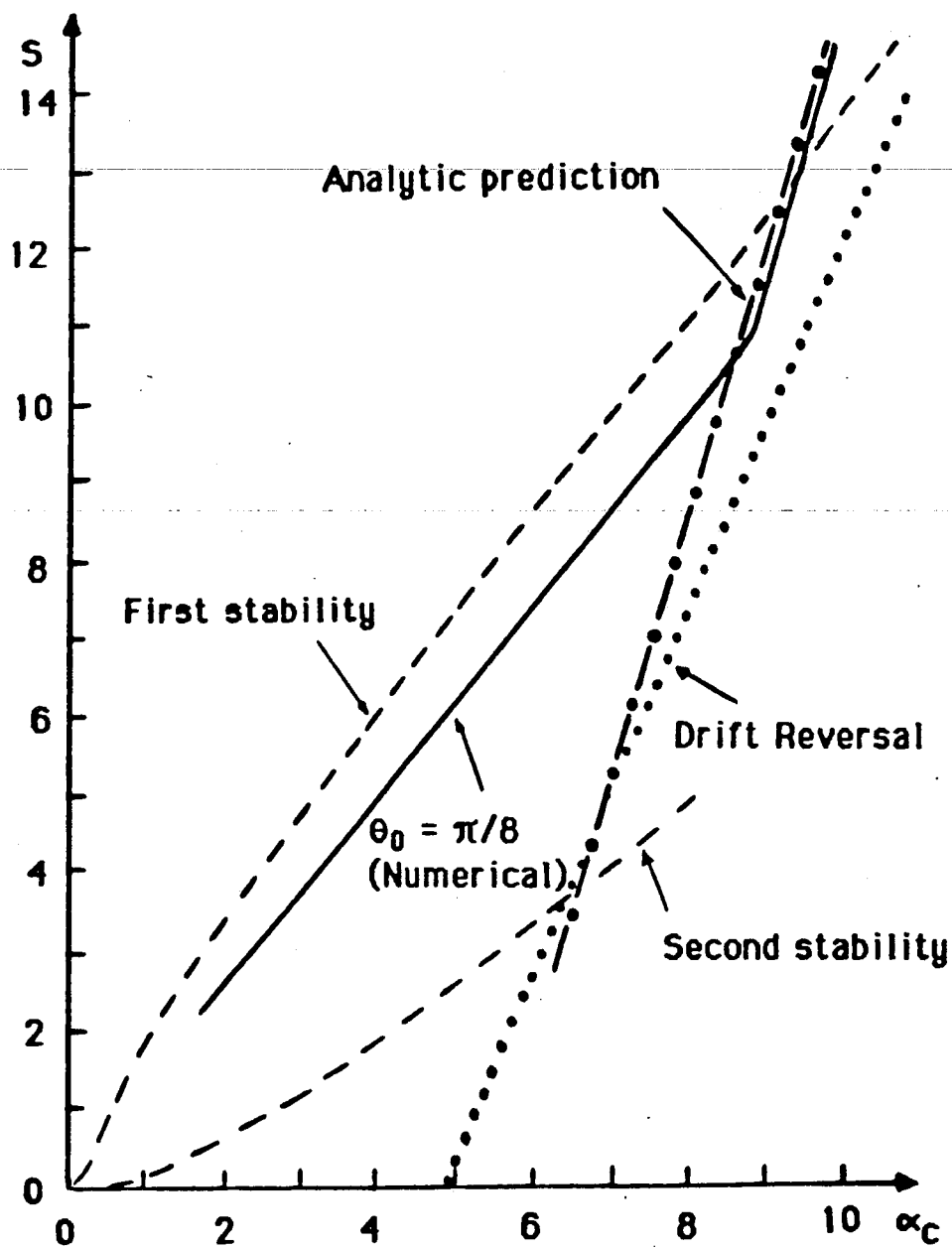


Fig. 2.10 Analytic prediction of discrepancy

for  $\theta_0 = \pi/8$



Notice that when the denominator  $V$  does not vanish, we obtain

$$\Phi(\theta_0) = 1 + \frac{\theta_0^2}{2} \left\{ -\alpha_c - \frac{\alpha_h}{2} + \frac{\alpha_h}{2 \left[ 1 - \frac{\alpha_c}{2q^2} \right]} \right\} + \dots, \quad (2.87)$$

where the first two terms in the curly bracket come from the interchange term and the third term comes from the compressional contribution of the hot particles. Using the maximum value for  $\alpha_h$  allowed by condition (2.85), we obtain

$$\Phi(\theta_0) = 1 - \frac{\alpha_c}{4} \theta_0^2 + O(\theta_0^4). \quad (2.88)$$

Thus, by comparing Eq. (2.88) with Eq. (2.87) for  $\alpha_h = 0$ , we see that when hot particles are introduced the function  $\Phi$  decreases more slowly in the first trapped particle region than in the absence of energetic particles, which implies enhanced stability

## 2.6 STABILITY BOUNDARIES FOR DIFFERENT PROFILES OF THE HOT PARTICLE PRESSURE

In Fig. (2.11) we show the effect on stabilization for various profiles of  $P_{\perp h}$ , with  $\theta_0 = \pi/4$ . The dash-dot line shows the stability boundary for the square profile, the solid line that for a concave profile, and the dash-cross line the results for a convex pressure profile, with its maximum at  $\theta = 0$ . The results show that even when the fluid part of the potential is larger for a concave profile than for one with its maximum at  $\theta = 0$ , the kinetic part is more stabilizing for the second case. We also show in Fig. 2.11 the stability boundary for a smooth hot particle pressure profile (dashed curve).

## 2.7 OFF-ANGLE MODES

The motivation for studying modes that peak off the midplane is to test stability for all possible ballooning modes. We have already stated that the ballooning modes corresponding to marginal stability have the general property of symmetry.

$$\Phi(-\theta, -\theta_k) = \Phi(\theta, \theta_k) .$$

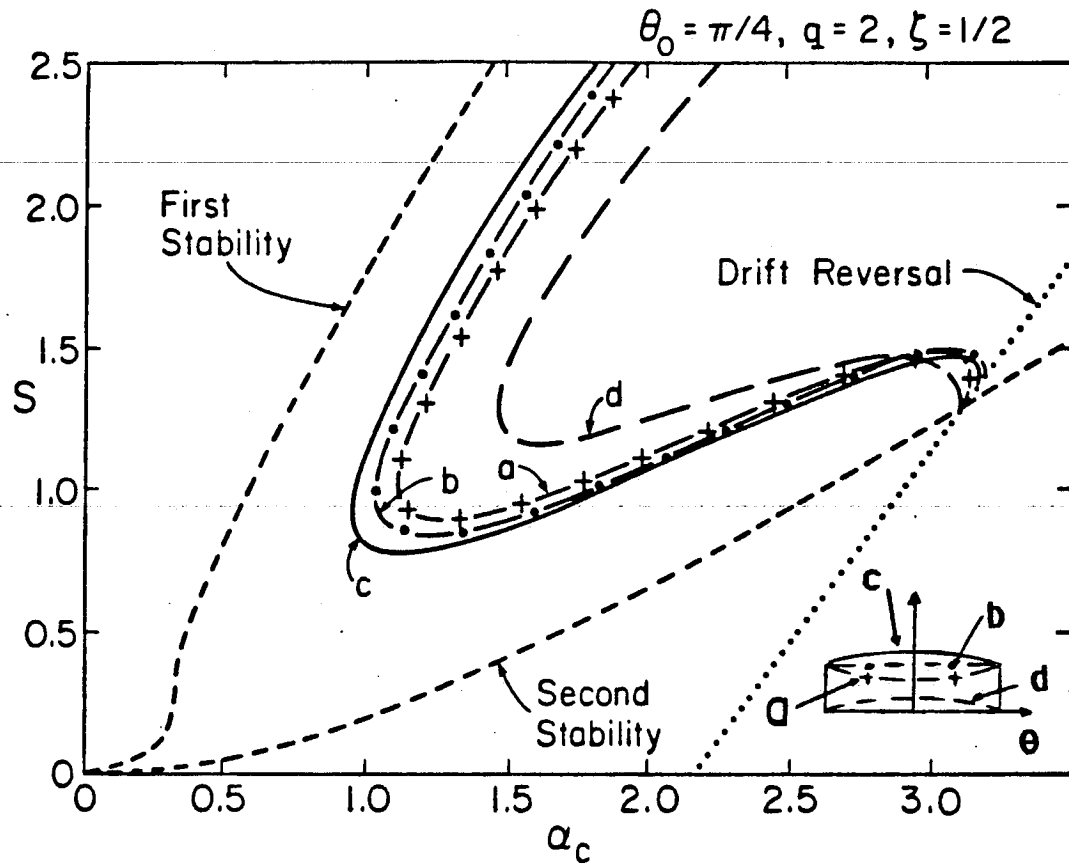


**Fig 2.11 Marginal stability for various profiles with  $\alpha_h$  set equal to the maximum value allowed by drift non-reversal.**

Thus, for  $\theta_k \neq 0$ , they are no longer symmetric about  $\theta = 0$ ; in fact numerical results seem to indicate that they are not even symmetric about the position of the maximum. In Fig. (2.12), we show the stability boundaries for off-angle modes with and without hot particles. The numerical results were obtained for values of the shear  $S$  up to 2.0 and for values of  $\alpha_c$  up to 4.0. When hot particles were considered,  $\theta_0 = \pi/4$ ,  $q = 2$ , and  $\zeta = 0$  were used. For comparison, we plot the curves corresponding to  $\theta_k = 0$  that were already shown in Fig. (2.5). The short dashed lines (-----) are the stability boundaries without hot particles, and the long dashed line (— —) is the stability boundary with hot particles. With the solid line (——) we have plotted the results for  $\theta_k = 3\pi/8$  when hot particles were not present; the stability boundary when they are present is plotted with a dot-dashed line (. \_ . \_ . \_ .).

We see that, without hot particles, there are two stable regions for off-angle modes, in the parameters space of  $S$  and  $\alpha_c$ . When  $\theta_k \neq 0$ , stability is less stringent for first stability, but more stringent for second stability: *i.e.*, at a fixed value for the shear, the marginal  $\alpha_c$  value increases for off-midplane modes. In fact it can be seen in Fig. (2.12) that the second stable region is greatly reduced

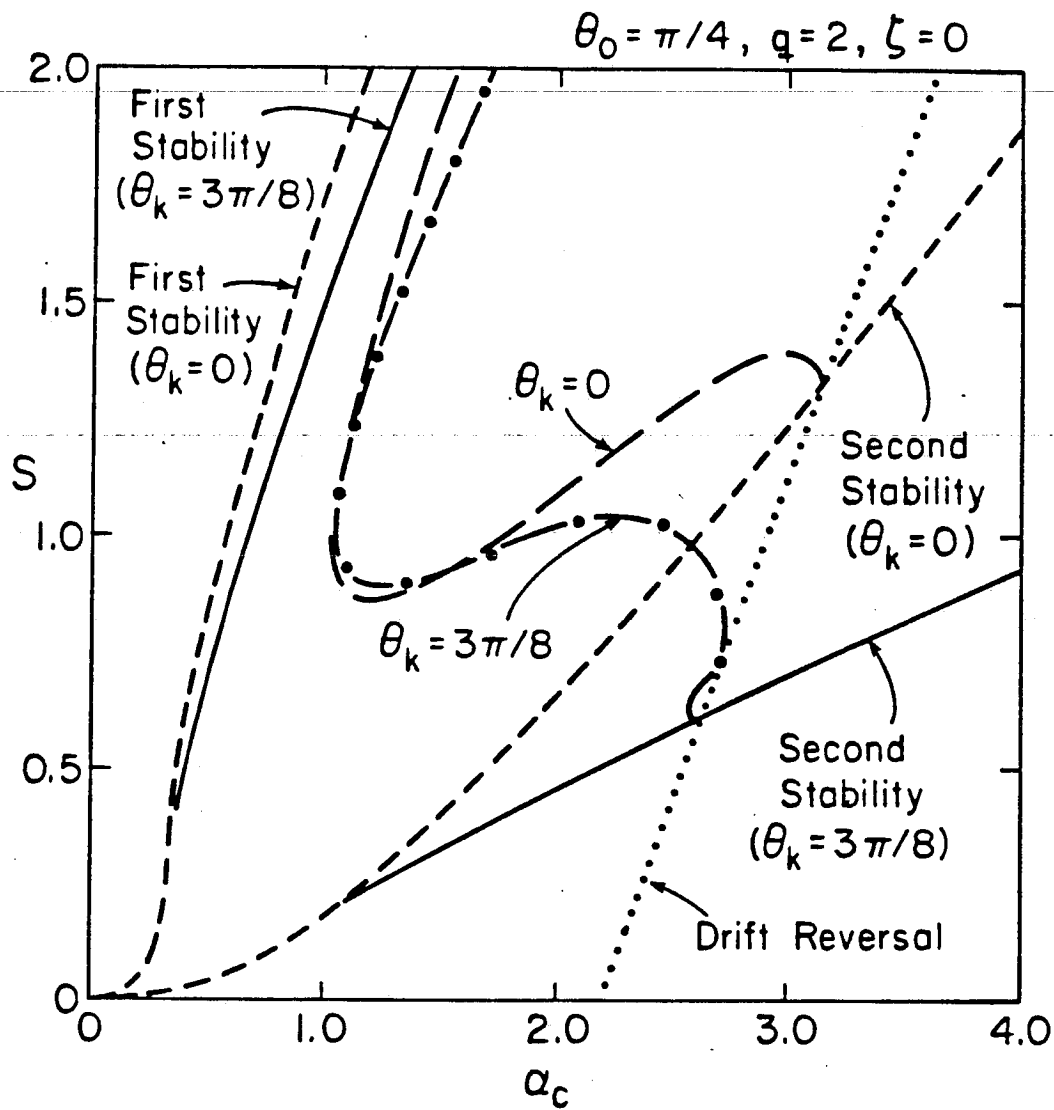


Fig. 2.12 Stability boundaries for  $\theta_k = 0$  and  $\theta_k = 3\pi/8$ ,  
with and without energetic particles

when  $\theta_k$  increases from 0 up to  $3\pi/8$ , without much improvement in the first stable region. For  $\theta_k > 3\pi/8$ , the second stability boundary does not change significantly in comparison with that for  $\theta_k = 3\pi/8$ , but the first stability boundary does, as can be seen in Fig. 2.13, where the stability boundaries for  $\theta_k = 3\pi/8$  and  $\theta_k = \pi/2$  are shown. The hot particles have a strong stabilizing role for these modes, because a large part of the unstable region becomes stable when hot particles are introduced. The "clockwise rotation" of the unstable region in the  $S$  versus  $\alpha_c$  plane is a consequence of the change (as  $\theta_k$  is varied) of the minimum of the canonical potential, which is where the modes corresponding to marginal stability tend to be localized.<sup>2,46</sup> Also the large variation of the second stability boundary when  $\theta_k$  is increased reflects a large change in the geodesic curvature for finite  $\theta_k$ .

## 2.8 CONCLUSIONS

In this chapter we have presented a theoretical description of the physical behavior of non-resonant, non-drift-reversed highly energetic particles in tokamak and of their effect on the stability of

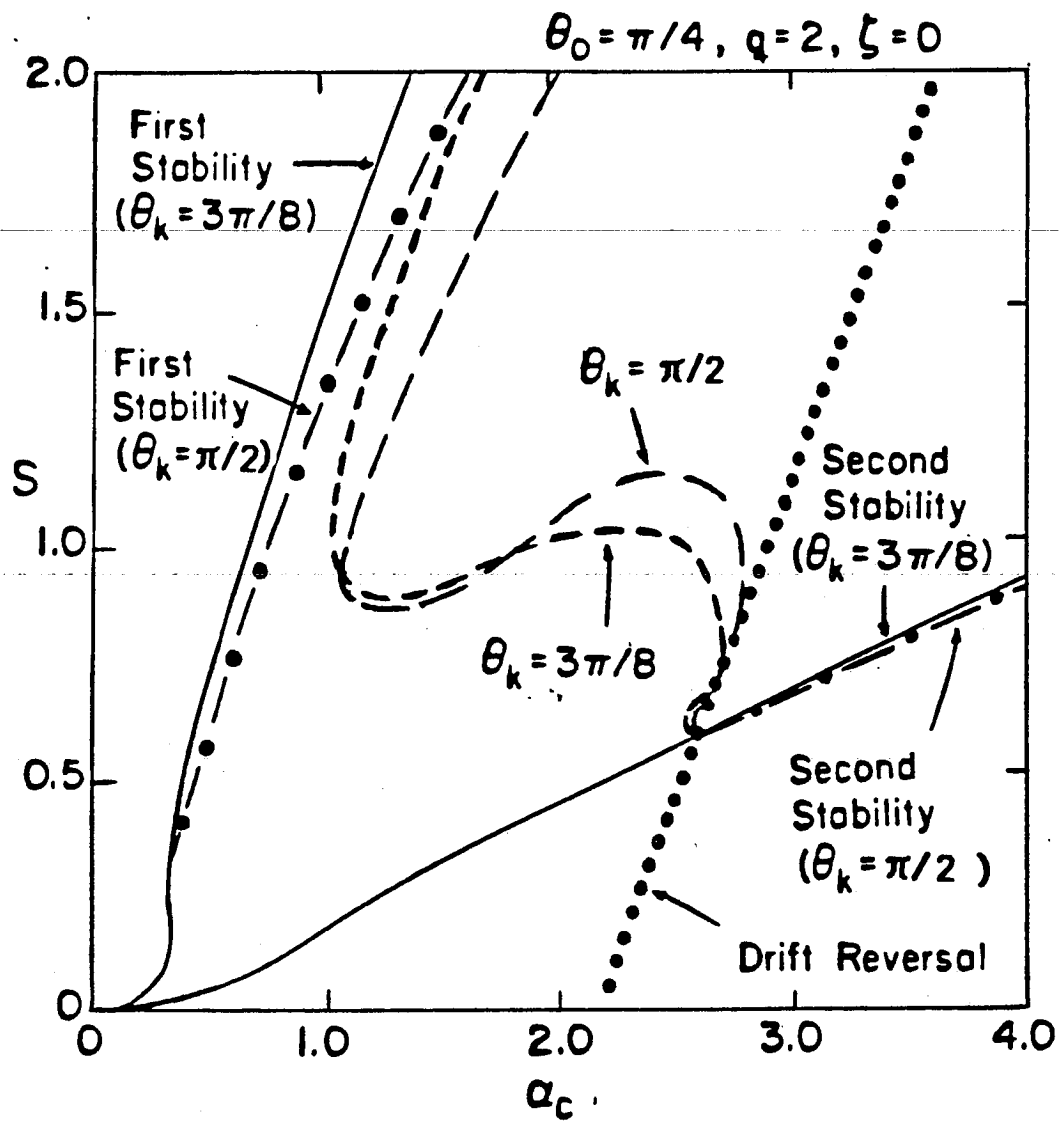


Fig. 2.13 The same as Fig. 2.12, for  $\theta_k = 3\pi/8$

and  $\theta_k = \pi/2$

ideal MHD ballooning modes. We have confirmed in detail the result initially predicted by Rosenbluth *et al.*,<sup>11</sup> that hot particles whose pressure is greater than a threshold value which is roughly comparable to the pressure value of the core plasma are able to completely stabilize the ideal ballooning mode. The significance of this result is that it allows for direct stable access into the high-beta second stability regime of operation.

In elaborating this theory, we noticed that the original stability estimate of Rosenbluth *et al.*, based as it is on a Schwartz inequality approximation for a lower bound to the potential energy, fails at finite shear values, for example, when  $S > 2.4$  for a hot trapped particle halfwidth of  $\pi/2$ . The result from their method is still valid, since their Schwartz method provides a sufficient condition for stability. However, it cannot be taken as a reliable guide to the actual stability boundary, since it indicates that at these higher values for the global shear, the presence of hot particles is destabilizing, whereas the energy principle clearly indicates a purely stabilizing contribution. We have resolved this discrepancy by constructing a better lower bound for marginal stability. This was done by exploiting an additional degree of freedom in the Schwartz inequality. The resulting stability predictions are both more favorable and more reasonable. We conjecture, in fact, that at low shear values,



the Schwartz lower bound is close to the real stability boundary, whereas at the high shear values, it deviates from the actual situation, while the upper bound approaches it. The improved Schwartz lower bound, by means of its internal pitch angle weighting, is able to make the transition from low to finite shear values without significant deviation from the real stability curve.

We also investigated various simple poloidal profiles for the pressure of the energetic species. The simplest of these is the square-top profile that was also used by Rosenbluth *et al.*; formally, this profile has a problem with the mirror anisotropy coefficient  $\tau$  being singular and even negative at the endpoints of the profile, although this isolated singular behavior appears not to affect greatly the global properties of ballooning modes. A smoothed profile that avoids this question was also studied, as well as a concave type of profile with fewer particles on the tokamak midplane than off, although still not drift reversed. Somewhat better stability was predicted for those profiles that peak on the midplane. The reason seems to be that the non-fluid response of highly energetic particles contributes stabilization when the particles are trapped in a region of unfavorable curvature. This behavior is quite contrary to usual MHD dynamics, where bad curvature implies instability, and is a consequence of the hot particles responding not to  $E \times B$  displacements

of the magneto-fluid, but instead responding primarily to variations in the magnetic field strength, which enters through the perturbation of the magnetic gradient-B drift of the hot particles. With this in view, it is clearly preferable to concentrate most of the hot particles where the curvature is worst. The stability results for the various profiles, then, differ slightly according to the value of the line average of the pressure-weighted curvature.

Another point explored numerically in this chapter concerned the detailed structure of the first and second stability boundaries for modes that do not necessarily peak at the tokamak midplane. In a high-mode-number analysis of ballooning modes localized on a single flux surface, the zero in poloidal angle,  $\theta_k$ , of the phase eikonal of perturbed quantities enters as a free parameter. We have numerically explored how the stability boundaries change as this parameter is varied. In general, the stability boundary on the first stability side improves -- *i. e.*, the marginal  $\alpha_c$  value increases, for fixed shear and with  $\alpha_h$  at its maximum value as allowed by the non-drift-reversal condition--, whereas it becomes worse as it approaches the second stability side. A stable avenue from first to second stability still exists, although at lower shear values than for zero  $\theta_k$ .

## CHAPTER III

### RESONANT DESTABILIZATION OF BALLOONING MODES BY ENERGETIC PARTICLES

#### 3.1 INTRODUCTION

In Chap. II it was shown that ideal ballooning modes can be stabilized by the presence of hot particles in a tokamak plasma. The energy of the hot particles must be very high in order to satisfy the nonresonant ( $\overline{\omega}_{dh} \gg \omega$ ) condition of this theory. For example, for reactor parameters, it was pointed out that this condition would require energies on the order of few MeV. Hot particles produced by currently available neutral beam injection or rf heating methods may not be this energetic. Moreover, even if highly energetic particles are created by fusion processes or by other means, they will eventually be slowed down by collisions with the background plasma and have their energy reduced. Also, their pitch angle distribution function will be broadened if the energy is not sufficiently high.<sup>48</sup> Thus it is important to study the interaction of the core plasma with moderately energetic particles, for which the nonresonant decoupling condition is not satisfied.

Indeed, experimental observations on the PDX tokamak seem to indicate that, for certain parameters, beam-injected hot ions are able to excite ideal ballooning modes through wave-particle resonant interaction with the plasma at the beam ion magnetic curvature drift frequency.<sup>5,47</sup> Fig. 3.1 reproduces the experimental results, presented in Ref. 47, for the excitation of MHD modes when moderately energetic ions were introduced into the PDX tokamak with nearly perpendicular injection. The excitations were recorded as time-varying fluctuations in the poloidal magnetic field, as measured with a Mirnov loop diagnostic during the process of heating the plasma. In the observed oscillations, it was possible to distinguish two modes with different frequencies. The dominant mode usually occurred at a frequency of 15-20 KHZ. There was also a higher-frequency "precursor" mode at frequencies of around 80-100 KHZ. The lower-frequency oscillations were dubbed "fishbone oscillations" on account of the shape of their Mirnov signal and were later interpreted by Chen *et al.*<sup>25</sup> as beam-ion-induced excitations of the  $m=n=1$  internal kink mode. The higher frequency precursor oscillations also had the fishbone feature that the oscillation frequency was close to the curvature drift frequency of the beam ions,  $\omega \approx \bar{\omega}_{dh}$ . In fact, the ratio of the precursor frequency to the frequency of the  $n=1$  fishbones was close to the measured toroidal mode number  $n=4-6$  of the precursor. However, the high-frequency oscillations tended to

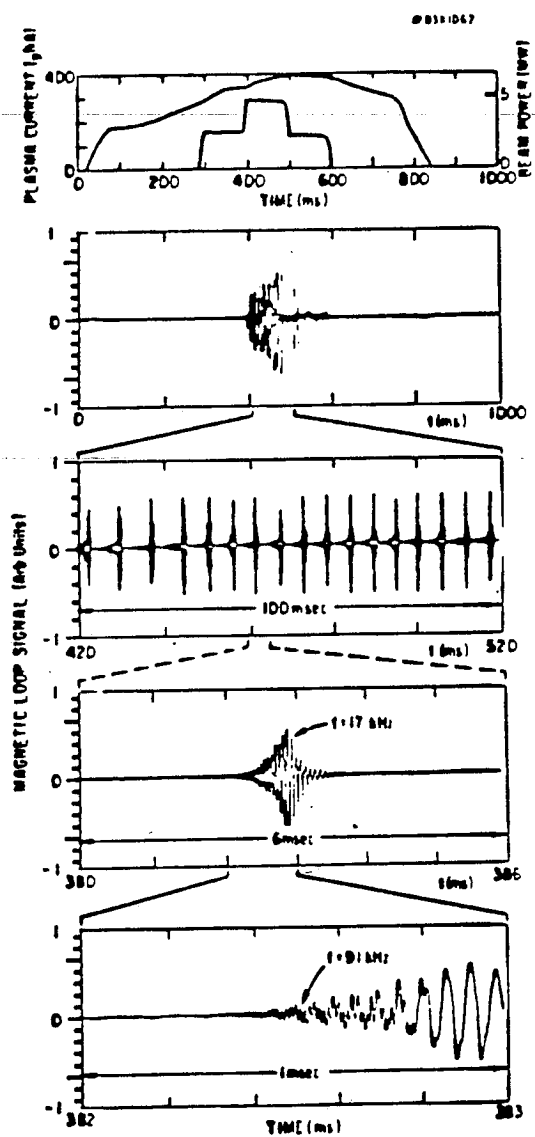


Fig. 3.1 Observations of MHD modes excited by energetic particles by K. Mc Guirre, *et al.*<sup>47</sup> in the PDX tokamak

occur at beam heating powers higher than the threshold power level for fishbones. Noting that this and other features of the precursor are suggestive of ballooning modes, Weiland and Chen<sup>27</sup> proposed to explain these excitations as MHD ballooning modes excited by trapped hot ions. Their theory for these "balloon-bone" oscillations was developed in the limit of weak shear and rather low beta values for the beam ions.

In this chapter we present a complimentary description of how ideal MHD ballooning modes can be resonantly destabilized by energetic trapped particles. Our theory is both analytical and numerical and seeks to describe the "balloon-bone" oscillations for finite shear and beta values. We also obtain the effect of varying either the trapped ion pressure or the core plasma pressure. The development of our theoretical investigation may be summarized as follows. We start our study of the "balloon-bone" oscillations from the quadratic form for the ideal, linear, high-mode-number equations that the electromagnetic perturbed fields satisfy.<sup>14,38</sup> The quadratic form can be divided into a fluid potential and a non-local kinetic part. The resonant response of the plasma at the drift frequency of the hot particles occurs in this non-local part. Certain approximations are then adopted to make the problem analytically tractable. One of these approximations is to use a delta-function model in order to

localize the resonant response of the energetic particles at the center of their trapped region. The exact form for the frequency dependence of the resonant term is calculated for a slowing-down energy distribution function. An integro-differential ballooning mode equation is then obtained that contains the spatially localized resonant response, along with the inertial response of the plasma. We shall take the ratio  $\omega_{dh}/\omega_A$  to be small compared to unity. This assumption is consistent with our consideration of only moderately energetic hot particles (since  $\omega_{dh}/\omega_A \propto T_h$ ). It is also consistent with the measured parameters for the PDX experiment that observed the fishbone oscillations and the high frequency precursor fluctuations.

We note that  $\omega \simeq \omega_{dh} \ll \omega_A$  implies that the plasma pressure is nonnegligible to the degree that the shear Alfvén-ballooning mode frequency is much below the Alfvén frequency:  $\omega \ll \omega_A$ . The high frequency MHD spectrum therefore remains intact when  $\omega_{dh}/\omega_A$  is small. Since the typical frequency for MHD ballooning modes is much lower than the Alfvén frequency, we may take  $\omega/\omega_A \sim \omega_{dh}/\omega_A \ll 1$ , so that the inertial term is unimportant except at large values of  $S\theta$ . Thus we can divide the field line into two regions: an inner region ( $S\theta \sim 1$ ) in which the inertial response is not important, and an outer inertial region  $S\theta \gg 1$  in which that term is important. We

numerically solve the integro-differential equation in the inner region and fit the results to an analytically derived asymptotic form for the wave function. In the outer region, a similar two-space-scale analysis leads to the inertial solution, which, when asymptotically matched to the inner MHD solution, yields a dispersion relation for the complex frequency  $\omega$ . The marginal stability boundaries are then obtained by a Nyquist analysis of this dispersion relation. The window in parameter space for stable operation with respect to the "balloon-bone" modes is finally presented.

This chapter is divided into 7 parts. In Sec 3.2 , we briefly review the assumptions. In Sec. 3.3, we obtain the ballooning mode equation, which is then solved in Sec. 3.4. In Sec. 3.5 we present the numerical results, and in Sec. 3.6 we derive some approximate analytical stability conditions. Finally, in Sec. 3.7 , we give our conclusions.

### 3.2 ASSUMPTIONS

We review some of the assumptions already explained in Chapter II. We consider energetic particles that are mirror confined on the unfavorable-curvature outer side of the tokamak. We also suppose that the population of hot particles is fairly anisotropic,



$P_{th}/P_{ch} < 1$ . We will consider the energetic particle beta and the core plasma beta to be comparable,  $\alpha_h \sim \alpha_c$ . (Note that in Ref. 30  $\alpha_h/\alpha_c \sim 0(\epsilon)$  was taken, where  $\epsilon \ll 1$  is the inverse aspect ratio.) Also, throughout this chapter, we will consider the square hot particle pressure profile of Eq. (2.18) with  $\eta=0$ . We want to investigate the stability of MHD-like modes (hence, finite parallel electric field effects are ignored) in the large-mode-number eikonal limit. The ballooning representation will be needed for the perturbed quantities, and finite Larmor radius and finite banana width effects will be neglected. Finally, we are interested in modes with frequencies  $\omega_{*i} < \omega \cong \omega_{dh} < \omega_{*h}$ , where  $\omega_{dh}$  and  $\omega_{*h}$  are the magnetic gradient-B and diamagnetic drift frequencies for the hot species and  $\omega_{*i}$  is the background ion diamagnetic frequency. Other assumptions and approximations will be explained in the course of the theoretical development to follow.

### 3.3 BALLOONING MODE EQUATION

#### 3.3.a QUADRATIC FORM AND THE BALLOONING MODE EQUATION

We obtain the ballooning mode equation beginning from the quadratic form for the equations of motion, with the hot species in the high bounce frequency limit: <sup>14,38</sup>

$$\delta W_f + \delta W_k + \delta I = 0 \quad (3.1)$$

Here,  $\delta W_f$  is the fluid part of the energy:

$$\delta W_f = \frac{1}{2} \int \frac{d\ell}{B} \left[ \frac{|\nabla S|^2}{B^2} |B \cdot \nabla \phi|^2 + |Q_{\parallel} - B \mathbf{e} \cdot \boldsymbol{\kappa} \phi|^2 - \mathbf{e} \cdot \boldsymbol{\kappa} \left[ \mathbf{e} \cdot \tilde{\nabla} P_{\parallel} + \frac{\sigma}{\tau} \mathbf{e} \cdot \tilde{\nabla} P_{\perp} \right] |\phi|^2 \right] \quad (3.2)$$

In Eq. (3.2),  $\phi$  is the perturbed electrostatic potential (the equilibrium electrostatic potential is assumed to be zero),  $Q_{\parallel}$  is the Lagrangian magnetic field perturbation parallel to the magnetic field,  $\mathbf{e} = \mathbf{B} \times \nabla S / B^2$ , and  $\tilde{\nabla} = \nabla - (\nabla B) \partial / \partial B$ . We are using the ballooning representation where  $S$  is the eikonal phase for the perturbed field quantities. The first term on the right-hand side of Eq. (3.2) is the stabilizing bending part of the fluid potential, the second one is the magnetic compressional term, and the last one is the destabilizing interchange free energy term. The kinetic part of the energy,  $\delta W_k$ , is given by

$$\delta W_k = \frac{-1}{2} \int \frac{d\ell}{B} \int dE d\mu \frac{B}{V_{\parallel}} \left[ \frac{\omega - \omega_{*h}}{\omega - \bar{\omega}_{dh}} \right] \frac{\partial F_h}{\partial E} \left[ \frac{\mu Q_{\parallel} + V_{\parallel}^2 \mathbf{e} \cdot \boldsymbol{\kappa} \phi}{\mu Q_{\parallel} + V_{\parallel}^2} \right]^2 \quad (3.3)$$

and involves an integration over velocity space quantities. The inertial energy,  $\delta I$ , is given by

$$\delta I = \left( \frac{1}{2} \right) \omega^2 \int \frac{d\ell}{B} \frac{|\nabla S|^2}{V_A^2} \phi^2 . \quad (3.4)$$

We can split  $\delta W_k$  into two pieces, one independent of  $\omega$  and another one containing the resonant dependence on  $\omega - \bar{\omega}_{dh}$ , as follows:

$$\delta W_k = \left( \frac{1}{2} \right) \int \frac{d\ell}{B} \int dE d\mu \left[ \frac{B}{V_I} \right] \left[ \frac{\omega_{*h}}{\omega_{dh}} - \frac{\omega}{(\omega - \bar{\omega}_{dh})} \times \right. \\ \left. \frac{(\omega_{*h} - \bar{\omega}_{dh})}{\omega_{dh}} \right] \frac{\partial F_h}{\partial E} \left\{ \frac{\mu Q_i + V_i^2 \mathbf{e} \cdot \mathbf{x} \phi}{\omega_{dh}} \right\}^2 . \quad (3.5)$$

The first term in the square parenthesis is the zero-frequency part of the kinetic potential energy, and the second is the finite frequency resonant part.

In order to make progress in our semi-analytical treatment we use a Schwartz inequality to estimate the zero frequency part of  $\delta W_k$ , which is then combined with  $\delta W_f$ . In the finite-frequency resonant part of  $\delta W_k$ , we make the following low beta approximation for the magnetic field

$$Q_1 \cong B \mathbf{e} \cdot \mathbf{x} \phi \quad (3.6)$$

Also, in the resonant part of  $\delta W_k$ , we assume that the energetic particles are deeply trapped, so that

$$\overline{(\mu B + V_1^2) \mathbf{e} \cdot \mathbf{x} \phi(\theta)} \cong \phi(\theta_n) \overline{(\mu B + V_1^2) \mathbf{e} \cdot \mathbf{x}} \quad (3.7)$$

Here,  $\theta_n = 2\pi n$  is the center of the  $n^{\text{th}}$  trapped particle interval. Using the Euler-Lagrange equations for the quadratic form (3.1), we now obtain the following equation for  $\phi$ :

$$\begin{aligned} B \cdot \nabla \left[ \frac{\sigma |\nabla S|^2}{B^2} B \cdot \nabla \phi \right] + \frac{\rho \omega^2}{B^2} |\nabla S|^2 \phi + \mathbf{e} \cdot \mathbf{x} \left[ \mathbf{e} \cdot \nabla P_{\parallel} + \frac{\sigma}{\tau} \mathbf{e} \cdot \nabla P_{\perp} \right] \phi \\ + R(\theta) = (\mathbf{e} \cdot \mathbf{x}) \left[ \mathbf{e} \cdot \nabla P_{\parallel h} + \frac{\sigma}{\tau} \mathbf{e} \cdot \nabla P_{\perp h} \right] \Lambda \end{aligned} \quad (3.8)$$

where

$$\begin{aligned} R(\theta) = \mathbf{e} \cdot \mathbf{x} \phi(\theta_n) \int \frac{dE d\mu}{V_1} \left[ \frac{\omega_{dh} - \omega_{*h}}{\omega_{dh}} \right] \left[ \frac{\omega}{\omega - \bar{\omega}_{dh}} \right] \times \\ \left[ \frac{\partial F_h}{\partial E} \right] \overline{(\mu B + V_1^2) \mathbf{e} \cdot \mathbf{x}} \quad (3.9) \end{aligned}$$

The first term on the left hand-side of Eq. (3.8) comes from the bending term in the fluid potential, the second one from the inertial term, the third one comes from the interchange term, and the fourth comes from the finite-frequency resonant part of the kinetic part of the energy. On the right-hand side appears the compressional term due only to the trapped hot particles.

We now assume that the effect of the resonant term in the ballooning equation can be localized to the center of the  $n^{\text{th}}$  trapped particle region at  $\theta = \theta_n$  as follows:

$$R(\theta) \rightarrow \sum_n \Phi(\theta_n) \delta(\theta - \theta_n) \left[ \frac{1}{2\theta_0} \right] \int_{\theta_n - \theta_0}^{\theta_n + \theta_0} d\theta R(\theta) = T(\omega) \sum_n \delta(\theta - \theta_n) \Phi(\theta_n) \quad (3.10)$$

where  $2\theta_0$  is the width of the trapped particle interval.

We now use our model equilibrium and the ballooning representation<sup>37</sup> to rewrite Eq. (3.8) as

$$\frac{d}{d\theta} \left[ 1 + h^2(\theta) \right] \frac{d}{d\theta} \Phi(\theta) + \Omega^2 \left[ 1 + h^2(\theta) \right] \Phi(\theta) + \sum_n \delta(\theta - 2\pi n) \Phi(2\pi n) \times$$

$$T(\omega) + \left[ \alpha_c + \left[ \frac{\alpha_h}{2} \right] H(\theta) \right] D(\theta) \Phi(\theta) = \left[ \frac{\alpha_h}{2} \right] H(\theta) D(\theta) \Lambda^{(n)} \quad (3.11)$$

Eq. (3.11) will serve as our basic equation to study the "balloon bone" modes. The various quantities in Eq. (3.11) are defined as follows. Corresponding to the square-top hot particle pressure profile, we have

$$h(\theta) = S\theta - \alpha_c \sin\theta - \left[ \frac{\alpha_h}{2} \right] g(\tilde{\theta}) \quad (3.12)$$

where, from Eq. (2.40),

$$g(\tilde{\theta}) = \begin{cases} - \left[ 1 + \frac{\tilde{\theta}}{\pi} \right] \left[ \sin\theta_0 - \theta_0 \cos\theta_0 \right], & -\pi \leq \tilde{\theta} \leq -\theta_0 \\ \sin\tilde{\theta} - \left[ \frac{\tilde{\theta}}{\pi} \right] \left[ \sin\theta_0 + (\pi - \theta_0) \cos\theta_0 \right], & |\tilde{\theta}| \leq \theta_0 \\ \left[ 1 - \frac{\tilde{\theta}}{\pi} \right] \left[ \sin\theta_0 - \theta_0 \cos\theta_0 \right], & \theta_0 \leq \tilde{\theta} \leq \pi \end{cases} \quad (3.13)$$

Here,  $\tilde{\theta}$  is  $\theta$  modulo  $2\pi$ , such that  $|\tilde{\theta}| \leq \pi$ . Furthermore, as in Chap. II, we use  $D(\theta) = \cos\theta + h(\theta) \sin\theta$ . The function  $H = H(\theta_0 - |\theta - 2n\pi|)$  is the Heaviside function, representing the functional form of the hot particle pressure profile in  $\theta$ :

$$H(\theta) = \begin{cases} 1 & , \quad 2\pi n - \theta_0 \leq \theta \leq 2\pi n + \theta_0 , \quad \text{integer } n \\ 0 & , \quad \text{elsewhere} \end{cases} \quad (3.14)$$

The integral term in Eq. (3.11) is the same as in Chap. II for an unweighted Schwartz inequality, viz. ,

$$\Lambda^{(n)} = \frac{\int_{2\pi n - \theta_0}^{2\pi n + \theta_0} D(\theta) \Phi(\theta) d\theta}{\int_{2\pi n - \theta_0}^{2\pi n + \theta_0} \left[ D(\theta) - \frac{\alpha_c}{2q^2} \right] d\theta} \quad (3.15)$$

The inertial term in Eq. (3.11) involves the normalized frequency  $\Omega = \omega / \omega_A$  , where  $\omega_A = V_A / qR$  is the Alfvén frequency. Finally, the quantity  $T(\omega)$  in Eq. (3.11), which represents the resonant trapped particle response, is given (for  $\bar{\omega}_{dh} / \omega_{*h} \ll 1$ ) by

$$T(\omega) = - \left[ \frac{q^2}{B_T^2} \right] \int_{2\pi n - \theta_0}^{2\pi n + \theta_0} d\theta' D(\theta') \int d\Gamma \mu B \frac{\partial F_h}{\partial r} \left[ \frac{\omega}{\omega - \bar{\omega}_{dh}} \right] \quad (3.16)$$

### 3.3.b FORM OF THE RESONANT TERM FOR A SLOWING-DOWN ENERGY DISTRIBUTION FUNCTION

We now calculate the explicit form for  $T(\omega)$ , using a slowing-down type of energy distribution for the hot particles,

$$f(E, \lambda) = n_0 E^{-3/2} H(E_m - E) \frac{\lambda^{5/2}}{\sqrt{B_0 - \lambda}} H(B_0 - \lambda) \quad (3.17)$$

where  $E_m$  is the maximum energy (*i.e.*, injection energy) of the hot particles and the dependence on  $\lambda = E/\mu$  is taken from Eq. (2.52) with  $\eta = 0$ . Then we can write Eq. (3.16) for  $T(\omega)$  as

$$T(\omega) = \frac{\alpha_h}{2\pi} \int_{-\theta_0}^{\theta_0} d\theta D(\theta) \int_0^{E_m} \frac{dE}{E_m} \int_B^{B_0} d\lambda \frac{1}{\sqrt{\lambda - B} \sqrt{B_0 - \lambda}} \left[ \frac{\omega}{\omega - \bar{\omega}_{dh}} \right] \quad (3.18)$$

Since  $B(\theta)$  is even, we can let

$$\int_{-\theta_0}^{\theta_0} d\theta \rightarrow 2 \int_0^{\theta_0} d\theta$$

We recall that the hot particle bounce-averaged drift frequency is given by



$$\bar{\omega}_{dh} = \frac{\int_{tr} \frac{d\ell}{V_i} \omega_{dh}}{\int_{tr} \frac{d\ell}{V_i}}$$

where the integrals are over the trapped particle region. Thus

$$\bar{\omega}_{dh} \cong \frac{\int_0^{\theta_0} \frac{d\theta}{\sqrt{\cos\theta - \cos\theta_0}} D(\theta)}{\int_0^{\theta_0} \frac{d\theta}{\sqrt{\cos\theta - \cos\theta_0}}} \left[ \frac{c}{q_h} \right] (\mu B_0) \left[ -\frac{qn}{rRB_T} \right] \quad (3.19)$$

For  $\theta_0 \ll 1$ , we approximate  $D(\theta) \cong \cos\theta$ . (The other terms could be handled but we ignore them for simplicity.) Then we find

$$\bar{\omega}_{dh} \cong \left[ \frac{c}{q_h} \right] (\mu B_0) \left[ -\frac{qn}{rRB_T} \right] \left[ \frac{2E(k_0^2)}{K(k_0^2)} - 1 \right] = \left[ \frac{E}{E_m} \right] \left[ \frac{B_0}{\lambda} \right] \bar{\omega}_{dm} \quad (3.20)$$

Here,  $k_0 = \sin(\theta_0/2)$ ;  $K$  and  $E$  are the complete elliptic integrals of the first and second kinds; and  $\bar{\omega}_{dm}$  is the magnetic precessional drift

frequency evaluated at the maximum energy  $E_m$  and at the pitch angle that corresponds to the turning point  $\theta_0$ :

$$\bar{\omega}_{dm} = \frac{cE_m}{q_h B_0} \left[ -\frac{qn}{rR} \right] \left[ \frac{2E}{K} - 1 \right]. \quad (3.21)$$

We can do the energy integral to obtain

$$T(\omega) = -\frac{\alpha_h}{\pi} \int_0^{\theta_0} d\theta D(\theta) \int_B^{B_0} d\lambda \frac{1}{\sqrt{\lambda-B} \sqrt{B-\lambda}} \times$$

$$\left[ \frac{\omega}{\bar{\omega}_{dm}} \right] \left[ \frac{\lambda}{B_0} \right] \ln \left[ 1 - \frac{\bar{\omega}_{dm} B_0}{\omega \lambda} \right] \quad (3.22)$$

Defining  $x = \lambda/B_0$ ,  $W = \omega/\bar{\omega}_{dm}$ , and  $b(\theta) = B/B_0$ , we obtain

$$T(W) = -\frac{\alpha_h}{\pi} \int_0^{\theta_0} d\theta D(\theta) \int_b^1 dx \frac{x}{\sqrt{x-b} \sqrt{1-x}} W \ln \left[ 1 - \frac{1}{xW} \right] \quad (3.23)$$

Now we change variables  $d\theta = (d\theta/db) db$  and then reverse the order of integrations. Note that for small  $\theta_0$ , we have

$$b = \frac{1 - \varepsilon \cos\theta}{1 - \varepsilon \cos\theta_0} \cong 1 - \varepsilon \left[ \cos\theta - \cos\theta_0 \right]$$

and

$$\frac{db}{d\theta} = \varepsilon \sin\theta = \varepsilon \sqrt{1 - [\cos\theta_0 + (1-b)/\varepsilon]^2} \cong \varepsilon \sqrt{2(1 - \cos\theta_0) - (2/\varepsilon)(1-b)}$$

$$= \sqrt{2\varepsilon} \sqrt{b - b_{\min}} \quad (3.24)$$

Hence we find that

$$\int_b^{\theta_0} d\theta \int_{b(\theta)}^1 dx = \int_{b_{\min}}^1 \frac{db}{\varepsilon \sqrt{1 - [\cos\theta_0 + (1-b)/\varepsilon]^2}} \int_b^1 dx$$

$$= \int_{b_{\min}}^1 dx \int_{b_{\min}}^x \frac{db}{\varepsilon \sqrt{1 - [\cos\theta_0 + (1-b)/\varepsilon]^2}} \quad (3.25)$$

Therefore, we obtain

$$T(W) = -\frac{\alpha_h}{\pi} \int_{b_{\min}}^1 dx \frac{x}{\sqrt{1-x}} W \ln \left[ 1 - \frac{1}{xW} \right] x$$

$$\int_{b_{\min}}^x \left[ \frac{db}{\epsilon} \right] \frac{D[\theta(b)]}{\sqrt{x-b} \sqrt{1 - [\cos\theta_0 + (1-b)/\epsilon]^2}} \quad (3.26)$$

For small  $\epsilon \ll 1$ , the range of integration for  $b$  is tiny, and we can approximate  $D(\theta) \cong 1$ . We change variables to

$$u = \sqrt{x-b}, \quad \frac{du}{db} = -\frac{1}{2\sqrt{x-b}}, \quad \frac{db}{\sqrt{x-b}} = -2du$$

and rewrite  $T(w)$  as

$$T(w) = -\frac{\alpha_h}{\pi} \int_{b_{\min}}^1 dx \frac{xw}{\sqrt{1-x}} \ln \left[ 1 - \frac{1}{xw} \right] \sqrt{2/\epsilon} x$$

$$\int_0^1 d \left[ \frac{u}{\sqrt{x-b_{\min}}} \right] \frac{1}{\left\{ 1 - \left[ \frac{u}{\sqrt{x-b_{\min}}} \right]^2 \right\}^{\frac{1}{2}}} \quad (3.27)$$

The second integral on the right side of Eq. (3.27) is equal to  $\pi/2$ .

Therefore

$$T(w) = -\frac{\alpha_h}{2} \sqrt{2/\epsilon} \int_{b_{\min}}^1 dx \frac{xw}{\sqrt{1-x}} \ln \left[ 1 - \frac{1}{xw} \right] = -\frac{\alpha_h}{2} \sqrt{2/\epsilon} I(w). \quad (3.28)$$

We write  $b_{\min} = 1 - \delta$ , where  $\delta = \varepsilon(1 - \cos\theta_0) \cong \varepsilon(\theta_0^2/2)$  for  $\theta_0 \ll 1$ .

We now investigate the remaining integral in Eq. (3.28):

$$\begin{aligned}
 I(W) &= \int_{1-\delta}^1 dx \frac{xW}{\sqrt{1-x}} \ln \left[ 1 - \frac{1}{xW} \right] \\
 &\cong \int_{1-\delta}^1 dx \frac{W}{\sqrt{1-x}} \left[ \ln \left[ x - \frac{1}{W} \right] - \ln x \right] \\
 &= W \int_0^\delta dt \frac{1}{\sqrt{t}} \ln(q-t) - W \int_{1-\delta}^1 dx \frac{\ln x}{\sqrt{1-x}} \quad (3.29)
 \end{aligned}$$

The integrals in Eq. (3.29) can be performed with the use of formula (...) of Ref. 48. However, care must be taken at the points  $W=0$ ,  $1$ , and  $(1-\delta)^{-1}$ ; here we need to use analytic continuation and indent the real- $W$  contour into the upper half  $W$ -plane by putting tiny semi-circles at these critical points. This procedure satisfies causality, which requires  $\text{Im}(\omega) > 0$ .

The final result is  $T(W) = \text{Re } T(W) + j \text{Im } T(W)$ , with

$$\text{Re } T(W) = -\alpha_h \sqrt{2/\epsilon} W \left\{ \sqrt{\delta} \ln \left| 1 - \frac{1}{W(1-\delta)} \right| - \ln \left| \frac{1+\sqrt{\delta}}{1-\sqrt{\delta}} \right| + U \right\} \quad (3.30)$$

where

$$U = \begin{cases} \sqrt{1-1/W} \ln \left| \frac{\sqrt{\delta} + \sqrt{1-1/W}}{\sqrt{\delta} - \sqrt{1-1/W}} \right|, & -\infty < W < 0; \text{ and} \\ & 1 < W < \infty \\ 2\sqrt{1/W-1} \tan^{-1} \left[ \sqrt{\delta / [(1/W)-1]} \right], & 0 < W < 1 \end{cases} \quad (3.31)$$

and with

$$\text{Im } T(W) = \begin{cases} 0, & -\infty < W < 0 \text{ and } (1-\delta)^{-1} < W < \infty \\ -\alpha_h \sqrt{2/\epsilon} (\pi W \sqrt{\delta}) = -\pi \alpha_h W \sqrt{2(1-\cos\theta_0)}, & 0 < W < 1 \\ -\alpha_h \sqrt{2/\epsilon} \pi W \left[ \sqrt{\delta} - \sqrt{1-(1/W)} \right], & 1 < W < (1-\delta)^{-1} \end{cases} \quad (3.32)$$

Plots of  $\text{Re } T(W)$  and  $\text{Im } T(W)$  as function of the normalized frequency  $W$  are given in Fig. 3.2 respectively, for  $\epsilon = 0.3$  and  $\theta_0 = \pi/4$ . Note that the  $\theta$  integration in Eq. (3.18) has the effect of smoothing what would otherwise be singular when  $W=1$ . A similar type of smoothing has been achieved <sup>26</sup> by means of a radial average in the fishbone theory for internal kink modes.

### 3.4 SOLUTION OF THE RESONANT BALLOONING MODE EQUATION

The goal in this section is to obtain the dispersion relation for the "balloon-bone" modes. Since the ballooning mode frequency is well below that for Alfvén waves, *i.e.*,  $\omega \sim \bar{\omega}_{dh} \ll \omega_A$ , the inertial term is unimportant until large  $\theta$  values. Therefore, as sketched in Fig. 3.3, we divide field line space into an inner region, which we call the MHD region, and an outer inertial region. We solve the ballooning mode equation in both regions and match the solutions asymptotically to obtain the dispersion relation.

#### 3.4.a SOLUTION IN THE INTERIOR MHD REGION

From now on we assume that the dominant resonant trapped particle response is a single  $\delta$ -function at  $\theta = 0$ , where the mode is

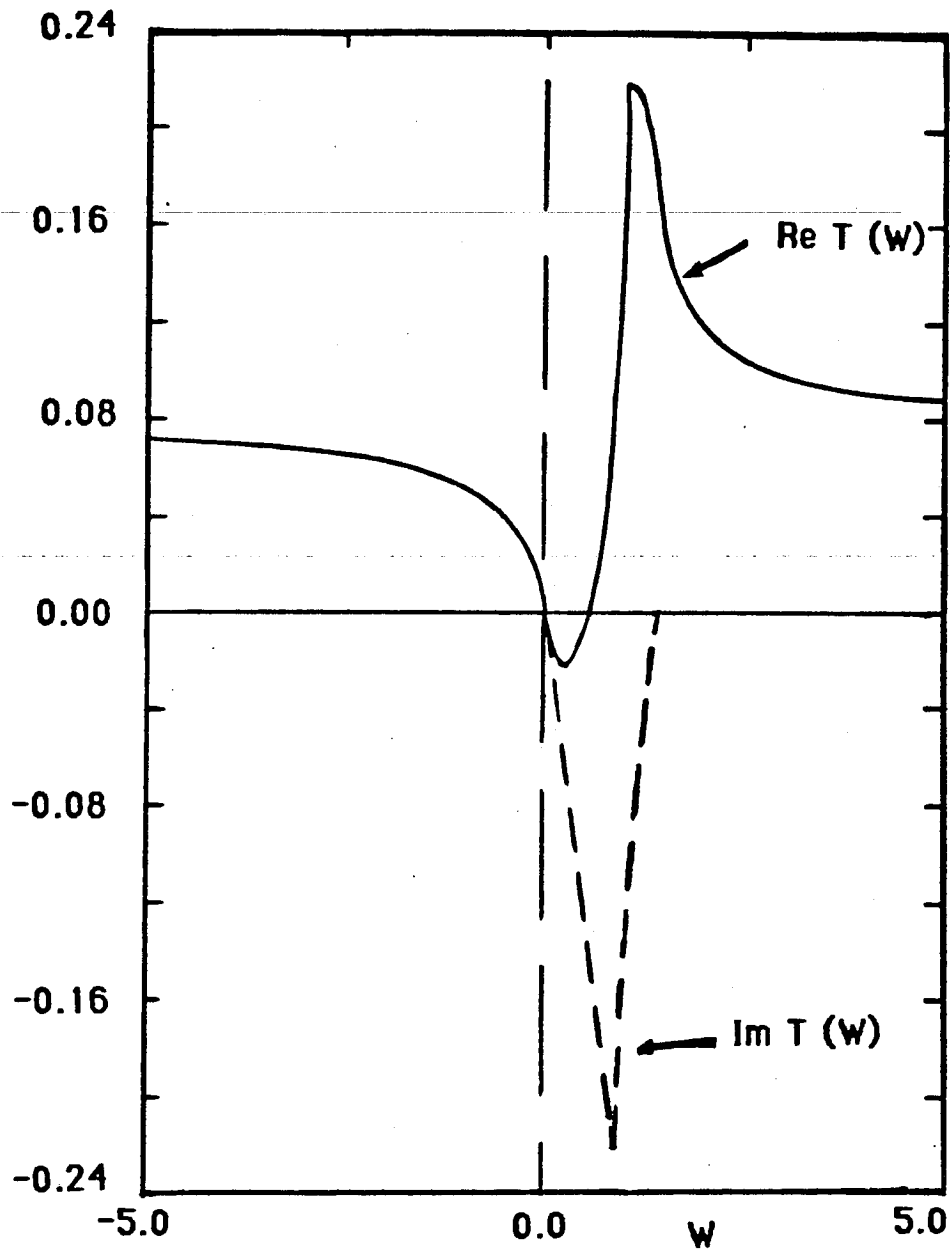


Fig. 3.2 Real and imaginary parts of  $T(w)$  versus  $W = \omega / \omega_{dm}$  for  $\alpha_c = \alpha_h = 0.05$ ,  $\epsilon = 0.3$ ,  $\bar{\omega}_{dm} / \omega_A = 0.2$ , and  $S = 0.5$ .



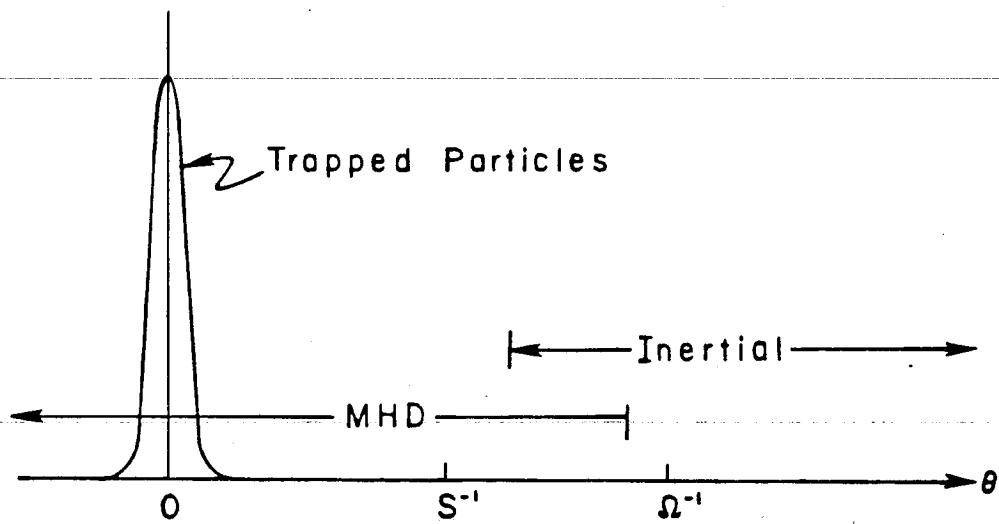


Fig. 3.3 Ideal MHD and inertial regions in ballooning space.

most strongly peaked. Then, the equation to be solved in each interval  $|\theta - 2n\pi| \leq \pi$ , for  $n=0, \pm 1, \pm 2, \dots$ , is

$$\frac{d}{d\theta} \left[ 1+h^2(\theta) \right] \frac{d}{d\theta} \Phi(\theta) + \left[ \alpha_c + \frac{\alpha_h}{2} H \right] D(\theta) \Phi(\theta) = \left[ \frac{\alpha_h}{2} \right] H(\theta) D(\theta) \Lambda^{(n)} \quad (3.33)$$

with 
$$\left. \frac{d}{d\theta} \ln \Phi \right|_{\theta=0^+} = -T(\omega) \quad (3.34)$$

as the boundary condition at the origin .

Two independent solutions of Eq. (3.33) are  $\Phi_{\text{even}}$  and  $\Phi_{\text{odd}}$ , distinguished by their respective parities at  $\theta=0$ . We shall normalize them such that  $\Phi_e(0)=1$ ,  $\Phi'_e(0)=0$ ,  $\Phi_o(0)=0$ , and  $\Phi'_o(0)=1$ , where the prime denotes  $d/d\theta$ . Thus, by virtue of Eq. (3.34), the total interior solution is given by

$$\Phi_{\text{in}} = \Phi_{\text{even}} - T(\omega) \Phi_{\text{odd}} \quad (3.35)$$

Having written down the formal solution in the inner region, we now desire to obtain the explicit asymptotic form for large  $\theta$ . This will be done by expanding Eq. (3.33) in powers of  $\theta^{-1} \ll 1$  and

solving for  $\Phi$  order by order. Noting that the coefficients in the ballooning mode equation (3.33) contain both oscillatory and secular dependence on  $\theta$ , we separate the  $\theta$  variation by introducing two space scales, *viz.*,  $\tilde{\theta}$  for the rapid oscillatory variation (with period  $2\pi$ ) and  $Z=S\theta$  for the slow secular variation. Next we assume that the solution  $\Phi$  can be expanded as<sup>49</sup>

$$\Phi(\theta) \sim \theta^\mu \left\{ 1 + \theta^{-1} f_1(\tilde{\theta}) + \theta^{-2} f_2(\tilde{\theta}) + \dots \right\} \quad (3.36)$$

The procedure outlined here is the well-known Mercier asymptotic analysis.<sup>50,51</sup>

One significant difference with the usual Mercier treatment is that Eq. (3.33) is an integro-differential equation. Therefore a way must be devised to handle the integral term,  $\Lambda^{(n)}$ . In the  $n^{\text{th}}$  trapped particle interval,  $|\theta - 2n\pi| \leq \theta_0$ , we note that for large  $n \gg 1$  (or, equivalently, large  $\theta$ ), we have

$$Z = S\theta = S(2\pi n + \tilde{\theta}) = S\theta_n + S\tilde{\theta} \approx S\theta_n. \quad (3.37)$$

Now, in the expression (3.15) for  $\Lambda^{(n)}$ , we translate the variable of integration back to the basic trapped interval  $(-\theta_0, \theta_0)$  and then

expand for  $\theta_n \gg \tilde{\theta}$ , valid for  $n \gg 1$ :

$$\Lambda^{(n)} = \frac{\int_{-\theta_0}^{\theta_0} d\tilde{\theta} \left[ D(\tilde{\theta}) + S\theta_n \sin\tilde{\theta} \right] \left[ \theta_n + \tilde{\theta} \right]^\mu \left\{ 1 + \left[ \theta_n + \tilde{\theta} \right]^{-1} f_1(\tilde{\theta}) + \dots \right\}}{\int_{-\theta_0}^{\theta_0} \left[ D(\tilde{\theta}) - \frac{\alpha_c}{2q^2} \right] d\tilde{\theta}}$$

$$\cong (S\theta_n)^\mu \left\{ \lambda_0 + (S\theta_n)^{-2} \lambda_2 + \dots \right\}$$

$$\cong Z^\mu \lambda_0 - (S\tilde{\theta})^\mu \lambda_0 Z^{\mu-1} + Z^{\mu-2} \left[ \lambda_2 + \mu(\mu-1) \frac{\lambda_0}{2} \right] + \dots$$

(3.38)

As is heuristically shown in Fig. 3.4, we have thus been able to convert the integral term  $\Lambda^{(n)}$  from a piecewise constant function to a slowly varying continuous function in  $Z$  with asymptotically small dependence on the sawtooth function  $\tilde{\theta}$ . The coefficient  $\lambda_0$  in Eq. (3.38) involves averages of equilibrium quantities over a trapped particle interval and is given by

$$\lambda_0 = \frac{\sin\theta_0 + S(\sin\theta_0 - \theta_0 \cos\theta_0)(1+\mu)}{\sin\theta_0 + S(\sin\theta_0 - \theta_0 \cos\theta_0) - \left[ \frac{\alpha_c}{4} \right] (2\theta_0 - \sin 2\theta_0) - \left[ \frac{\alpha_c \theta_0}{2q^2} \right]}$$

(3.39)

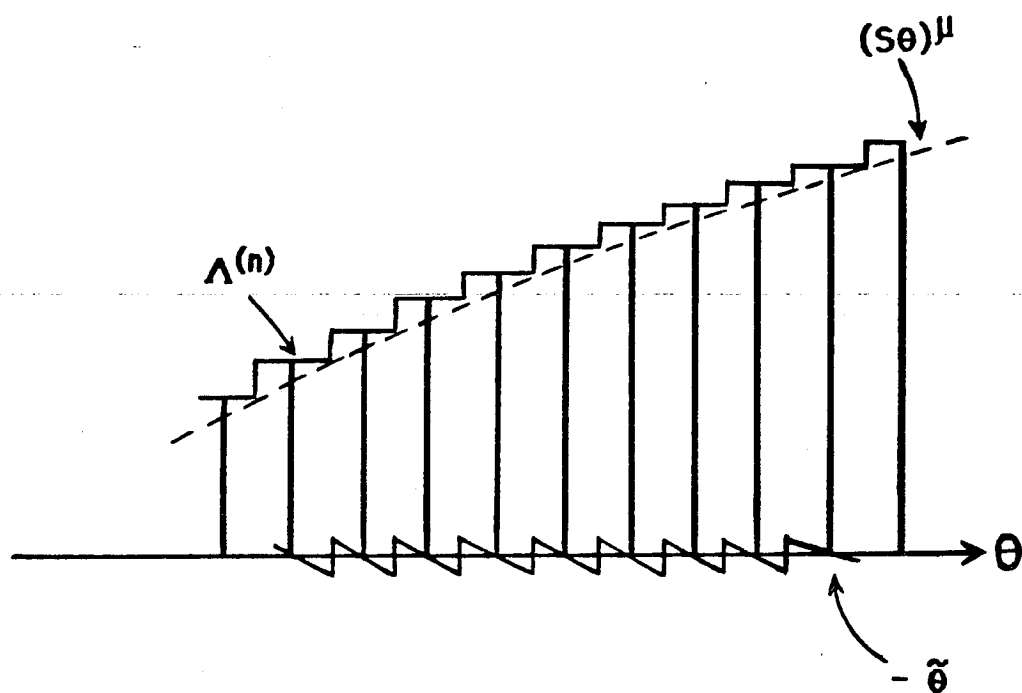


Fig. 3.4 Piecewise constant  $\Lambda^{(n)}$  and slowly continuous function  $(S\theta)^\mu$

It will be not necessary to know  $\lambda_2$  in order to obtain the Mercier exponent,  $\mu$ .

Using Eqs. (3.36) and (3.38), we find that the ballooning equation (3.33) in  $O(Z^{\mu+1})$  can be solved to give

$$f_1(\tilde{\theta}) = \alpha_c \sin\theta + \frac{1}{2} (1-\lambda_0) \alpha_h g(\tilde{\theta}). \quad (3.40)$$

With this information for  $f_1$ , we then average in  $\tilde{\theta}$  the differential equation for  $f_2$  and obtain the following indicial equation for the Mercier exponent  $\mu$  :

$$\mu(\mu+1) - D_h = 0 \quad (3.41)$$

with

$$D_h = \frac{\left[ \frac{\alpha_c \alpha_h}{4\pi S^2} \right] \sin\theta_0 \left[ \theta_0 \left[ 1 + \frac{1}{q^2} \right] - \frac{1}{2} \sin 2\theta_0 \right]}{\sin\theta_0 + S t_0 - \left[ \frac{\alpha_c}{2} \right] \left[ \theta_0 \left[ 1 + \frac{1}{q^2} \right] - \frac{1}{2} \sin 2\theta_0 \right] + \left[ \frac{\alpha_h}{2\pi} \right] t_0^2} \quad (3.42)$$

when  $t_0 = \sin\theta_0 - \theta_0 \cos\theta_0$ . The two solutions of Eq. (3.41) are

$$\mu_{\pm} = -\frac{1}{2} \pm \sqrt{1/4 + D_h} \quad (3.43)$$

(From now on, in general we will drop the subscript and let  $\mu = \mu_+$ , with  $\mu_- = -1 - \mu$ .)

In Fig. 3.5 we have plotted the exponent  $\mu = \mu_+$  as a function of  $\alpha_c$ , for various values of  $\alpha_h$  and with the parameters  $\theta_0 = \pi/4$ ,  $q = 1.5$ , and  $S = 0.5$ . Note that the value of  $\mu$  increases with  $\alpha_c$  and with  $\alpha_h$ . In fact, for the parameters of Fig. 3.6,  $\mu$  is singular at  $\alpha_c \cong 2.47$ .

Since there are two solutions for the Mercier exponent, the general asymptotic solution for  $\Phi$  will be a superposition, written as

$$\begin{aligned} \Phi(\theta) \sim M\theta^\mu \left\{ 1 + \theta^{-1} f_1(\tilde{\theta}) + \theta^{-2} f_2(\tilde{\theta}) + \dots \right\} \\ + N\theta^{-1-\mu} \left\{ 1 + \theta^{-1} \bar{f}_1(\tilde{\theta}) + \theta^{-2} \bar{f}_2(\tilde{\theta}) + \dots \right\} \end{aligned} \quad (3.44)$$

Here,  $\bar{f}_m(\tilde{\theta})$  is the same as  $f_m(\tilde{\theta})$ , except that  $\mu$  is replaced by  $-1-\mu$ . Without any energetic component, we have  $\mu = 0$  and the asymptotic solution assumes the familiar form  $\Phi \sim M + N/\theta$ . Applying the oscillation theorem used in Chap. II, we see that the ideal mode is stable when  $M \geq 0$  (where the equality holds for the marginal case). Also since  $\Phi$  may correspond to even or odd parity, we label the coefficients as  $M_e$  and  $N_e$ , or  $M_o$  and  $N_o$ , respectively.

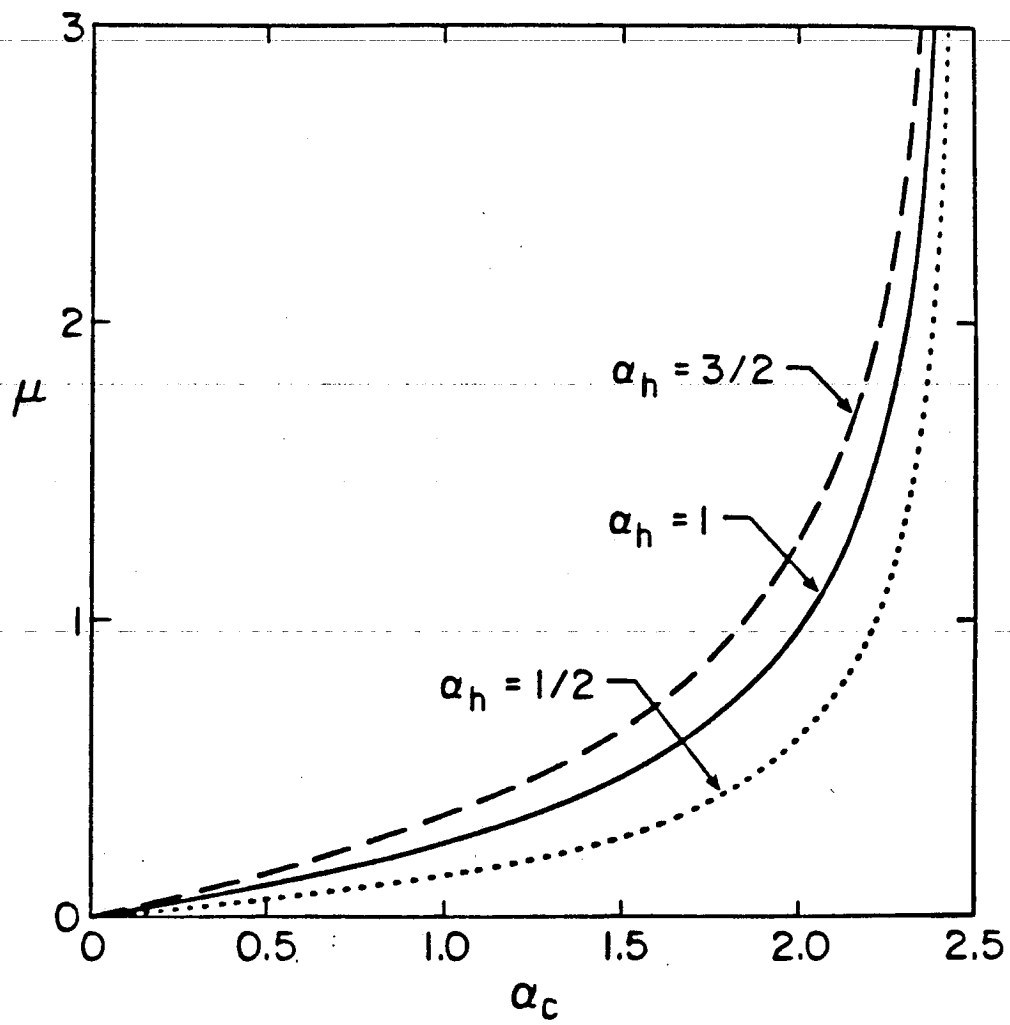


Fig. 3.5 Mercier exponent  $\mu$  as a function  $\alpha_c$  for various values of  $\alpha_h$



In this analytical treatment of the asymptotic solution, the Mercier coefficients  $M_{e,0}$  and  $N_{e,0}$  are not determined. We obtain them by matching the asymptotic expression for  $\Phi$  in Eq. (3.44), with the even and odd solutions of the integro-differential equation (3.33), obtained numerically. Notice that when  $\mu \gtrsim 0.5$ , the  $Mf_2\theta^{\mu-2}$  term is the same magnitude as the  $N\theta^{-1-\mu}$  term, and hence it is necessary to find  $f_2(\tilde{\theta})$  and subtract its effect on  $\Phi$  in order to obtain  $N_{e,0}$ .

The equation for  $f_2(\tilde{\theta})$ , generated from Eq. (3.33) in  $O(Z^\mu)$ , can be solved to give

$$f_2(\tilde{\theta}) = c_1 + \frac{df_1}{d\tilde{\theta}} + \alpha_c \left[ \sin\theta + \frac{g}{2} \right] f_{1-\mu(\mu+1)} \frac{S^2 \tilde{\theta}^2}{2} + \mu S \alpha_h \lambda_0 \tilde{\theta} g \frac{g}{2} \\ + \left[ 1 - H \left[ \theta_0 - |\tilde{\theta}| \right] \right] \left[ \frac{\alpha_h}{2} \right] (1 - \lambda_0) \sin\theta_0 (\theta_0 - \tilde{\theta}) \quad (3.45)$$

The constant  $c_1$  in Eq. (3.45) can be obtained numerically. It is also possible to derive this constant analytically from the solubility condition obtained<sup>51</sup> as the  $\tilde{\theta}$ -average of the  $O(Z^{\mu-2})$  equation for  $f_4(\tilde{\theta})$ .

For the parameters  $S = 0.5$ ,  $\theta_0 = \pi/4$ , and  $q = 1.5$ , we show in Figs. 3.6 and 3.7 plots of the various Mercier coefficients as functions of  $\alpha_c$ , corresponding to  $\alpha_h = 0$  and  $\alpha_h = 1$ , respectively. In these pictures the stable region for ballooning modes corresponds to the regions where the coefficient  $M_e$  is positive. In Fig. 3.8 where the coefficient  $M_e$  is shown for  $\alpha_h = 0, 0.5, 1.0$ , and  $1.5$ , it can be seen that introducing hot particles reduces the unstable region.

#### 3.4.b SOLUTION IN THE EXTERIOR INERTIAL REGION .

To find an analytical solution of the ballooning mode equation in the exterior inertial region where  $\theta \sim \omega_A/\omega_{dh} \gg 1$ , we repeat the Mercier analysis for an integro-differential equation, but keep the inertial  $\Omega^2$  term. Thus, we start with the equation

$$\frac{d}{d\theta} (1+h^2) \frac{d\phi}{d\theta} + \Omega^2 (1+h^2) \phi + \left[ \alpha_c + \left[ \frac{\alpha_h}{2} \right] H \right] D\phi = \left[ \frac{\alpha_h}{2} \right] H\Delta \quad (3.46)$$

For this finite frequency analysis, we also use a double scale treatment of the differential equation; however, noticing that the differential equation does not admit a power series solution, we try the following form, where  $\phi_1/\phi_0 \sim Z^{-1} \ll 1$ :

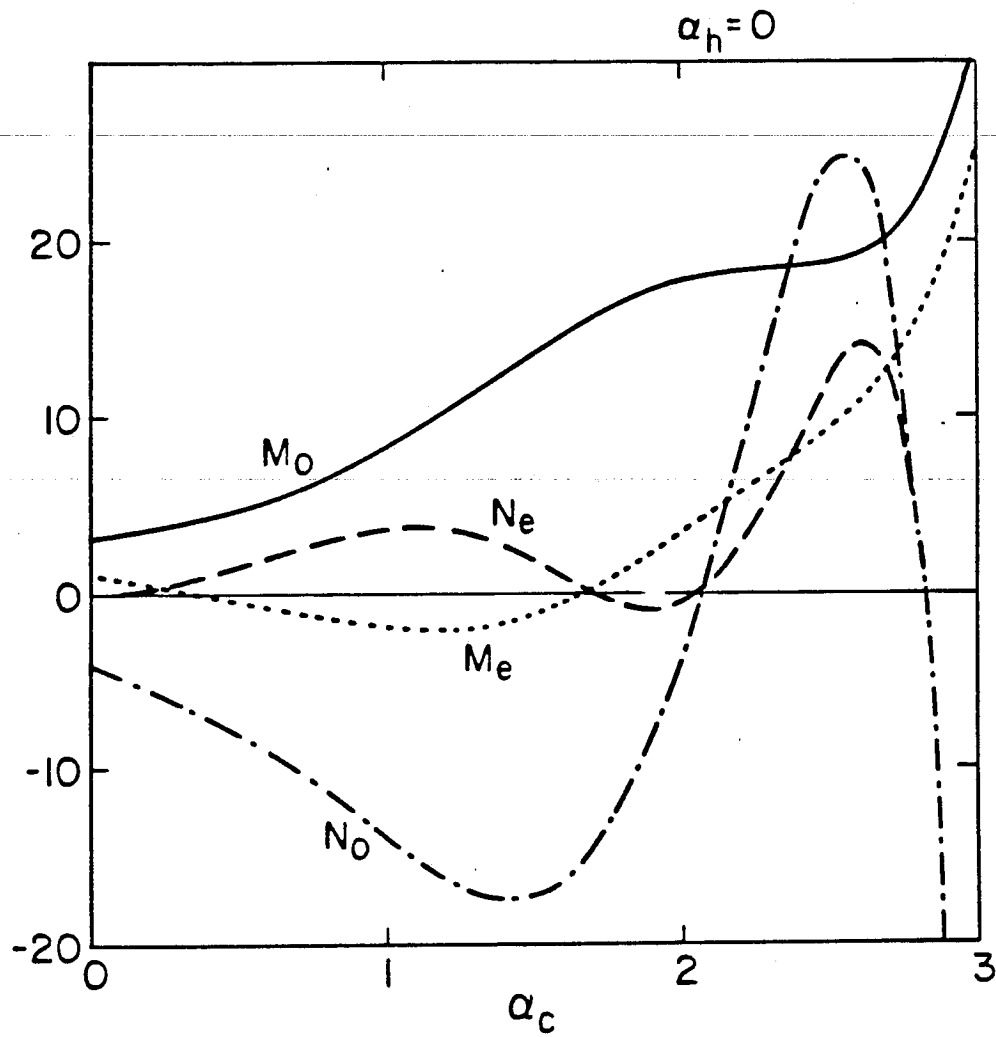


Fig. 3.6 Mercier coefficients as functions of  $\alpha_c$  for  $\alpha_h = 0$ , with  $\theta_0 = \pi/4$ ,  $q = 1.5$ , and  $S = 0.5$ .

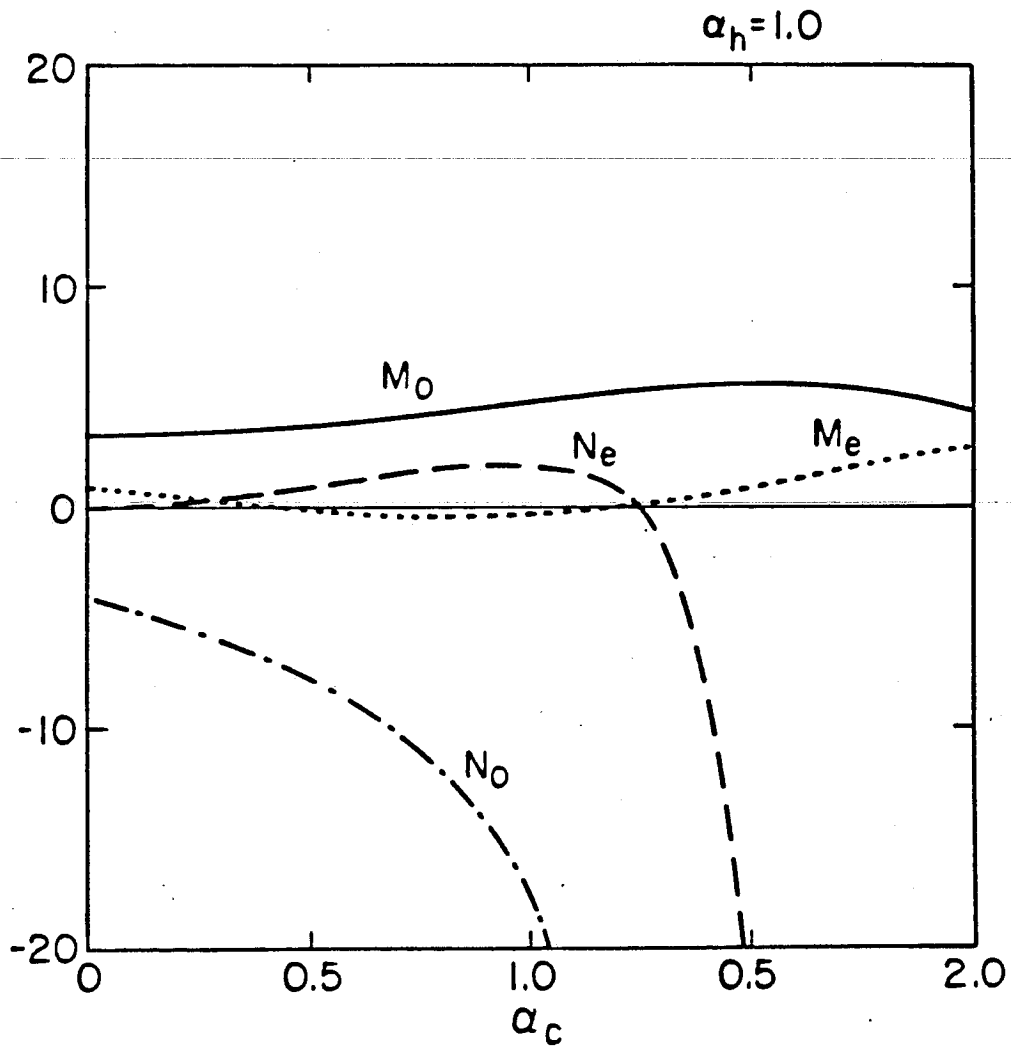


Fig. 3.7 Mercier coefficients as functions of  $\alpha_c$  for  $\alpha_h=1$ , with  $\theta_0=\pi/4$ ,  $q=1.5$ , and  $S=0.5$

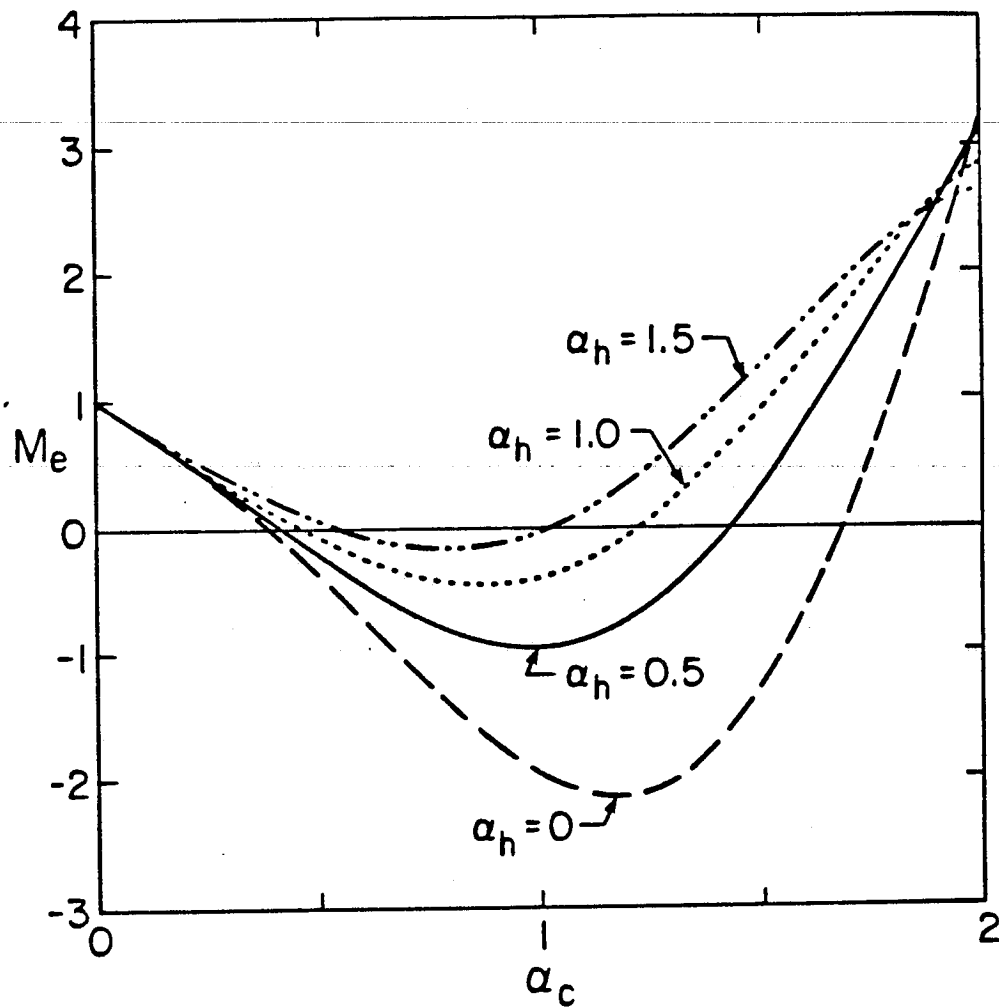


Fig. 3.8 Mercier coefficient  $M_e$  as a function of  $\alpha_c$  .  
for various values of  $\alpha_h$  , with  $\theta_0 = \pi/4$  ,  
 $q = 1.5$ , and  $S = 0.5$

$$\Phi(\tilde{\theta}) = \Phi_0(Z) + \Phi_1(Z, \tilde{\theta}) + \Phi_2(Z, \tilde{\theta}) + \dots \quad (3.47)$$

Actually, we find *a posteriori* that we should take the particular form

$$\Phi_1(Z, \tilde{\theta}) = \frac{\Phi_0(Z)}{Z} P(\tilde{\theta}) + \left[ \frac{\partial \Phi_0}{\partial Z} \right] Q(\tilde{\theta}) \quad (3.48)$$

with  $P$  and  $Q$  are periodic functions of  $\tilde{\theta}$  with period  $2\pi$ .

We expand the integral term again as follows:  $\Lambda^{(n)} = \lambda/\Delta$ ,

where

$$\Delta = \int_{-\theta_0}^{\theta_0} d\theta \left[ D(\theta) - \frac{\alpha_c}{2q^2} \right] \quad (3.49)$$

and

$$\begin{aligned} \lambda &\cong \int_{-\theta}^{\theta_0} d\theta \left[ D(\tilde{\theta}) + Z_n \sin\theta \right] \left\{ \Phi_0(Z_n) + \left[ s\tilde{\theta} \frac{\partial \Phi_0}{\partial Z_n} + \Phi_1(Z_n, \tilde{\theta}) \right] \right. \\ &\quad \left. + \left[ \frac{1}{2} (s\tilde{\theta})^2 \frac{\partial^2 \Phi_0}{\partial Z_n^2} + \frac{s\tilde{\theta}}{\partial Z_n} \frac{\partial \Phi_1}{\partial Z_n} + \Phi_2(Z_n) \right] + \dots \right\} \\ &= Z_n \frac{\partial \Phi_0}{\partial Z_n} (J + K_Q) + \Phi_0 (1 + K_P) + O(Z_n^{-2}) \quad (3.50) \end{aligned}$$

In Eq. (3.50) for  $\lambda$ , we have defined the quantities

$$I = \int_{-\theta_0}^{\theta_0} d\tilde{\theta} D(\tilde{\theta}) \quad (3.51)$$

$$J = \int_{-\theta_0}^{\theta_0} d\tilde{\theta} S\tilde{\theta} \sin\theta \quad (3.52)$$

and

$$\begin{Bmatrix} K_P \\ K_Q \end{Bmatrix} = \int_{-\theta_0}^{\theta_0} d\tilde{\theta} \sin\theta \begin{Bmatrix} P(\tilde{\theta}) \\ Q(\tilde{\theta}) \end{Bmatrix} \quad (3.53)$$

Finally, we therefore obtain

$$\Lambda \equiv \frac{\left[ 1 - S\tilde{\theta} \frac{\partial}{\partial Z} \right] \left[ (1 + K_P) \Phi_0(Z) + (J + K_Q) Z \frac{\partial \Phi_0}{\partial Z} \right]}{\Delta} \quad (3.54)$$

The equation obtained from Eq. (3.46) in  $O(2)$  separates into two equations for the functions  $P$  and  $Q$  in  $\Phi_1$ , which may be solved to yield

$$P(\tilde{\theta}) = \alpha_c \sin\theta + \left[ \frac{\alpha_h}{2} \right] \left[ \frac{1 - 1 + K_P}{\Delta} \right] g(\tilde{\theta}) \quad (3.55a)$$

$$Q(\tilde{\theta}) = - \left[ \frac{\alpha_h}{2} \right] \left[ \frac{J+K_Q}{\Delta} \right] g(\tilde{\theta}) \quad (3.55b)$$

Then, the solubility condition that is obtained by taking the  $\tilde{\theta}$ -average of the  $O(Z^0)$  equation gives a differential equation for the slowly varying function  $\Phi_0(Z)$ :

$$\frac{d}{dZ} \left[ Z^2 \frac{d\Phi_0}{dZ} \right] + \left[ \frac{\Omega^2/S^2}{1+\eta_h} \right] Z^2 \Phi_0 - D_h \Phi_0 = 0 \quad (3.56)$$

$$\eta_h = \frac{\alpha_h J (J+K_Q)}{2S^2 \Delta} \quad (3.57)$$

For  $\Omega^2 \rightarrow 0$ , we recover the Mercier power law solution

$$\Phi_0 \sim Z^\mu \quad (3.58)$$

with the Mercier exponent given by Eq. (3.41), as before.

For  $\Omega^2 \neq 0$ , Eq. (3.56) has an exact solution in terms of Bessel functions:

$$\Phi_0 = Y^{-1/2} J_{\pm \sqrt{1/4+D}}(Y) \quad (3.59)$$

$$\text{with } Y = \left[ \frac{\Omega Z}{S} \right] \frac{1}{\sqrt{1+\eta_h}}$$



We choose to take the particular combination of Bessel functions that yields an outgoing wave at  $\theta \rightarrow \infty$  :

$$\Phi_{\text{out}} = Y^{-1/2} H_{\mu+1/2}^{(1)}(Y) \quad (3.60)$$

This solution has the desired asymptotic behavior to satisfy the outgoing boundary condition for  $Y \gg 1$ :

$$\Phi_{\text{out}} \sim Y^{-1} \exp \left[ i \left[ Y - \frac{\pi\mu}{2} \right] \right]. \quad (3.61)$$

Its small argument form, which will be needed for the matching to the inner MHD solution, is given by

$$\Phi_{\text{out}} \propto -i\pi \left[ \frac{\Omega}{2\sqrt{1+\eta_h}} \right]^{1+2\mu} \frac{\exp(-i\mu\pi)}{\cos(\pi\mu) \Gamma\left[\mu + \frac{1}{2}\right] \Gamma\left[\mu + \frac{3}{2}\right]} \theta^\mu - \theta^{-1-\mu} \quad (3.62)$$

### 3.5 DISPERSION RELATION AND RESULTS

In order to obtain the dispersion relation we match the asymptotic (Mercier) form of  $\Phi_{\text{in}}$  given in Eq. (3.44) to the small

argument form of the Hankel function for  $\Phi_{\text{out}}$  given in Eq. (3.62).

Thus, the dispersion relation for the "balloon-bone" modes is obtained as

$$\frac{M_e - T(\omega) M_0}{N_e - T(\omega) N_0} = i \left[ \frac{\Omega}{2\sqrt{1+\eta_h}} \right]^{1+2\mu} \frac{\pi \exp(-i\pi\mu)}{\Gamma\left[\mu + \frac{1}{2}\right] \Gamma\left[\mu + \frac{3}{2}\right] \cos(\pi\mu)} \quad (3.63)$$

A somewhat more transparent way to rewrite the dispersion relation is as follows:

$$G(\omega) = T(\omega)$$

$$-\frac{\left[ M_e M_0 - \sin(\mu\pi) (M_e N_0 + M_0 N_e) Q + N_e N_0 Q^2 \right] + i Q \cos(\mu\pi) (M_e N_0 - M_0 N_e)}{M_0^2 - 2M_0 N_0 \sin(\mu\pi) Q + N_0^2 Q^2} = 0 \quad (3.64)$$

with  $Q(\omega) = (\Omega/2\sqrt{1+\eta_h})^{1+2\mu} \pi/\Gamma(\mu+1/2) \Gamma(\mu+3/2) \cos(\mu\pi)$ . In Eq.

(3.64), the resonant effect of the energetic particles is isolated in the first term on the right-hand side. The second term represents the

ideal MHD contribution, coming through the Mercier coefficients  $M_e$  and  $N_{e,0}$ , as well as the outgoing flux inertial contribution, incorporated in the  $Q(\omega)$  quantity.

At zero frequency, since  $T(0) = 0$ , we find that the dispersion relation (3.64) reduces to  $G(0) = -M_e/M_0 = 0$ . This reproduces the marginal stability condition,  $M_e \geq 0$ , for nonresonant ballooning modes studied in Chap. II, since  $M_e$  depends on the values of the equilibrium parameters, including that for the hot particle pressure  $\alpha_h$ .

At finite frequencies, we note that  $T(\omega)$  peaks at a somewhat large value near resonance,  $\omega/\bar{\omega}_{dm} \approx 1$ , whereas the second term on the right-hand side of Eq. (3.64) remains  $O(1)$  in magnitude. Therefore, since  $T(\omega)$  is linearly proportional to  $\alpha_h$ , we suspect that only small values of  $\alpha_h$  need to be considered for the resonant branch, such that  $\mu, \eta_h \ll 1$ ; the validity of this approximation may be checked *a posteriori*. In this limit the dispersion relation simplifies to

$$G(\omega) = T(\omega) - \frac{\left[ M_e M_0 + \Omega^2 N_e N_0 \right] - i\Omega \left[ M_e N_0 - M_0 N_e \right]}{M_0^2 + \Omega^2 N_0^2} = 0. \quad (3.65)$$

The stability characteristics of the simplified dispersion relation, Eq. (3.65), can be analyzed by means of Nyquist diagrams. Thus, we plot the real and imaginary parts of  $G(\omega)$  against each other, for frequencies  $\omega$  on a contour that runs along the real  $\omega$  axis, indented above the point  $\omega = \bar{\omega}_{dm}$ , and encircles the upper half  $\omega$  plane. Since  $G(\omega)$  has a pole in the upper half  $\omega$ -plane at  $\omega/\omega_A = iM_0/|N_0|$ , if a Nyquist plot of  $\text{Re } G(\omega)$  versus  $\text{Im } G(\omega)$  for real frequencies encircles the origin ( $G = 0$ ) then there is no instability.<sup>52</sup> In Fig. 3.9, we show a typical Nyquist diagram, for the parameters  $\alpha_h = 0.05$ ,  $\alpha_c = 0.05$ ,  $S = 0.5$ ,  $q = 1.5$ , and  $\theta_0 = \pi/4$ . Since the Nyquist plot in Fig. 3.9 does encircle the origin, the "balloon-bone" mode is stable for these parameters. By varying the parameters  $\alpha_c$  and  $\alpha_h$ , we obtain the stable operating regime for these modes.

Figure 3.10 shows the stability boundaries for both the zero-frequency nonresonant branch ( $\omega/\bar{\omega}_{dh} \approx 0$ ) and the finite-frequency resonant branch ( $\omega/\bar{\omega}_{dh} \approx 1$ ), plotted as functions of  $\alpha_c$  and  $\alpha_h$ , with  $\theta_0 = \pi/4$ ,  $S = 0.5$ ,  $q = 1.5$  and  $\bar{\omega}_{dh}/\omega_A = 0.2$ . The nonresonant stability boundary shown here is merely a cross-plot of the corresponding boundary in a display like that of Fig. 2.4, except that the implicit  $\alpha_h$  variation is made explicit in Fig. 3.10, which takes

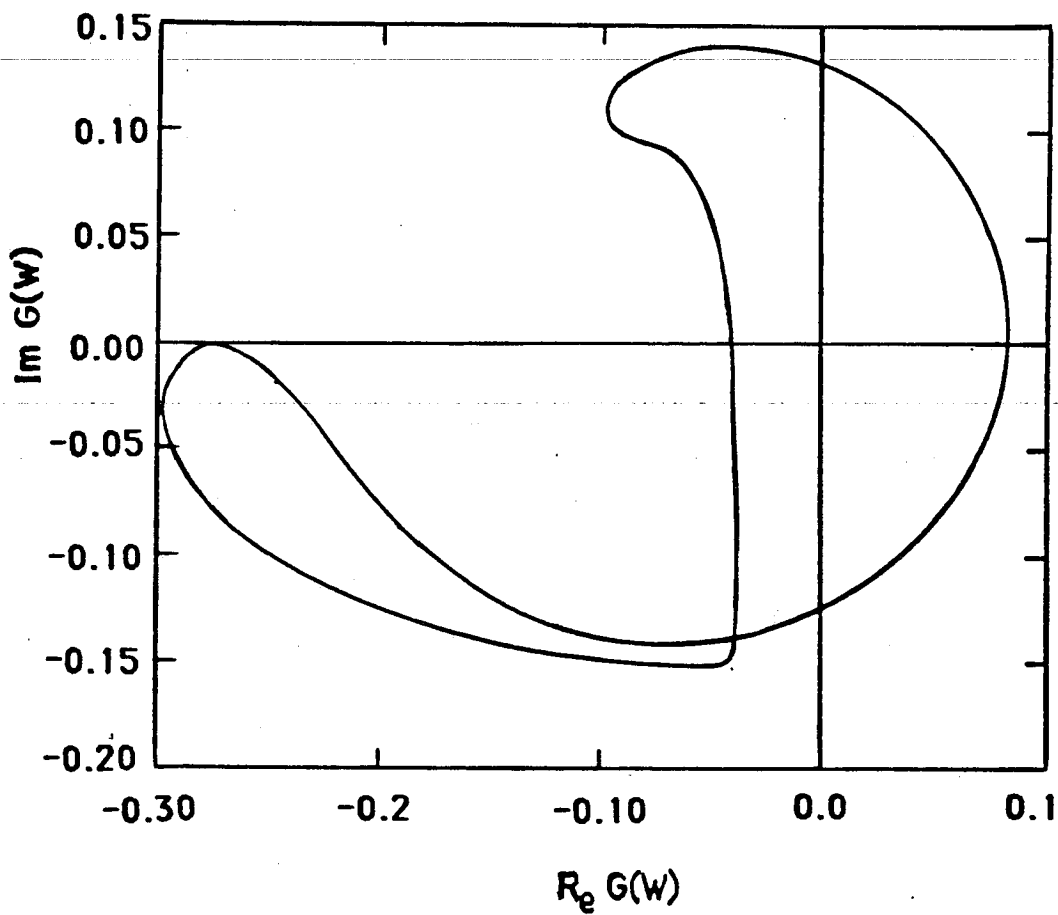


Fig. 3.9 Imaginary part of  $G(w)$ , versus Real part of  $G(w)$ , with  $\varepsilon = 0.3$ ,  $\alpha_h = \alpha_c = 0.05$ ,  $q = 1.5$ ,  $S = 0.5$ , and  $\theta_0 = \pi/4$ .

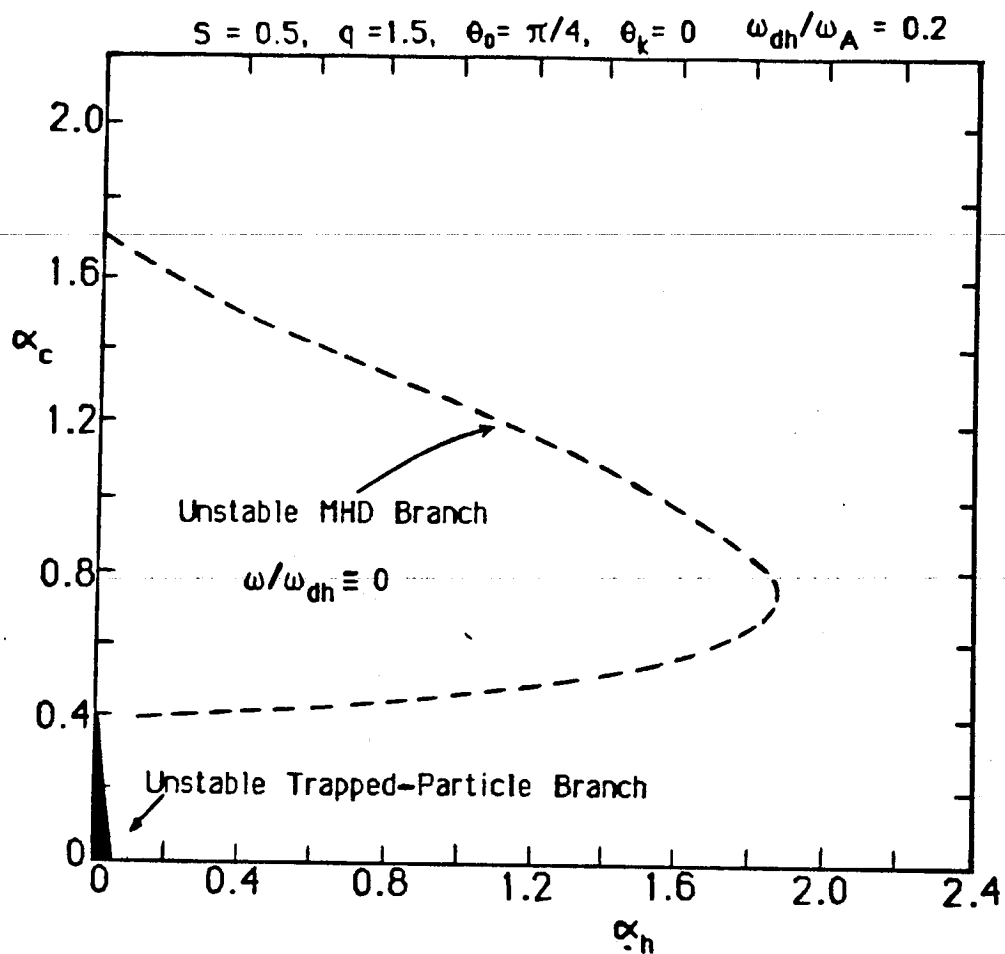


Fig. 3.10 Marginal stability boundaries in  $\alpha_c$  and  $\alpha_h$  parameter space for the MHD and trapped-particle-induced ballooning mode branches for  $\bar{\omega}_{dh}/\omega_A = 0.2$ ,  $\epsilon = 3$ ,  $S = 0.5$ , and  $\theta_0 = \pi/4$

shear to be fixed. Without any energetic particles ( $\alpha_h = 0$ ), Fig. 3.10 shows first and second stability regions in  $\alpha_c$ , separated by an unstable zone in which  $M_e < 0$ . If one were to ignore their resonant interaction, then it would appear that the introduction of energetic particles with sufficient pressure ( $\alpha_h \gtrsim 1.9$ ) could allow the system to gain access to the high  $\alpha_c$  second stability regime while avoiding the zero-frequency unstable zone. However, when the resonant "balloon bone" branch is taken into consideration, one finds a rather low threshold in  $\alpha_h$  that therefore reduces the stable region—*i.e.*, stable with respect to both branches of the ballooning mode—to the rather small area in the lower left-hand corner of Fig. 3.10.

Figure 3.11 shows a similar plot of the stability boundaries, but for the larger value of  $\bar{\omega}_{dh}/\omega_A = 0.6$ . The size of the stable region increases with the increased value of  $\omega_{dh}/\omega_A$ , since this ratio is proportional to the energy of hot particles. For sufficiently energetic particles, the mode becomes predominantly nonresonant as the balloon bone stability boundary moves out to large  $\alpha_h$ . However, this limit requires values for  $\bar{\omega}_{dh}/\omega_A$  that are larger than those allowed by the initial assumptions of our theoretical description. Consequently, we

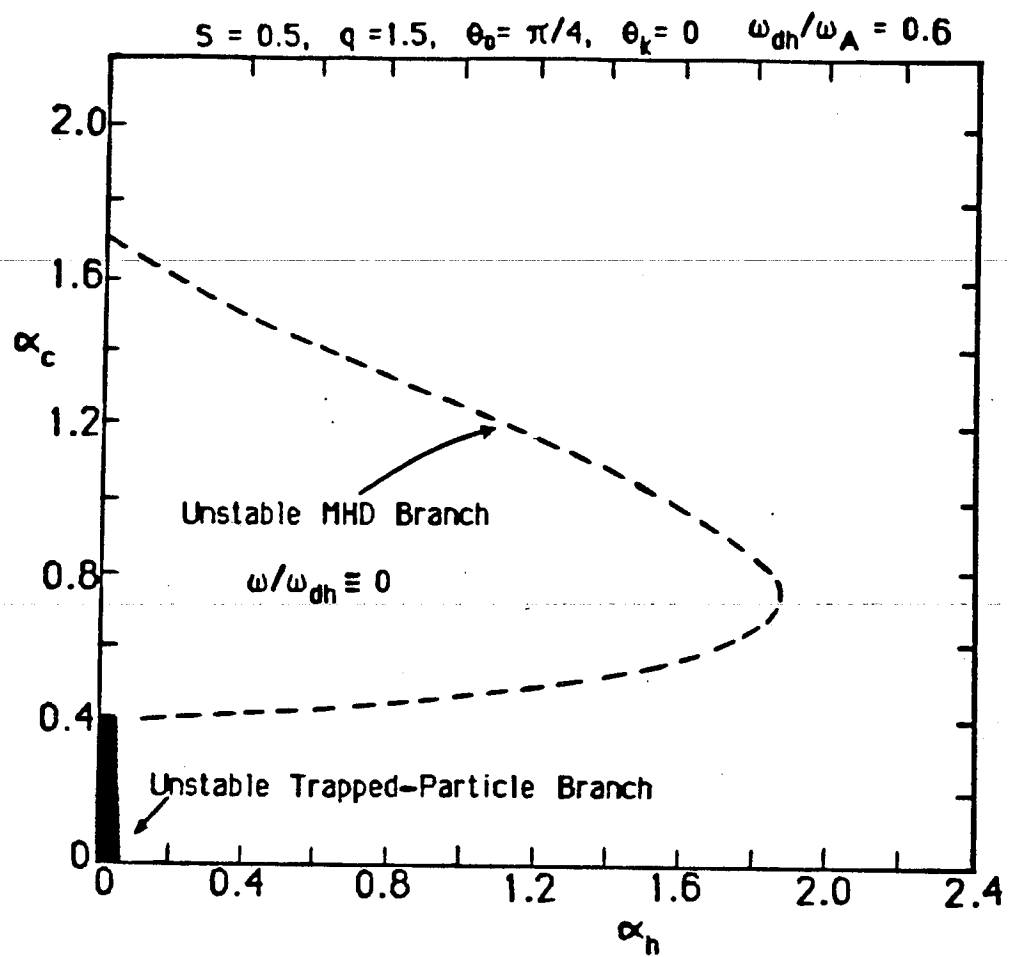


Fig. 3.11 The same as Fig. 3.10, except  $\bar{\omega}_{dm}/\omega_A = 0.6$



can only detect the incipient trend with increased energy. We can say for the parameters characteristic of the PDX experiment, however that  $\omega_{dh}/\omega_A \ll 1$  and that therefore these energetic trapped particle-induced ballooning instabilities were present.

### 3.6 APPROXIMATE STABILITY CONDITIONS

Here we will analytically derive some approximate stability conditions for the resonant mode, by visually inspecting the Nyquist diagrams.

The Nyquist plot of the second term in the dispersion relation, *viz.*,  $G(\omega)-T(\omega)$ , is roughly an ellipse that encircles the origin if  $M_e > 0$ . This explains why  $M_e > 0$  is the stability condition for the zero-frequency nonresonant branch. When the resonant term  $T(\omega)$  is included, the roughly elliptical shape is distorted into a shape like that shown in Fig. 3.9. The largest distortion occurs near the resonant frequency  $\omega \simeq \bar{\omega}_{dm}$ . Indeed, the Nyquist plot of  $\text{Re } G$  versus  $\text{Im } G$  can be made to no longer encircle the origin if  $\text{Re } T$  is sufficiently positive and  $\text{Im } T$  is sufficiently negative. We can quantify these two conditions for instability as follows:

$$\operatorname{Re} G \left[ \omega \simeq \bar{\omega}_{dm} \right] \cong \operatorname{Re} T \left[ \omega \simeq \bar{\omega}_{dm} \right] - \frac{M_e}{M_0} > 0 \quad (3.66)$$

and

$$\begin{aligned} \operatorname{Im} G \left[ \omega \simeq \bar{\omega}_{dm} \right] &\cong \operatorname{Im} T \left[ \omega \simeq \omega_{dm} \right] \\ &+ \frac{\left[ \frac{\bar{\omega}_{dm}}{\omega_A} \right] \left[ M_e N_0 - M_0 N_e \right]}{M_0^2} < 0 \end{aligned} \quad (3.67)$$

Here, we have neglected the  $\Omega^2$  terms in  $G(\omega)$  since  $\omega_{dh}/\omega_A \ll 1$ .

Referring to Eqs. (3.30)-(3.32), we find

$$\begin{aligned} \operatorname{Re} T \left[ \frac{\omega}{\bar{\omega}_{dm}} = 1 \right] &= -\alpha_h \sqrt{2/\epsilon} \left[ \sqrt{\delta} \ln \left[ \frac{\delta}{1-\delta} \right] - \ln \left[ \frac{1+\sqrt{\delta}}{1-\sqrt{\delta}} \right] \right] \\ &\cong \alpha_h \left[ 2 - \ln \delta \right] \theta_0 \end{aligned} \quad (3.68)$$

$$\operatorname{Im} T \left[ \frac{\omega}{\bar{\omega}_{dm}} = 1 \right] = -\pi \alpha_h \sqrt{2(1-\cos\theta_0)} \cong -\pi \theta_0 \alpha_h, \quad (3.69)$$

where the approximate forms are valid for  $\delta = \epsilon(1-\cos\theta_0) \cong \epsilon\theta_0^2/2 \ll 1$ .

A further simplification of Eqs. (3.66) and (3.67) can be effected by noting a Wronskian-type relationship among the Mercier coefficients. Beginning with the  $\alpha_h \ll 1$  ballooning equations for the even and odd parity modes,

$$\frac{d}{d\theta} (1+h^2) \frac{d\Phi_{e,o}}{d\theta} + \alpha_c D(\theta) \Phi_{e,o} \cong 0, \quad (3.70)$$

we cross-multiply and subtract to obtain the relationship

$$\left[ 1+h^2(\theta) \right] \left[ \Phi_e \left[ \frac{d\Phi_o}{d\theta} \right] - \Phi_o \left[ \frac{d\Phi_e}{d\theta} \right] \right] = \text{const. in } \theta \quad (3.71)$$

By virtue of our chosen normalizations for  $\Phi_e$  and  $\Phi_o$  at  $\theta = 0$ , at which point  $h(\theta) \cong S\theta - \alpha_c \sin\theta \rightarrow 0$ , we find the constant on the right-hand side of Eq. (3.71) to be equal to unity. At large  $\theta \gg 1$ , we have  $\Phi_{e,o} \sim M_{e,o} \theta^\mu + N_{e,o} \theta^{-1-\mu}$ , hence

$$\Phi_e \Phi_o' - \Phi_o \Phi_e' \sim -2 \left[ M_e N_o - M_o N_e \right] \left[ \mu + \frac{1}{2} \right] / \theta^2 \quad (3.72)$$

But because  $h(\theta) \sim S^2 \theta^2$ , we obtain the relationship

$$M_e N_o - M_o N_e = - \frac{1}{(1+2\mu)S^2} \cong - \frac{1}{S^2}, \quad (3.73)$$

valid for the  $\alpha_h \ll 1$  limit being considered here.

Finally, we will focus our attention near ideal marginal stability,  $|M_e| \ll 1$ , and assume that the values of  $M_0$  and  $N_0$  are little changed from their values at  $\alpha_c = 0$ . The latter may be obtained from the  $\alpha_c = 0$  odd parity solution of Eq. (3.70):

$$\Phi_0 = \frac{1}{S} \tan^{-1}(S\theta) - \frac{\pi}{2S} - \frac{1}{S^2 \theta} , \quad (3.74)$$

hence  $M_0 \cong \pi/2S$  and  $N_0 \cong -1/S^2$ . For  $|M_e| \ll 1$ , the Wronskian relationship (3.73) yields  $N_e \cong 2/\pi S$ .

Now we are ready to re-write the approximate stability conditions (3.66) and (3.67).

If  $M_e < 0$ , the zero frequency nonresonant ( $\omega/\omega_{dh} \simeq 0$ ) branch is unstable.

If  $M_e > 0$ , the finite-frequency resonant ( $\omega/\omega_{dh} \simeq 1$ ) branch is unstable if both of the following conditions are satisfied:

$$\alpha_c > \frac{2SM_e}{\pi\theta_0} (2 - \ln \delta)^{-1} \quad (3.75)$$

and

$$\alpha_h > \frac{4}{\theta_0 \pi^3} \left[ \frac{\bar{\omega}_{dm}}{\omega_A} \right] \quad (3.76)$$

For  $\epsilon = 0.3$  and the other parameters the same as in Fig. 3.12, we obtain from Eq. (3.75) with  $\alpha_c = 0$  the threshold value of  $\alpha_h \cong 0.09$ , whereas near the  $\alpha_c$  value for ideal marginal stability, Eq. (3.76) gives a threshold of  $\alpha_h \cong 0.03$ ; these estimated values check with the numerical results in Fig. 3.12.

For small values of  $\omega_{dh}/\omega_A \ll 1$ , Eq. (3.75) is the more stringent stability condition, away from ideal marginal stability. We note that Weiland and Chen<sup>27</sup> obtained only the equivalent of Eq. (3.76) because they used a singular resonant response (*i.e.*,  $\delta \rightarrow 0$ ) and considered the marginal stability situation ( $M_e = 0$ ).

### 3.7 CONCLUSIONS

In this chapter, we have elaborated a semi-analytical theory for the "balloon-bone" modes, *i.e.*, unstable ballooning modes excited by wave-particle resonance at the curvature drift frequency of trapped energetic particles. In our analysis for finite values of the pressure and the shear, we are able to obtain the Mercier exponent analytically and the Mercier coefficients numerically. In particular, the plot of the coefficient  $M_e$  contains all the stability information

for the enhanced stability of nonresonant ballooning modes that is due to hot particles: namely, that for large enough hot particle pressure  $\alpha_h$ , it is possible to have stability ( $M_e > 0$ ) for all core plasma pressures  $\alpha_c$ . By using the asymptotic Mercier information, we performed a numerical Nyquist analysis of the stability of resonant modes, which predicts fairly restrictive ballooning instability. We have also presented approximate analytical stability conditions for this mode. This beam ion-induced ballooning instability may explain the high-frequency fishbone precursor oscillations that were observed in the PDX experiment.

## CHAPTER IV

### RESISTIVE BALLOONING STABILITY WITH HIGHLY ENERGETIC PARTICLES

#### 4.1 INTRODUCTION

In Chapter II, we found that highly energetic particles—such as alpha particles, neutral-beam injected ions, or cyclotron-wave-heated electrons or ions—could nonresonantly enhance the stability of ideal ballooning modes. In Chapter III it was found that moderately energetic particles can lead to wave-particle resonant destabilization of ideal ballooning modes. In this chapter, we now explore the possibility of residual resistive ballooning instabilities. Recently, the behavior of the resistive interchange-ballooning modes in the presence of moderately energetic, resonant particles was examined by Biglari and Chen,<sup>34</sup> with the restriction of rather low beta for the hot species. Here, we will investigate the effect of highly energetic, *i.e.*, non-resonant, finite beta particles on the stability of resistive ballooning modes.

The plan for our study of resistive ballooning stability in the presence of energetic particles will be as follows. First, we will

derive the coupled system of equations appropriate for the resistive modes. As in Chapter III, in the large- $\theta$  resistive region we employ a double-scale analysis for an integro-differential equation and derive a differential equation for the nonoscillating part of the eigenmode. Then, the solution in the small- $\theta$  ideal MHD region is matched asymptotically with its exactly known Mercier-type form to the solution for the resistive layer, with hot particles in both regions. In the limit of finite beta and finite shear, but deeply trapped hot particles, we derive a dispersion relation for the complex frequency of the resistive ballooning modes, as a function of the usual  $\Delta'$  quantity that controls resistive stability. The limits of small and large  $\Delta'$  reproduce certain scalings with fractional powers of the resistivity that may be identified with well-known modes. In general, the  $\Delta'$  quantity is obtained by numerically solving the ideal ballooning equation and extracting the ratio of the non-oscillatory "small" and "large" components. Analytic expressions for  $\Delta'$  have also been derived in various low beta cases. Finally, the above treatment will be carried out for the case in which the effects of parallel compressibility and cross-field transport are included.



## 4.2 DERIVATION OF RESISTIVE BALLOONING MODE EQUATIONS

The traditional derivation of the resistive ballooning mode equations is based on the collisional fluid equations of motion, written in a form appropriate for a single-fluid, weakly resistive, charge-neutral plasma of electrons and ions. The presence of energetic particles introduces another plasma component, one which cannot adequately be described by fluid equations, due to their very high diamagnetic energy. A kinetic equation must be used for the dynamics of the energetic component.

For the behavior of the fluid-like core plasma, we can still write down the following resistive hydromagnetic equations for mass conservation,

$$\frac{\partial}{\partial t} \rho_c + \nabla \cdot (\rho_c \mathbf{U}_c) = 0 \quad (4.1)$$

for momentum,

$$\rho_c \frac{d}{dt} \mathbf{U}_c = \frac{1}{c} (\mathbf{J}_c \times \mathbf{B}) + Q_c \mathbf{E} - \nabla P_c \quad (4.2)$$

for energy (i.e., the adiabatic equation of state),

$$\frac{d}{dt} \left[ P_c \rho_c^{-\gamma} \right] = 0 \quad (4.3)$$

and for the resistive Ohm's law,

$$\mathbf{E} + \frac{1}{c} (\mathbf{U}_c \times \mathbf{B}) = \boldsymbol{\eta} \cdot \mathbf{J}_c \quad (4.4)$$

Here,  $\rho_c = M_i N_i$  is the mass density (approximately given by that of the core plasma ions),  $\mathbf{U}_c$  is the single-fluid center of mass velocity,  $\mathbf{J}_c$  is the sum of the core plasma electron and ion currents,  $P_c$  likewise is the core plasma pressure (assumed to be isotropic), the convective time derivative is  $d/dt = \partial/\partial t + \mathbf{U}_c \cdot \nabla$ ,  $\Gamma_s = 5/3$  is the adiabatic index for the ratio of specific heats of an isotropic fluid, and  $\boldsymbol{\eta} = \eta_{\parallel} \mathbf{b} \mathbf{b} + \eta_{\perp} (\mathbf{I} - \mathbf{b} \mathbf{b})$  is the dyadic resistivity, with  $\mathbf{b} = \mathbf{B}/B$  a unit vector in the direction of the magnetic field  $\mathbf{B}$ ,  $Q_c$  is the charge density,  $\mathbf{E}$  is the electric field, and  $\mathbf{I}$  is the unit dyadic.

The behavior of the non-fluid energetic plasma component will be described by the collisionless Vlasov equation. The appropriate form of the kinetic equation for low-frequency linear perturbations will be quoted shortly. For our purposes at present, we note that Eqs. (4.1) and (4.2) are exact moments of the kinetic equation, and therefore we can write down similar equations that include the hot particle species:

$$\frac{\partial}{\partial t} \rho + \nabla \cdot (\rho \mathbf{U}) = 0 \quad (4.5)$$

$$\rho \frac{d}{dt} \mathbf{U} = \frac{1}{c} (\mathbf{J} \times \mathbf{B}) - \nabla P_c - \nabla \cdot \mathbf{P}_h \quad (4.6)$$

Here,  $\rho = \rho_c + \rho_h$  is the total mass density,  $\mathbf{U}$  and  $\mathbf{J}$  are the total fluid velocity and current, and  $\mathbf{P}_h = P_{\parallel h} \mathbf{b}\mathbf{b} + P_{\perp h} (\mathbf{I} - \mathbf{b}\mathbf{b})$  is the anisotropic pressure of the hot species. Finally, we add the Maxwell equations

$$\nabla \times \mathbf{E} + \frac{1}{c} \frac{\partial}{\partial t} \mathbf{B} = 0 \quad (4.7)$$

$$\nabla \times \mathbf{B} = \frac{4\pi}{c} \mathbf{J}, \quad (4.8)$$

where neglect of the displacement current is valid in the limit of low frequency. Overall charge neutrality implies, furthermore, that  $\nabla \cdot \mathbf{J} = 0$ .

Briefly consider the steady-state equilibrium equations. For simplicity, we assume there is no equilibrium electrostatic potential; hence,  $\mathbf{E} = 0$  and  $J_{\parallel} = 0$  in equilibrium. Neglecting the small resistive equilibrium flow, we obtain from Eqs. (4.6) and (4.8) the equations for perpendicular pressure balance,

$$\frac{1}{B} \nabla_{\perp} B + \left[ \frac{4\pi}{\tau B^2} \right] \nabla_{\perp} P_{\perp} = \left[ \frac{\sigma}{\tau} \right] \mathbf{x} . \quad (4.9)$$

and parallel pressure balance,

$$\mathbf{b} \cdot \nabla P_{\parallel} = \frac{1}{B} (P_{\parallel} - P_{\perp}) \mathbf{b} \cdot \nabla B . \quad (4.10)$$

Here,  $\sigma = 1 + 4\pi (P_{\perp} - P_{\parallel}) / B^2$  and  $\tau = 1 + 4\pi [(1/B^2) (\partial P_{\perp} / \partial B)]$  are the firehose and mirror mode anisotropy coefficients,  $\mathbf{x} = (\mathbf{b} \cdot \nabla) \mathbf{b}$  is the magnetic field line curvature, and  $\nabla = \nabla - (\nabla B) \partial / \partial B$ , with  $P_{\parallel, \perp}$  the components of the total pressure  $\mathbf{P} = \parallel P_c + P_h$ .

We now consider how to express the equations that describe a linear perturbation of the system. We shall assume that perturbed quantities, to be designated with a tilde, vary in time as  $\exp(\gamma t)$ , with  $\gamma$  related to the complex frequency  $\omega$  of the mode by  $\gamma = -i\omega$ . Equations (4.1) - (4.4) for the core plasma yield

$$\mathbf{J}_{\perp c} = \frac{\tilde{\mathbf{E}}_{\perp}}{\eta_{\perp}} , \quad (4.11)$$

$$\mathbf{J}_{\perp c} = \frac{\left\{ \gamma \rho_c \tilde{\mathbf{E}}_{\perp} + \frac{1}{c} \left[ \frac{1}{c} (\mathbf{J}_c \times \tilde{\mathbf{B}}) + Q_c \tilde{\mathbf{E}} - \nabla \tilde{p}_c \right] \times \mathbf{B} \right\}}{\left[ \gamma \rho_c \eta_{\perp} + \frac{B^2}{c^2} \right]} \quad (4.12)$$

and

$$\begin{aligned}
 U_c = & \frac{-\mathbf{b} \cdot (\mathbf{B} \cdot \nabla \beta_c + \mathbf{B}' \cdot \nabla P_c)}{\alpha \rho_c B} \\
 & + \frac{\left\{ \frac{1}{c} (\mathbf{E}'_{\perp} \times \mathbf{B}) + \eta_{\perp} \left[ \frac{1}{c} (\mathbf{J}_c \times \mathbf{B}') + Q_c \mathbf{E}' - \nabla \beta_c \right] \right\}}{\left[ \alpha P_c \eta_{\perp} + \frac{B^2}{c^2} \right]} \quad (4.13)
 \end{aligned}$$

Due to the presence of the hot species, we note that  $Q_c = -e_h N_h \neq 0$ , where  $e_h$  is the (signed) charge of the hot particles and  $N_h$  is their density. However, we wish to consider the energetic component to be very hot, but low in density, such that their pressure is comparable to the core plasma pressure. Therefore, we will take  $N_h/N_i \ll 1$  and let  $Q_c \rightarrow 0$  and thus neglect electrostatic (i.e., charge separation-related) effects in favor of diamagnetic (i.e., pressure-related) effects due to the hot particles.

Also note that in the Ohm's law, we have neglected collisions between the hot particles and the core ions and electrons, since presumably this contribution would be small, on the order of  $N_h/N_i \ll 1$ . Also, most of the parallel current is carried by circulating

electrons, and hence  $\mathcal{J}_{ic} \cong \mathcal{J}_{ie}$  and  $\eta$  refers to Spitzer resistivity. Moreover,  $\mathcal{J}_{ih} \cong 0$  since the hot particles are assumed to be trapped. The perturbed fluid velocity, given in Eq. (4.13), is seen to be dominated by the  $\mathbf{E} \times \mathbf{B}$  contribution. The energetic particles, however, have a negligible  $\mathbf{E} \times \mathbf{B}$  response, due to their large gradient-B drift frequency, which we take to be greater than the fluctuation frequency in this nonresonant theory. Thus, we may neglect  $\tilde{\mathbf{U}}_h$  and, again in the limit  $N_h/N_i \rightarrow 0$ , obtain the perturbed perpendicular current of the energetic component from perturbed pressure balance as

$$\mathcal{J}_{\perp h} \cong \frac{c}{B} (\mathbf{b} \times \nabla \cdot \tilde{\mathcal{P}}_h) - \frac{J_{\perp h}}{B^2} (\mathbf{B} \cdot \tilde{\mathcal{B}}) \quad (4.14)$$

Having solved for the perturbed currents and fluid velocity, we now proceed to derive a set of coupled equations for the remaining field quantities  $\tilde{\mathcal{E}}$ ,  $\tilde{\mathcal{B}}$ , and  $\tilde{\mathcal{P}}$ . Equivalently, if we introduced the electrostatic potential  $\tilde{\phi}$  and the vector potential  $\tilde{\mathcal{A}}$ , where  $\mathbf{E} = -\nabla\tilde{\phi} - \partial\tilde{\mathcal{A}}/c$  and  $\tilde{\mathcal{B}} = \nabla \times \tilde{\mathcal{A}}$ , we need to develop equations relating  $\tilde{\phi}$ ,  $\tilde{\mathcal{A}}_{\parallel}$ ,  $\tilde{\mathcal{A}}_{\perp}$ ,  $\tilde{\mathcal{B}}_{\parallel}$ , and  $\tilde{\mathcal{P}}$ . This will be done in the limit of large toroidal mode numbers,  $n \gg 1$ , such that the variation of a perturbed quantity across a field line is much larger than the variation along the line. Following Chance *et al.*,<sup>20</sup> we therefore adopt the following orderings:

$$\nabla'_{\perp} \sim n \gg 1,$$

$$\nabla'_{\perp} \sim \delta \sim \nabla \sim \beta_c \sim P \sim \tilde{E}_{\perp} \sim \tilde{B} \sim n^2 \eta_{\perp} \sim 1 \quad (4.15)$$

$$\tilde{E}_{\perp} \sim A \sim \tilde{\phi} \sim 1/n \ll 1$$

where  $\nabla'$  means a derivative of a perturbed quantity.

We now derive the field equations.

(1) Vorticity equation: Quasi-charge neutrality implies

$$\nabla \cdot \tilde{\mathbf{J}} = \mathbf{B} \cdot \nabla \left[ \frac{\tilde{J}_{\perp}}{B} \right] + \nabla \cdot \tilde{\mathbf{J}}_{\perp} = 0 \quad (4.16)$$

Since  $\tilde{J}_{\perp} \sim O(n)$ , we should look for terms of the same order in  $\nabla \cdot \tilde{\mathbf{J}}_{\perp}$ . Thus, we obtain

$$\mathbf{B} \cdot \nabla \left[ \frac{\mathbf{B} \cdot \tilde{\mathbf{J}}}{B^2} \right] - \left[ \frac{\alpha \rho_i c^2}{B^2} \right] \nabla_{\perp}^2 \tilde{\phi} + \frac{c}{B} (\mathbf{b} \times \mathbf{x}) \cdot \nabla_{\perp} (2\tilde{\beta}_c + \tilde{\beta}_{th} + \tilde{\beta}_{lh}) = 0 \quad (4.17)$$

(2) Quasi-static force balance equation: If we take the cross product of Eq. (4.6), linearly perturbed, with  $\mathbf{B}$  and note that  $\tilde{\mathbf{J}}_{\perp} \cong -(4\pi/c) \mathbf{b} \times \nabla_{\perp} \tilde{B}_{\perp} \sim O(n)$ , whereas  $\tilde{\mathbf{U}} \cong \tilde{\mathbf{U}}_c \sim O(1)$  from Eq. (4.13), then we obtain

$$\mathbf{B} \times \nabla_{\perp} (\mathbf{B} \cdot \tilde{\mathbf{B}} + 4\pi \tilde{\beta}_{\perp}) = 0. \quad (4.18)$$

This condition expresses the "annihilation" of the compressional Alfvén mode in the low-frequency regime of interest.

(3) Ampere's law: The parallel component of Eq. (4.8) yields

$$-\frac{4\pi}{c} \mathbf{B} \cdot \tilde{\mathbf{J}} = \left[ \frac{4\pi}{c\eta_{\perp}} \right] \left[ \mathbf{B} \cdot \nabla \tilde{\phi} + \frac{\alpha}{c} \mathbf{B} \cdot \tilde{\mathbf{A}} \right] = \nabla_{\perp}^2 (\mathbf{B} \cdot \tilde{\mathbf{A}}) \quad (4.19)$$

(4) Core Plasma Pressure Evolution Equation: Eqs. (4.1) and (4.3) imply

$$\alpha \tilde{\beta}_c + \tilde{\mathbf{U}}_c \cdot \nabla P_c + \Gamma_s P_c \nabla \cdot \tilde{\mathbf{U}}_c = 0 \quad (4.20)$$

The  $O(n)$  part of  $\nabla \cdot \tilde{\mathbf{U}}_c$  is zero, which indicates incompressibility at this order. The next order terms of Eq. (4.20) give

$$\begin{aligned} & \mathbf{B} \cdot \nabla \left[ \frac{1}{\alpha \rho_i B^2} \left[ \mathbf{B} \cdot \nabla \tilde{\beta}_c + \tilde{\mathbf{B}} \cdot \nabla P_c \right] \right] + \left[ \frac{\eta_{\perp} c^2}{B^2} \right] \nabla_{\perp}^2 \tilde{\beta}_c \\ & - \left( \frac{2c}{B} \right) (\mathbf{b} \times \mathbf{x}) \cdot \nabla_{\perp} \tilde{\phi} - \left[ \frac{B^2 + 4\pi P_c \Gamma_s}{B^2 P_c \Gamma_s} \right] \left[ \alpha \tilde{\beta}_c - \frac{c}{B} (\mathbf{b} \times \nabla P_c) \cdot \nabla_{\perp} \tilde{\phi} \right] \\ & - \frac{4\pi}{B^2} \left[ \alpha \tilde{\beta}_{\perp h} - \frac{c}{B} (\mathbf{b} \times \nabla P_{\perp h}) \cdot \nabla_{\perp} \tilde{\phi} + \frac{c}{B} (P_{\perp h} - P_{\parallel h}) (\mathbf{b} \times \mathbf{x}) \cdot \nabla_{\perp} \tilde{\phi} \right] = 0 \end{aligned} \quad (4.21)$$



(5) Energetic species pressure equation: The perturbed tensor pressure for the hot species can be written as

$$\begin{aligned} \tilde{P}_h = & \int d\Gamma \left[ M_h v_{\perp}^2 \mathbf{b} \mathbf{b} + \mu B (\mathbf{I} - \mathbf{b} \mathbf{b}) \right] \tilde{f}_h \\ & + \tilde{\mathbf{B}}_{\perp} \frac{\partial}{\partial B} P_h + \left[ \frac{P_{\parallel} - P_{\perp}}{B} \right] (\mathbf{b} \tilde{\mathbf{B}}_{\perp} + \tilde{\mathbf{B}}_{\perp} \mathbf{b}). \end{aligned} \quad (4.22)$$

The perturbed pressure consists of an intrinsic contribution (the first term) due to the perturbed particle distribution function  $\tilde{f}_h$ , as well as two geometrical contributions associated with perturbing the magnitude (second term) and the direction (third term) of the magnetic field.

The perturbed distribution function (without finite Larmor radius effects) is

$$\tilde{f}_h = e_h \tilde{\phi} \left[ \frac{\partial F_h}{\partial B} \right] - \mu \frac{\tilde{\mathbf{B}}_{\parallel}}{B} \left[ \frac{\partial F_h}{\partial \mu} \right] + \tilde{g}_h \quad (4.23)$$

where  $\tilde{g}_h$  satisfies

$$\left[ \mathbf{v}_{\perp} \mathbf{b} \cdot \nabla - i(\omega - \omega_{dh}) \right] \tilde{g}_h = i(\omega - \omega_{*h}) \frac{\partial F_h}{\partial E} \left[ e_h \left[ \tilde{\phi} - \frac{\mathbf{v}_{\perp} \cdot \tilde{\mathbf{A}}_{\perp}}{c} \right] + \mu \tilde{\mathbf{B}}_{\perp} \right] \quad (4.24)$$

In writing the drift kinetic equation, Eqs. (4.23) and (4.24), we have introduced the usual high-mode-number eikonal representation for the transverse variation of perturbed quantities. In this representation we can express

$$\mathbf{E} = \mathbf{b} \left[ -\mathbf{b} \cdot \nabla \tilde{\phi} - \frac{\gamma}{c} \tilde{A}_{\parallel} \right] - i \tilde{\phi} \nabla S + \frac{i \gamma \tilde{B}_{\parallel}}{c |\nabla S|^2} (\mathbf{b} \times \nabla S)$$

$$\mathbf{A} = \mathbf{b} \tilde{A}_{\perp} - \frac{i \tilde{B}_{\perp}}{|\nabla S|^2} (\mathbf{b} \times \nabla S)$$

$$\mathbf{B} = \mathbf{b} \tilde{B}_{\perp} - i \tilde{A}_{\perp} (\mathbf{b} \times \nabla S)$$

$$\mathbf{J} = \mathbf{b} \tilde{A}_{\perp} |\nabla S|^2 - i \tilde{B}_{\perp} (\mathbf{b} \times \nabla S).$$

It will be desirable in what follows to define

$$\tilde{A}_{\perp} = - \left( \frac{c}{\gamma} \right) \mathbf{b} \cdot \nabla \tilde{\Psi} . \quad (4.25)$$

(The ideal MHD condition,  $\tilde{E}_{\perp} = 0$ , corresponds to  $\tilde{\phi} = \tilde{\Psi}$ ).

As before, we assume that the energetic particles are trapped and satisfy the large bounce frequency condition  $V_{\perp} \mathbf{b} \cdot \nabla \gg \omega_{\text{dh}} \sim \omega$ . Then, we find from Eq. (4.24) to lowest order

$$\mathbf{V}_h \cdot \mathbf{b} \cdot \nabla \left[ \tilde{g}_h + e_h \left[ \frac{\omega - \omega_{*h}}{\omega} \right] \frac{\partial F_h}{\partial E} \Psi \right] = 0. \quad (4.26)$$

The next-order equation then determines  $\tilde{g}_h$  as

$$\begin{aligned} \tilde{g}_h = & - e_h \left[ \frac{\omega - \omega_{*h}}{\omega} \right] \frac{\partial F_h}{\partial E} \Psi \\ & - \left[ \frac{\omega - \omega_{*h}}{\omega - \omega_{dh}} \right] \frac{\partial F_h}{\partial E} \overline{\left[ \tilde{\Phi} - \tilde{\Psi} + \left[ \frac{\omega_{dh}}{\omega} \right] \tilde{\Psi} + \mu \tilde{\mathbf{B}}_h \right]}, \end{aligned} \quad (4.27)$$

where as before the overbar denotes a bounce average.

Thus, we obtain for the perturbed pressure

$$\begin{aligned} P_h = & B \tilde{\mathbf{B}}_h \left[ - \mathbf{b} \cdot \mathbf{b} (\sigma - 1) + (\mathbf{I} - \mathbf{b} \cdot \mathbf{b}) (\tau - 1) \right] \\ & - (\sigma - 1) (B \tilde{\mathbf{B}}_h + \tilde{\mathbf{B}}_h B) \\ & + (\mathbf{I} - \mathbf{b} \cdot \mathbf{b}) \left[ (\tilde{\Phi} - \tilde{\Psi}) B^2 \frac{\partial}{\partial B} \left[ \frac{e_h N_h}{B} \right] + B \tilde{\mathbf{B}}_h (\tau - 1) \right. \\ & \left. - \left[ \frac{c \tilde{\Psi}}{\omega} \right] \mathbf{e} \cdot \nabla P_{\perp h} \right] - \mathbf{b} \cdot \mathbf{b} \left[ (\tilde{\Phi} - \tilde{\Psi}) e_h N_h + B \tilde{\mathbf{B}}_h (\sigma - 1) \right. \\ & \left. + \left[ \frac{c \tilde{\Psi}}{\omega} \right] \mathbf{e} \cdot \nabla P_{\perp h} \right] \end{aligned}$$

$$\begin{aligned}
& - \int d\Gamma \left[ \mathbf{b} \mathbf{b} M_h V_h^2 + (\mathbf{I} - \mathbf{b} \mathbf{b}) \mu B \right] \left[ \frac{\omega - \omega_{*h}}{\omega - \bar{\omega}_{dh}} \right] \\
& \times \left[ \frac{\partial F_h}{\partial E} \right] \left[ e_h (\tilde{\Phi} - \tilde{\Psi}) + e_h \left[ \frac{\omega_{dh}}{\omega} \right] \tilde{\Psi} + \mu \tilde{\beta}_h \right] \quad (4.28)
\end{aligned}$$

At this point we drop the electrostatic terms in Eq. (4.28) by virtue of the condition  $N_h/N_i \ll 1$ ; we consider the nonresonant (i.e., highly energetic) limit  $\omega \ll \bar{\omega}_{dh}, \omega_{*h}$ ; and we recall our large aspect-ratio tokamak equilibrium with circular flux surfaces and radially localized pressure gradients. Because  $P_{\parallel h}/P_{\perp h}$  is of the order of the inverse aspect ratio, we may neglect  $P_{\parallel h}$  and also drop the curvature drift compared to the  $\nabla B$  drift in  $\omega_{dh}$ . Also, since the beta values are small compared to unity, we take  $\sigma, \tau \approx 1$ . We ignore the combination  $e_h (\tilde{\Phi} - \tilde{\Psi}) \propto N_h/N_i \ll 1$ . Then Eq. (4.28) reduces to an expression for the perpendicular component of the pressure:

$$\begin{aligned}
\tilde{\beta}_{\perp h} = & - \left[ \frac{c}{\omega} \right] \tilde{\Psi} (\mathbf{e} \cdot \nabla P_{\perp h}) + \int d\Gamma B \left[ \frac{\mathbf{e} \cdot \nabla F}{\mathbf{e} \cdot \nabla B} \right] \\
& \times \left[ \left[ \frac{\omega_{dh}}{\omega} \right] e_h \tilde{\Psi} + \mu \tilde{\beta}_h \right] \quad (4.29)
\end{aligned}$$

Finally, we introduce the ballooning representation for the perturbed quantities and investigate the stability of modes localized to a single flux surface. In this representation and with our model equilibrium, we recall that  $|\nabla S|^2 \rightarrow (nq/r)^2 (1+h^2)$ ,  $\mathbf{B} \cdot \nabla' \rightarrow (B_T/qR) \times (\partial/\partial\theta)$ ,  $\mathbf{e} \cdot \mathbf{x} \rightarrow -(nq/rRB_T) D(\theta)$ , and  $\mathbf{e} \cdot \nabla \rightarrow (nq/rB_T) (\partial/\partial r)$ . We will again use the square-top profile in poloidal angle  $\theta$  for the hot particle equilibrium pressure. Also, we will be investigating only modes whose integrated local shear,  $h(\theta)$ , vanishes at  $\theta = 0$ .

It is convenient to define the normalized pressure perturbations

$$\hat{p}_c = \frac{\gamma r B_T \tilde{\beta}_c}{i n c q \left[ \frac{dP_c}{dr} \right]}, \quad \hat{p}_{\perp h} = \frac{\gamma r B \tilde{\beta}_{\perp h}}{i n c q \left[ \frac{dP_{\perp h 0}}{dr} \right]} \quad (4.30)$$

It is also convenient to approximate the bounce average integrals in the expression for  $\tilde{\beta}_{\perp h}$ , Eq. (4.29), by line integrals. This approximation (which corresponds to the Schwartz inequality lower bound of Chap. II) does not violate the integrity of the integral nature of the equation, and it improves its tractability. Eliminating  $\tilde{\beta}_{\perp}$  in the integrand by means of quasi-static force balance, Eq.

perturbed fields. However, the analysis can be nontrivially simplified by working with a lower bound,  $\delta W_1$ , for the kinetic potential energy: *i.e.*,  $\delta W_1 \leq \delta W_k$ . This lower bound is derived by an application of the Schwartz inequality in the integral over velocity space. Unfortunately, the use of the Schwartz inequality imposes a maximum value on the hot particle pressure, since it requires that the hot particles not be drift reversed. Thus, the stability condition given by  $\delta W_k + \delta W_1 \geq 0$  in the non-resonant limit becomes only a sufficient, but not necessary, condition for stability. Therefore working with a lower bound for the kinetic potential, Rosenbluth *et al.* obtained a pessimistic estimate of stability. By solving the integro-differential equation for the ballooning mode perturbation in the ballooning space<sup>37</sup>, they found that direct access to the high-beta second stable regime for ballooning modes can be provided by the presence of the energetic particles.

In their treatment, however, an unexpectedly pessimistic result for the first stability boundary is obtained at large values of the global shear. This result was a consequence of using a pessimistic estimate of the total energy, which apparently is not very realistic at moderately large values of  $S$ . In the present work, we adopt their same assumptions and equilibrium model, but

$$\begin{aligned}
& + \frac{2\Gamma_s P_c}{RP'_c} D(\theta) \tilde{\phi} - \left[ \frac{\omega_s}{\omega_A} \right]^2 \left[ \frac{P'_{\perp h0}}{P'_c} \right] \times \\
& \left[ P_{\perp h} - H \tilde{\phi} - \left[ \frac{P'_{\perp h0}}{RP'_{\perp h0}} \right] H D(\theta) \tilde{\phi} \right] \quad (4.34)
\end{aligned}$$

Again,  $H = H(\theta_0 - |\theta - 2\pi l|)$ , and Eqs. (4.31) to (4.34) above are written for  $\theta$  in the interval  $(2\pi l \pm \pi)$ . We have defined  $\omega_s = c_s/qR$  and also

$$v_{\parallel, \perp} = \left[ \frac{nq}{r} \right]^2 \left[ \frac{c^2 \eta_{\parallel\perp}}{4\pi} \right] \quad (4.35)$$

in the remainder of this study we will assume isotropic resistivity,  $v_{\parallel, \perp} = v_r$ . Note that  $v_r = (nq)^2/\tau_r$ , where  $\tau_r = r^2/D_r$  is the resistive diffusion time and  $D_r = (c^2\eta/4\pi)$  is the resistive diffusion coefficient. Equations (4.31) to (4.34) will constitute the basic equations for our study of the effects of highly energetic particles on resistive ballooning stability.

Note that there are several space scales associated with Eqs. (4.31) - (4.34). Since  $h(\theta)$  is given by  $1 + S^2 \theta^2$  apart from oscillatory terms, we see that in the ideal region,  $\theta \sim 1$ , resistivity

and inertia may be neglected. They become significant at larger distances when  $\theta \sim \theta_r = (\gamma/v_r S^2)^{1/2} \gg 1$  and  $\theta \sim \theta_i = \omega_A/\gamma S \gg 1$ . The parallel compressibility and cross-field transport enter, respectively, when  $\theta \sim \theta_s = \omega_s/\gamma \gg 1$  and  $\theta \sim \theta_t = (\gamma/v_r S^2)^{1/2} \times (\omega_A/\omega_s) \gg \theta_r \gg 1$ . A self-consistent ordering for the growth rate  $\gamma$  is obtained when we order  $\theta_r \sim \theta_i$  and  $\theta_s \sim \theta_t$ ; this yields the basic resistive ballooning scaling of  $\gamma \sim \eta^{1/3}$ . In the following sections, we will solve Eqs. (4.31)-(4.34) in each of the three regions  $\theta \sim 1$ ,  $\theta \sim \theta_r$ , and  $\theta \sim \theta_s$  and match the solution to obtain the dispersion relation.

#### 4.3 SOLUTION IN THE IDEAL REGION

In this section we solve the eigenmode equations in the ideal region,  $S\theta \sim 1$ . In this region, all resistive and inertial effects may be ignored, and the equations reduce to the ideal ballooning mode equation, which we solve numerically to obtain values for the  $\Delta'$  quantity.

Analytically, it is very difficult to solve the ideal equation except for low beta. Thus, we will obtain analytical expressions for



$\Delta'$  in the low shear, low beta limit ( $\alpha_c \sim \alpha_h \sim S \ll 1$ ) and in the finite shear, low beta ( $\alpha_c \sim \alpha_h \ll 1, S \sim 1$ ) limit. Also, we obtain  $\Delta'$  analytically in two special limiting cases, one when  $\alpha_c = 0$  but  $\alpha_h$  is finite, and another when  $\alpha_h = 0$  and  $\alpha_c \ll 1$ .

#### 4.3.a NUMERICAL SOLUTION FOR $\Delta'$

Numerically,  $\Delta'$  was obtained by comparing the computed solution with the known asymptotic expression given in Eq. (3.44):

$$\Phi_{\text{ideal}} \sim M\theta^\mu \left[ 1 + \frac{f_1(\tilde{\theta})}{\theta} + \frac{f_2(\tilde{\theta})}{\theta^2} + \dots \right] + N\theta^{-1-\mu} \left[ 1 + \frac{\bar{f}_1(\tilde{\theta})}{\theta} + \dots \right]$$

where the Mercier exponent  $\mu$  has been previously defined in Eqs. (3.41) and (The function  $\bar{f}_1$  is the same as  $f_1$  except that  $\mu$  is replaced by  $-1-\mu$ .)

The functions  $f_1(\tilde{\theta})$  and  $f_2(\tilde{\theta})$  can be determined analytically by solving the large- $\theta$  version of the ballooning mode equation in successive powers of  $Z^{-1} \ll 1$ . Knowledge of  $f_1$  and  $f_2$  becomes useful when  $\alpha_h$  increases so as to make  $\mu$  finite. Specifically,  $f_m$  becomes significant when  $\mu \gtrsim (m-1)/2$ , and it must

be subtracted away before the coefficient,  $N$ , of the "small" term can be extracted. By integrating the equation for  $\Phi$  with the appropriate choice of parity at the origin and then comparing its values at successive points, e.g., at  $\theta = 2\pi l$  and  $2\pi(l+1)$ , for  $l \gg 1$ , we numerically obtain  $M$  and  $N$ . In Figs. (4.1) and (4.2), we present the results for  $\Delta' = N/M$  for  $\alpha_h = 0$ ,  $\alpha_h = 1.0$  and  $\alpha_h = 1.5$ , with even and odd parity, respectively.

#### 4.2.b ANALYTICAL SOLUTIONS FOR $\Delta'$

To be able to solve the ideal ballooning mode equation analytically almost always requires that one work in the low beta limit because of the mix of oscillatory and secular  $\theta$ -dependence in the coefficients of the differential equation. By considering low beta, it is possible to solve the differential equation order by order. In this way we have been able to obtain  $\Delta'$  analytically in the following cases.

(i) Low beta and low shear:  $\alpha_c \sim \alpha_h \sim S \ll 1$ .

When the shear is small we can work in the  $Z = S\theta \sim 1$  realm, but still expand the hot particle integral term as in Eq. (3.38) for

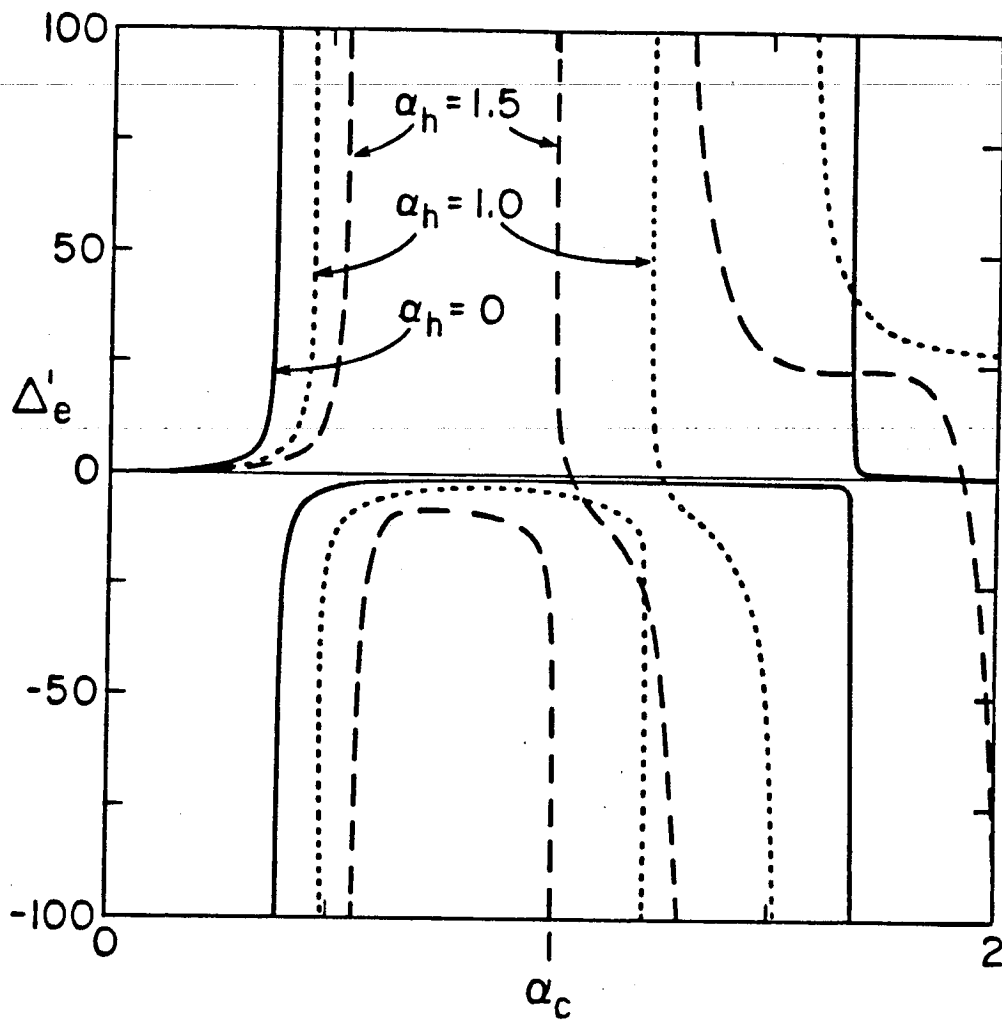


Fig. 4.1 Numerical results for  $\Delta'_e = N_e/M_e$   
for various values of  $\alpha_h$ .

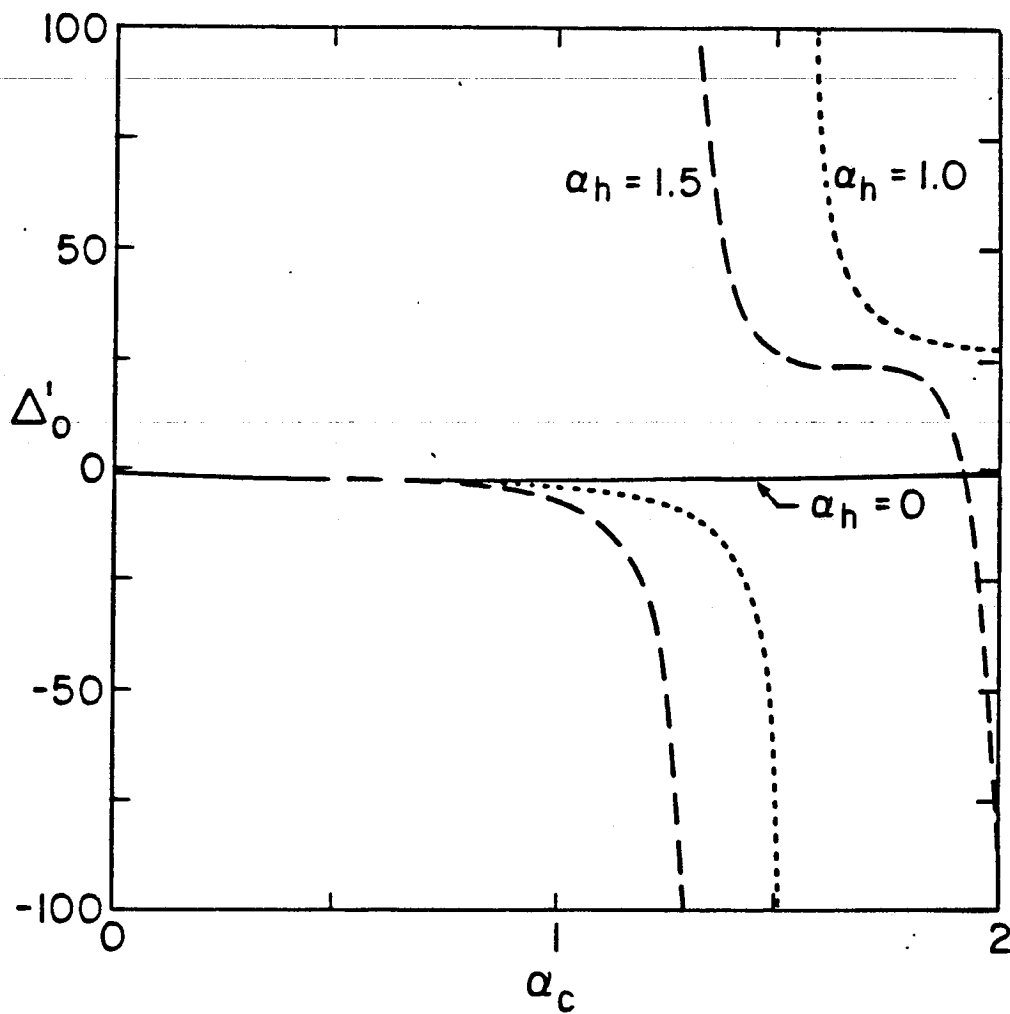


Fig. 4.2 Numerical results for  $\Delta_0' = N_0/M_0$

for various values of  $\alpha_h$

$\theta > 1$ . Introducing the secular and periodic space scales  $Z$  and  $\tilde{\theta}$ , respectively, where both are formally of  $O(1)$ , and expanding the solution  $\Phi$  in powers of  $\alpha_c = \epsilon \ll 1$ , as

$$\Phi = \Phi_0(Z) + \epsilon \Phi_1(\tilde{\theta}, Z) + \epsilon^2 \Phi_2(\tilde{\theta}, Z) + \dots, \quad (4.36)$$

we obtain a differential equation for the nonoscillatory part  $\Phi_0(Z)$

$$\frac{d}{dZ} (1+Z^2) \frac{d}{dZ} \Phi_0 - \mu_0 \Phi_0 = 0 \quad (4.37)$$

$$\text{with } \mu_0 = \left[ \frac{\alpha_c \alpha_h}{4\pi S^2} \right] \left[ \theta_0 \left[ 1 + \frac{1}{q^2} \right] - \frac{\sin(2\theta_0)}{2} \right].$$

The first and third terms in the square bracket on the left-hand side represent the curvature averaged over the trapped particle region; the second term in the square bracket represents the magnetic compression due to the hot particles, which in this low beta limit reduces to the so-called "ring" rigid response. Note that  $\mu_0$  is, in fact, the low beta/low shear limit of the Mercier exponent  $\mu$  given in Eq. (3.43).

Equation (4.37) has an exact solution:

$$\Phi_0(Z) = A \left[ P_{\mu_0}(t) + B Q_{\mu_0}(t) \right] \quad (4.38)$$

where  $t = iZ$  and where  $P_{\mu_0}$  and  $Q_{\mu_0}$  are Legendre functions of first order. By using the small argument forms for the Legendre functions, <sup>(40)</sup> we can determine the coefficient  $B$  by the choice of parity at the origin and the coefficient  $A$  by the normalization at the origin: *viz.*,  $\Phi_e(0) = 1$ ,  $\Phi_e'(0) = 0$ ,  $\Phi_o(0) = 0$ , and  $\Phi_o'(0) = 1$  where  $\Phi' = d\Phi/d\theta = Sd\Phi/dZ$ . Then we employ the large argument forms for the Legendre functions and extract the coefficients of the "large" and "small" terms. This process yields

$$\Delta'_e = \frac{\left[ \sin \left[ \frac{\pi\mu_0}{2} \right] \Gamma \left[ 1 + \mu_0 \right] \right]^2}{2^{2\mu_0} \cos(\pi\mu_0) \left[ \mu_0 + \frac{1}{2} \right] \left[ \Gamma \left( \frac{1}{2} + \mu_0 \right) \right]^2} \quad (4.39)$$

$$\Delta'_o = - \frac{\left[ \cos \left[ \frac{\pi\mu_0}{2} \right] \Gamma \left[ 1 + \mu_0 \right] \right]^2}{2^{2\mu_0} \cos(\pi\mu_0) \left[ \mu_0 + \frac{1}{2} \right] \left[ \Gamma \left( \mu_0 + \frac{1}{2} \right) \right]^2} \quad (4.40)$$

respectively, for the even and odd parity modes.

In Figs. 4.3 and 4.4 we have plotted these expressions for  $\Delta'_e$  and  $\Delta'_0$ .

The Legendre function solution for  $Z \sim 1$  (*i.e.*,  $\theta > 1$  since  $S \ll 1$ ) has also been checked against the solution for the non-oscillatory part of the eigenmode for  $\theta \sim 1$  (*i.e.*,  $Z \ll 1$ ). To obtain the solution in this latter region, we first expand the ballooning equation in powers of  $\alpha_c$  and then solve the equation corresponding to each order in individual trapped and untrapped intervals. We match the values for  $\Phi$  and  $\Phi'$  between successive intervals to satisfy continuity. This matching yields a difference equation for the secular (*i.e.*, nonoscillatory) part of the eigenmode, which in the  $\ell^{\text{th}}$  untrapped region, where  $\ell \gg 1$ , is given by

$$\Phi_{\ell \text{ even}} \left| \begin{array}{l} \sim 1 + \left[ \frac{a_0}{2} \right] (2\pi \ell S)^2 \approx 1 + \left[ \frac{a_0}{2} \right] Z^2. \\ \text{non-oscillatory} \end{array} \right. \quad (4.41)$$

This result is identical to what one obtains from the Legendre function solution of Eq. (4.38) in the limit  $Z \ll 1$ . Hence, the Legendre function solution is valid even for small  $Z$ , the reason being that the hot particle integral term does not contribute to the  $O(1)$  equation for  $\Phi_0(Z)$ , which contains the information about parity at  $\theta = 0$ .

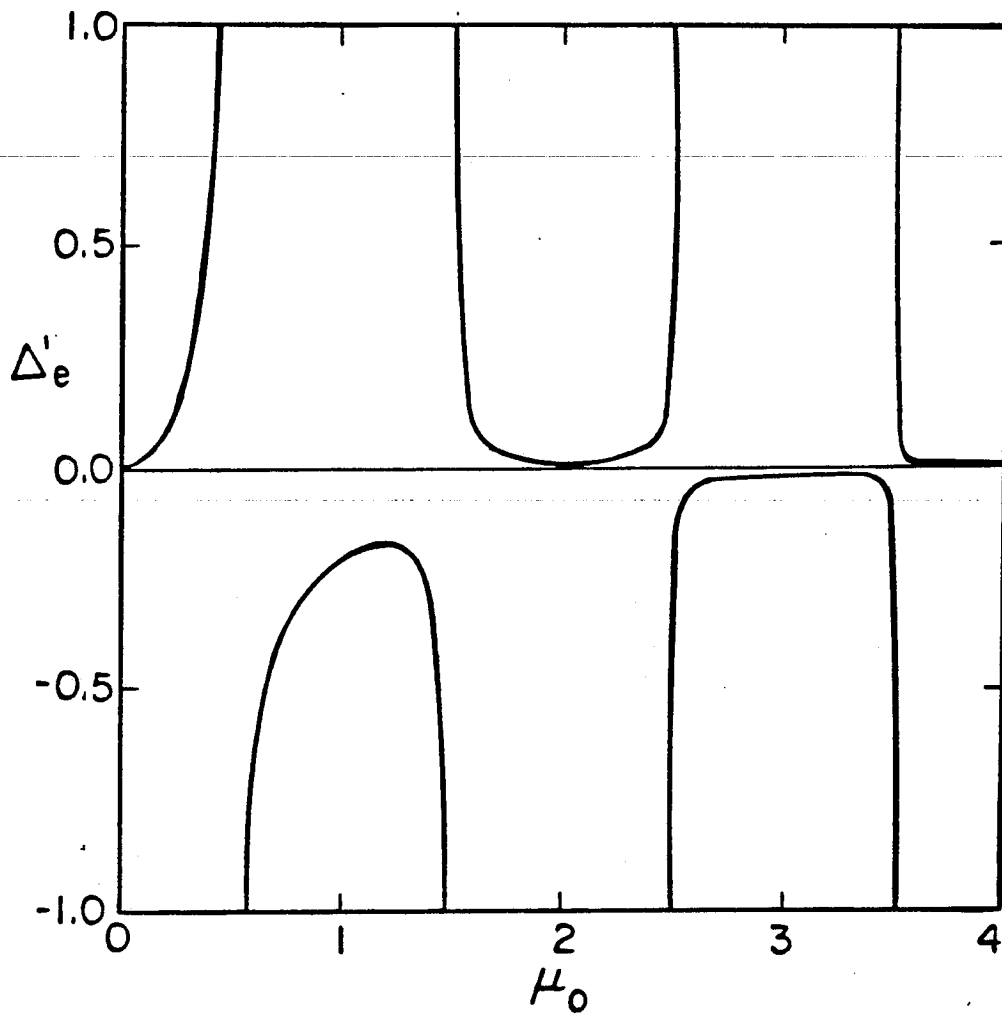


Fig. 4.3 Resistive parameter  $\Delta'_e$  in the limit of small  $\alpha_c$ ,  $\alpha_h$ , and  $S$ .



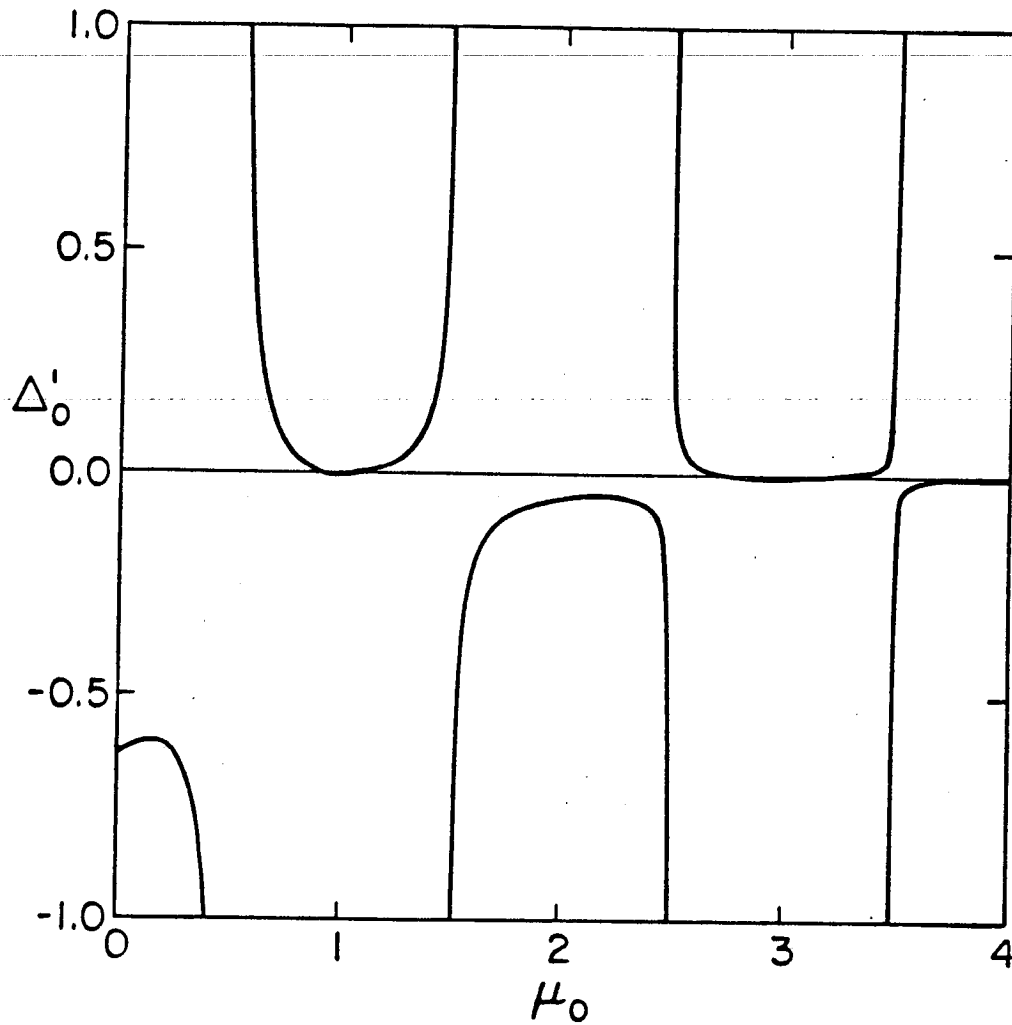


Fig. 4.4 Resistive parameter  $\Delta'_0$  in the limit of small  $\alpha_c$ ,  $\alpha_h$ , and  $S$

(ii) Low beta, but finite shear:  $\alpha_c \sim \alpha_h < 1$ ,  $S \sim O(1)$ .

We were motivated to study the finite shear limit by analogy with the work of Drake and Antonsen (without hot particles),<sup>54</sup> which showed that the low shear results for  $\Delta'$  derived by Strauss<sup>55</sup> could be generalized to the  $S \sim O(1)$  case.

In this limit, we again expand the solution  $\Phi$  and the ballooning equation in powers of the small parameter  $\alpha_c \ll 1$ , but we consider  $S$  to be finite. We solve the ballooning equation up to second order in  $\alpha_c$  and use the low beta relationship<sup>56</sup>

$$\Delta' = \frac{N}{M} \approx -\frac{1}{S\Phi_0} \lim_{\theta \rightarrow \infty} \left[ \left( 1 + S^2 \theta^2 \right) \frac{d\Phi_2}{d\theta} \right]_{\text{non-oscillatory}}, \quad (4.42)$$

which is valid for low beta - *i.e.*, when the Mercier exponent is small,  $\mu \ll 1$ . We obtain

$$\Delta'_{\text{even}} = \left[ \frac{\alpha_c}{2S} \right]^2 \pi (S + 2) \left[ 1 - \frac{S+2}{S} e^{-2/S} \right] \quad (4.43)$$

and

$$\Delta'_{\text{odd}} = -S^{-2} \quad (4.44)$$

However, the results for  $\Delta'$  given in Eq. (4.43) do not depend on  $\alpha_h$  and are, in fact, the same as the Drake-Antonsen results without hot particles.<sup>54</sup> The reason for this result is that  $(\alpha_c \alpha_h)/S^2 \sim O(1)$  is required to obtain a contribution from hot particles that is of the same order as the core plasma effects, as in the previous case treated in part (i).

(ii) Special zero beta cases:

$$(a) \alpha_c = 0, \alpha_h \neq 0.$$

When  $\alpha_c = 0$ , the even parity solution of the ideal ballooning mode equation is trivially seen to be

$$\Phi_{\text{even}} = 1 \quad (4.45)$$

Hence the corresponding Mercier coefficients are  $M_e = 1$  and  $N_e = 0$

The coefficient  $N_0$  can be easily found by using Eq. (3.44) for  $\Phi_{\text{odd}}$ .

We find

$$N_{\text{odd}} = \frac{-\left[\frac{1}{S^2}\right]}{\left[1 + \left[\frac{\alpha_h}{2S}\right] (1 - \Lambda_0) \left[\frac{t_0}{\pi}\right]\right]} \quad (4.46)$$

where  $\Lambda_0 = \sin\theta_0/(\sin\theta_0 + St_0)$  and  $t_0 = \sin\theta_0 - \theta_0 \cos\theta_0$ . In Fig. 4.5 we show the various Mercier coefficients, obtained numerically and plotted as functions of  $\alpha_h$  for the case when  $\alpha_c = 0$ . These agree very well with the analytic solutions in Eqs. (4.45) and (4.46). Note that the  $\alpha_h$  dependence is very weak for the odd modes and absent for the even modes.

$$(b) \alpha_h = 0, \alpha_c \ll 1.$$

As before, we expand the solution  $\Phi_0$  and the ballooning equation in powers of  $\varepsilon = \alpha_c \ll 1$ . Also, we employ the optimal ordering,  $S \sim O(\varepsilon^2)$  which is traditional in the absence of any hot particles. Proceeding to second order in  $\varepsilon$ , we obtain a solubility condition that yields the equation for the average part of the eigenfunction,  $\Phi_0(Z)$ :

$$\frac{d}{dZ} (1+Z^2) \frac{d}{dZ} \Phi_0 + \frac{\lambda}{(1+Z^2)^2} \Phi_0 = 0 \quad , \quad (4.47)$$

with

$$\lambda = \frac{2\alpha_c^2}{S} \left[ 1 - \frac{3}{16} \frac{\alpha_c^2}{S} \right] \sim 0 \quad (1) \quad (4.48)$$

In the  $\lambda \ll 1$  limit we can solve Eq. (4.47) perturbatively for the even parity solution:

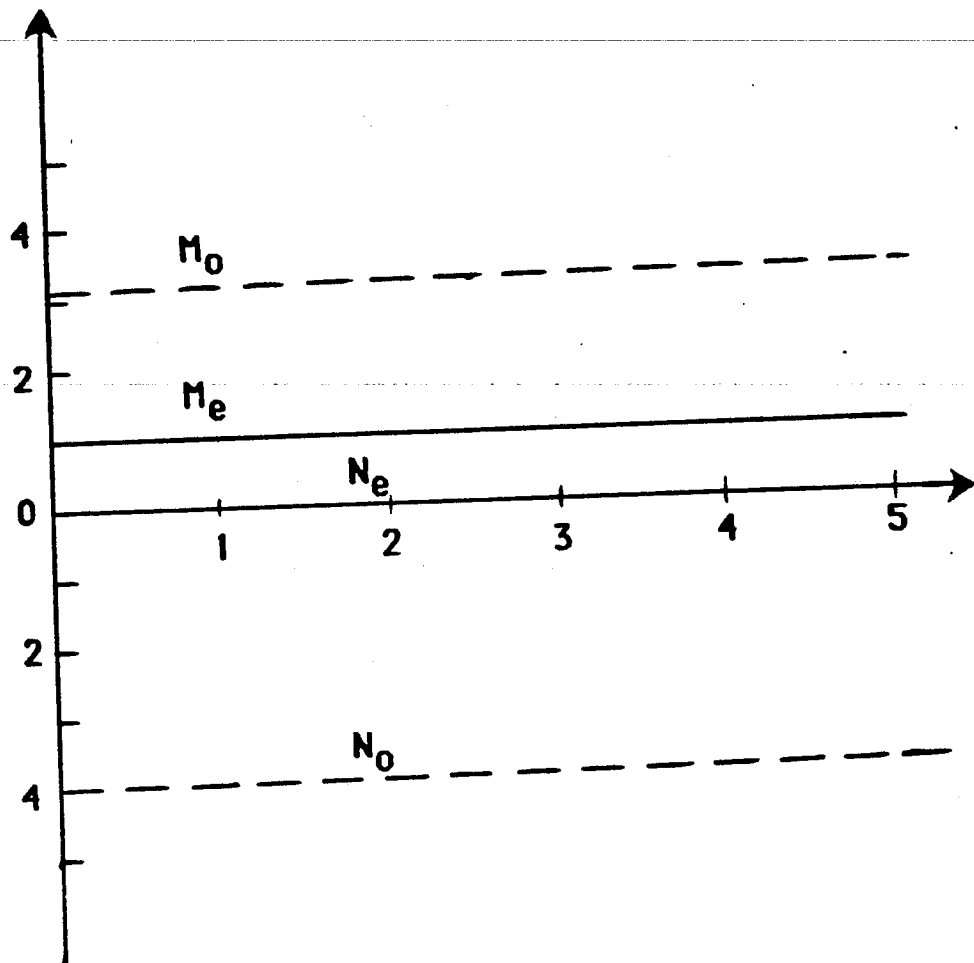


Fig. 4.5 Mercier coefficients for  $S = 0.5$ ,  
 $\theta_0 = \pi/4$ ,  $q = 1.5$ ,  $\theta_k = 0$ , and  $\alpha_c = 0$

$$\Phi_e \cong 1 + \left[ \frac{\lambda}{4} \right] \left[ (1 + Z^2)^{-1} - 1 - (\tan^{-1} Z)^2 \right] . \quad (4.49)$$

Considering the large  $Z$  limit for of this solution, we find

$$\Delta'_{\text{even}} \cong \frac{\pi \lambda}{4} \quad (4.50)$$

The odd parity solution is  $\Phi_0 = (1/S) \tan^{-1} Z$ , where the  $O(\lambda)$  correction is not necessary in order to obtain

$$\Delta'_{\text{odd}} \cong -\frac{2}{\pi} \quad (4.51)$$

For finite  $\lambda$ , we can find the solution by changing the independent variable to  $\xi = \tan^{-1} Z$ . Then Eq. (4.47) transforms to the Mathieu equation

$$\left[ \frac{d^2}{d\xi^2} + \frac{\lambda}{2} \left[ 1 + \cos 2\xi \right] \right] \Phi_0(\xi) = 0 \quad (4.52)$$

Let us consider the even parity solution at marginal stability. The eigensolution that is even about  $\xi \approx Z \approx 0$  and that satisfies the condition  $\Phi_0(\xi = \pi/2) = 0$ , which assures that  $\Phi_0(Z) \rightarrow 0$  for  $Z \rightarrow \infty$  (marginally stable), is

$$\Phi_0(\xi) = \frac{ce_1\left[\xi, -\frac{\lambda}{4}\right]}{ce_1\left[0, -\frac{\lambda}{4}\right]} \quad (4.53)$$

where  $ce_1$  is the first-order even periodic Mathieu function.<sup>57</sup> Using the power series for the characteristic value of this eigenmode,

$$\left[\frac{\lambda}{2}\right] \cong 1 + \left[-\frac{\lambda}{4}\right] - \left[-\frac{\lambda}{4}\right]^2 \frac{1}{8} + \left[-\frac{\lambda}{4}\right]^3 \frac{1}{64} - \dots \quad (4.54)$$

we obtain  $\lambda = 1.32$  at marginal stability. Also, we can examine the asymptotically large  $Z$  behavior of the solution by putting  $\xi = \pi/2 - 1/Z$  and expanding for  $Z^{-1} \ll 1$ :

$$\Phi_0 \approx -Z^{-1} \frac{ce_1\left[\frac{\pi}{2}, -\frac{\lambda}{4}\right]}{ce_1\left[0, -\frac{\lambda}{4}\right]} \quad (4.55)$$

Eq. (4.55) thus provides the value of  $N_e$  at marginal stability (where  $M_e = 0$ ); using the power series to evaluate the periodic functions, we find  $N_e = 0.85$ .

We can compare this result with the plot of  $N_e$ , for  $\alpha_h = 0$ , shown in Fig. 3.6. For  $S = 0.5$ , Eq. (4.48) shows that our calculated

value of  $\lambda = 1.32$  gives two marginal values,  $\alpha_c = 0.62$  and  $\alpha_c = 1.51$ . In Fig. 3.6, the zero-crossings of  $M_e$  (first and second stability points) occur at  $\alpha_c = 0.4$  and  $1.7$ , for which the corresponding values of  $N_e = 1.00$  and  $0.14$  were computed by solving the ballooning mode equation numerically. The analytical solution is fairly good at the first stability threshold, but not so good at second stability, which is understandable in view of the small beta assumption.

Marginal stability can also be studied variationally with a trial solution, for example,  $\Phi_0(Z) = a/\sqrt{a^2 + Z^2}$ . We find two stationary points for  $\lambda$ , the eigenvalue, as a function of  $a$ . One, at  $a = 1.00$ , yields  $\lambda = 1.33$  and  $N_e = 1.00$ ; however, although this point is stationary, it is not a minimum for  $\lambda(a)$ . The other, at  $a = 0.86$ , is a true minimizing value and gives  $\lambda = 1.32$  and  $N_e = 0.86$ , thus reproducing the Mathieu function results.



#### 4.4 SOLUTION IN THE RESISTIVE REGION

Having obtained numerical and analytical solutions in the ideal region ( $\theta \sim 1$ ), we now proceed to examine Eqs. (4.31)-(4.34) in the large- $\theta$  resistive region.

We can derive the asymptotic form of these equations by decomposing the  $\theta$  dependence of the field quantities as follows:

$$\tilde{\Phi}(\theta) = \Phi_0(Z) + \Phi_1(\tilde{\theta}_1 Z) + \Phi_2(\tilde{\theta} Z) + \dots \quad (4.56)$$

and likewise for  $\tilde{\Psi}$ ,  $\hat{P}_c$ , and  $\hat{P}_{\perp h}$ ; here  $\tilde{\theta} = \theta$  modulo  $2\pi$  represents the rapid periodic variation and  $Z=S\theta$  the slow, averaged behavior. As before in Chap. III, we expand the equation in powers of  $Z^{-1} \ll 1$ , where  $\Phi_1 \sim O(Z^{-1})$ , etc., and solve order by order. As for the resistive and inertia terms, we adopt the following maximal orderings:

$$\begin{aligned} v_r/\gamma &\sim (\gamma/\omega_A)^2 \sim v_r\omega_s^2/\gamma\omega_A^2 \sim O(Z^{-2}) \\ (\omega_s/\gamma)^2 &\sim Z^2 \end{aligned} \quad (4.57)$$

The lowest order solutions are easily obtained. Note that the lowest order of Eqs. (4.31) and (4.32) is ostensibly  $O(1)$ , whereas the lowest order of Eqs. (4.33) and (4.34) is  $O(Z^2)$ ; however, we treat them all simultaneously. One finds trivially that  $\Phi_0$ ,  $\Psi_0$ , and  $P_{c0}$  are functions only of  $Z$ . Expanding the integral term on the right-hand side of Eq. (4.31) for  $\theta \gg 1$ , one finds that

$$P_{ho}(Z) = H \left[ \theta_0 - |\tilde{\theta}| \right] \left[ \Psi_0(Z) - \frac{\lambda_0(Z)}{\Delta} \right]. \quad (4.58)$$

Here,

$$\lambda_0 = I \Psi_0(Z) + JZ \frac{d\Psi_0}{dZ} + Z\beta(Z) + (\alpha_c \theta_0/q^2) \left[ P_{c0}(Z) - \Psi_0(Z) \right] \quad (4.59)$$

$$\text{with } I = \int_{-\theta_0}^{\theta_0} d\tilde{\theta} D(\tilde{\theta}), \quad J = \int_{-\theta_0}^{\theta_0} d\tilde{\theta} S\tilde{\theta} \sin\tilde{\theta}, \quad \beta(Z) = \int_{-\theta_0}^{\theta_0} d\tilde{\theta} \sin\tilde{\theta} \Psi_1(\tilde{\theta}, Z),$$

$$\text{and } \Delta = 1 - (\alpha_c \theta_0/q^2).$$

The next order equations are slightly more complicated. As becomes clear from the expression (4.58) for  $P_{ho}$ , they involve an integro-differential equation in  $\tilde{\theta}$  for  $\Psi_1(\tilde{\theta}, Z)$ , which can be solved by the method of solution for a Fredholm equation with a separable kernel.<sup>45</sup>

The equations for the next, or "second", order are then averaged over the periodic  $\tilde{\theta}$  variation to give the so-called distilled equations for the average field quantities  $\Phi_0(Z)$ , etc. The algebra is somewhat tedious although straightforward, and so we do not reproduce it here (see appendix B).

Finally, we note that  $(\omega_s/\omega_A)^2 = 4\pi \Gamma_s P_c/B^2 \ll 1$  by our assumption of low beta and that  $P_c/RP_c' \ll 1$  by virtue of our localized gradient equilibrium model. Dropping these terms in the equation for the core plasma pressure, we obtain the following system:

$$\left[ 1 + \left[ \frac{v_r \omega_s^2}{\gamma \omega_A^2} \right] Z^2 \right] P_{co} = \left[ \frac{S\omega_s}{\gamma} \right]^2 \frac{d^2}{dZ^2} (P_{co} - \Psi_0) + \phi_0 \quad (4.60)$$

$$\frac{d}{dZ} \left[ Z^2 \frac{d\Psi_0}{dZ} \right] - \left[ \frac{\gamma}{S\omega_A} \right]^2 \frac{Z^2}{(1+\eta_h)} \Phi_0$$

$$-\beta_t \hat{D}_h \left[ P_{co} + \frac{ZJ}{2 \sin\theta_0} \frac{d}{dZ} (P_{co} - \Psi_0) \right] = 0 \quad (4.61)$$

$$\left[ 1 + \left[ \frac{v_r}{\gamma} \right] Z^2 \right] \frac{d\Psi_0}{dZ} = \frac{d\Phi_0}{dZ} \quad (4.62)$$

In Eq. (4.61),  $\eta_h$  is the same quantity as was previously defined in Eq. (3.57), and  $\beta_1 \hat{D}_h = \mu(\mu+1) = D_h$  where  $\mu$  is the Mercier exponent for the ideal ballooning mode and the quantity  $D_h$  is defined in Eq. (3.42).

Looking at Eqs. (4.60) - (4.62), we see that the resistive region can be divided into two subregions: one a region of intermediate resistivity where  $(v_r Z^2/\gamma) \sim O(1)$ , the other being the so-called deeply resistive region at still larger values of  $Z$  such that  $(v_r Z^2/\gamma) \sim (\omega_A/\omega_s)^2 \gg 1$ . We shall examine each of these regions in turn.

(i) Intermediate Resistivity Region:

Following Drake and Antonsen,<sup>54</sup> introduce the quantities

$$\gamma_r^3 = v_r S^2 \omega_s^4 / \omega_A^2$$

$$\beta_t = (\omega_s / \omega_A)^2$$

$$Z_t^2 = \gamma \omega_A^2 / v_r \omega_s^2$$

as well as the dimensionless variables  $W = Z/Z_t$  and  $\hat{\gamma} = \gamma/\gamma_r \sim O(1)$ .

Then the intermediate resistivity region corresponds to  $W^2 \sim \beta_1 \ll 1$ . Parallel resistivity effects [in Eq. (4.63)] are important here, whereas sonic compressibility [the first term on the right hand side of Eq. (4.60) and cross-field transport [the second term on the left hand side of Eq. (4.60)] do not contribute until  $W^2 \sim 1$ . Therefore, in the intermediate resistivity region ( $W^2 \sim \beta_1$ ), the resistive equations reduce to

$$\frac{d^2}{dW^2} (P_{co} - \Psi_0) = 0 \quad (4.63)$$

$$\frac{d}{dW} \left[ W^2 \frac{d\Psi_0}{dW} \right] = 0 \quad (4.64)$$

$$\left[ 1 + \frac{W^2}{\beta_1} \right] \frac{d\Psi_0}{dW} = \frac{d\Phi_0}{dW} \quad (4.65)$$

which can be easily solved to give

$$\Phi_0(Y) = a_1 - a_2 \left[ Y - \frac{1}{Y} \right] \quad (4.66)$$

$$\Psi_0(Y) = a_3 + a_2/Y \quad (4.67)$$

$$P_{co}(Y) = a_4 + a_5 Y + a_2/Y \quad (4.68)$$

where  $Y^2 = w^2/\beta_1 \sim O(1)$ . Note that for  $Y \ll 1$ , *i.e.*, approaching the ideal region, we recover  $\Phi_0 \approx \Psi_0 \approx P_{c0}$  as expected.

Also note that the dominant behavior of  $\Phi_0$  at small  $Y$  matches to the large- $\theta$  asymptotic form for  $\Phi$  in the ideal region as long as the Mercier exponent  $\mu \ll 1$ , which is guaranteed in the present analysis by our taking  $\hat{\Delta}_h \sim O(1)$ . This latter ordering means that the Mercier condition for interchange stability in the presence of energetic particles is well satisfied,  $|\beta_1 \hat{\Delta}_h| \ll 1/4$  and insures that the ideal stability properties do not dominate the behavior of the resistive modes. If we keep the  $O(\beta_1)$  terms in this intermediate resistivity region as small corrections, we can solve perturbatively to obtain  $\Phi_0$  up to next order as

$$\begin{aligned} \Phi_0 &= \left[ a_1 - a_2 \left[ Y - \frac{1}{Y} \right] \right] + \beta_1 \hat{\Delta}_h \left[ a_1 \left[ \ln Y + \frac{1}{2} Y^2 \right] \right. \\ &\quad \left. + a_6 \left[ \frac{1}{2} Y + \frac{1}{6} Y^3 \right] + a_2 \left[ Y \ln Y - Y - \frac{\ln Y}{Y} - \frac{1}{Y} \right] \right] \\ &\xrightarrow{Y \ll 1} a_1 (1 + \beta_1 \hat{\Delta}_h \ln Y) + \frac{a_2}{Y} (1 - \beta_1 \hat{\Delta}_h \ln Y) \\ &\cong a_1 Y^\mu + a_2 Y^{-1-\mu} \end{aligned} \tag{4.69}$$

where  $\mu = -1/2 + \sqrt{(1/4) + \beta_1 \hat{D}_h} \approx \beta_1 \hat{D}_h$ . The logarithmic correction terms, therefore, demonstrate the proper matching to the asymptotic ideal solution.

(ii) Deeply Resistive Region :

In this region, we have  $W^2 \sim 1$  and the equations become

$$(1 + W^2) P_{co} = \hat{\gamma}^{-3} \frac{d^2}{dW^2} P_{co} + \Phi_0 \quad (4.70)$$

and

$$\frac{d^2}{dW^2} \Phi_0 - \left[ \frac{\hat{\gamma}^3}{1 + \eta_h} \right] W^2 \Phi_0 - \hat{D}_h P_{co} + \hat{D}_h \left[ \frac{J}{2 \sin \theta_0} \right] \left[ W \frac{dP_{co}}{dW} \right] = 0. \quad (4.71)$$

Note that this region is electrostatic, since  $W^2(d\Psi_0/dW) = \beta_1(d\Phi_0/dW)$  implies that  $\Psi_0$  may be neglected (*i.e.*,  $\tilde{A}_1 \rightarrow 0$ ). At this point, for the sake of tractability, we will take the energetic particles to be deeply trapped:  $\theta_0 \ll 1$ . Then we may drop the last term in Eq. (4.71), since  $J = 2S(\sin\theta_0 - \theta_0 \cos\theta_0) \sim O(\theta_0^3)$ , and we may neglect  $\eta_h \sim O(\theta_0^5) \ll 1$ . Equations (4.70) and (4.71) are now coupled equations of the parabolic cylinder form and their solution is

$$\Phi_0 = a_7 U(c_+, x) + a_8 U(c_-, x) \quad (4.72)$$

and

$$P_{co} = - \left[ \frac{2 \hat{\gamma}^{3/2}}{\hat{D}_h} \right] \left[ a_7 c_+ U(c_+, x) + a_8 c_- U(c_-, x) \right] \quad (4.73)$$

where  $4c_{\pm} = \hat{\gamma}^{3/2} \pm (\hat{\gamma}^3 - 4\hat{D}_h)^{1/2}$  and  $U(c, x) = D_{-c-1/2}(x)$  is the asymptotically evanescent Whittaker function,<sup>57</sup> with  $x^2 = w^2 (2\hat{\gamma}^{3/2})$ .

The dispersion relation is obtained by matching from the ideal region to the intermediate resistivity region to the deeply resistive region. We note that our solutions have the same form as those obtained by Drake and Antonsen,<sup>54</sup> if we substitute our quantity  $\hat{D}_h$  for the negative of their quantity  $D$ . Therefore, we may simply quote the result for the final dispersion relation

$$\Delta' = \frac{2\Gamma(\frac{1}{4})}{\Gamma(\frac{3}{4})} \frac{(\hat{\gamma}^3 - 4\hat{D}_h)^{1/2}}{2\hat{\gamma}^{1/4}} \times \left[ \frac{\Gamma\left[\frac{1}{4} + \frac{c_-}{2}\right]}{\Gamma\left[\frac{3}{4} + \frac{c_-}{2}\right]} - \frac{\Gamma\left[\frac{1}{4} + \frac{c_+}{2}\right]}{\Gamma\left[\frac{3}{4} + \frac{c_+}{2}\right]} \right]^{-1} \quad (4.74)$$



where

$$\hat{\Delta}' = \Delta' \frac{\Gamma(\frac{1}{4})}{2\Gamma(\frac{3}{4})} \left[ \frac{\gamma_r / \omega_A}{\beta_t^{3/2}} \right] \quad (4.75)$$

#### 4.5 STABILITY ANALYSIS

It has been shown in Ref. 54 that various limits of a dispersion relation having the form of Eq. (4.74) can be investigated analytically. In particular, for  $\hat{\Delta}' \ll 1$ , one obtains  $\hat{\gamma} \{ [-D_h (4\ell+1)^2] / (4\ell+1) \}^{2/3}$  with  $\ell = 0, 1, 2, \dots$ ; as long as  $D_h > 0$  (which holds in the case of drift nonreversal), the only acceptable solutions are damped roots, implying stability. For  $\hat{\Delta}' \gg 1$ , two different roots can be found. One root, for which  $\hat{\gamma} \gg 1$ , yields a tearing mode type of scaling with resistivity for the growth rate:  $\gamma \propto \eta^{3/5} (\Delta')^{4/5}$ . The small  $\hat{\gamma} \ll 1$  root has the resistive ballooning mode scaling with resistivity:  $\hat{\gamma} \propto \eta^{1/3} (\Delta')^{-4}$ .

Moreover, because of the formal similarity between the dispersion relation obtained here and that analyzed in Ref. 54, we can use the numerical curve obtained in Ref. 54 for the relationship between the normalized driving energy  $\hat{\Delta}$  at marginal stability and the quantity  $\hat{D}_h$ , which represents the favorable contribution to the curvature provided by the energetic particles; see Fig. 4.6.

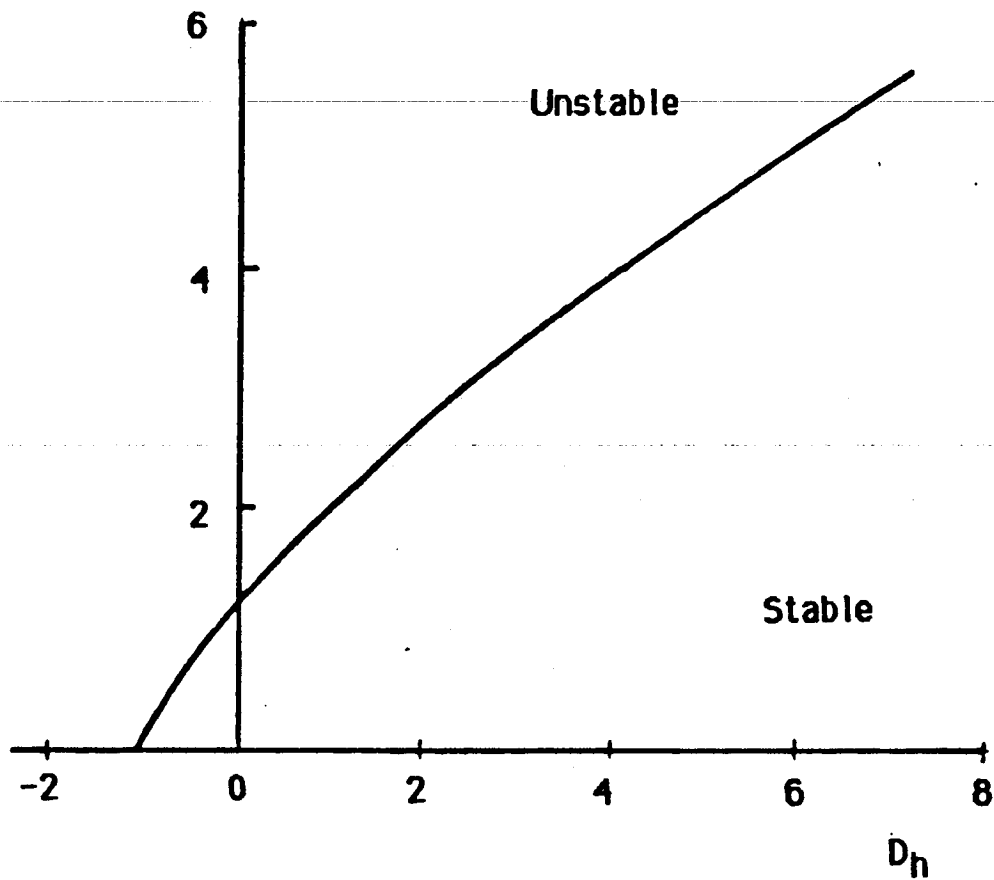


Fig. 4.6 A universal curve for the stability of resistive ballooning modes below the ideal threshold. The critical value of the driving energy,  $\Delta'_c$ , is plotted versus  $D_h$ . [From Drake and Antonsen paper, Ref. 54]

Finally we note that in the deeply trapped limit ( $\theta_0 \ll 1$ ), we have from Eq. (3.42) that

$$\delta_h \cong \left[ \frac{\alpha_c \alpha_c}{4\pi S^2} \right] \left[ \frac{\theta_0}{\beta_t} \right] \frac{1}{(q^2 - \alpha_c/2)} \quad (4.76)$$

Thus, the small  $\theta_0$  limit allows us to still consider finite values for  $\alpha_c$  and  $\alpha_h$ . Note that the denominator in Eq. (4.76) yields a singular behavior when  $\alpha_c = 2q^2$ ; this corresponds to the core pressure limit discovered in earlier studies of bumpy torus stability.<sup>(1)</sup> We stay below the value of  $\alpha_c$  corresponding to this threshold; nevertheless as  $\alpha_c$  increases and approaches this value,  $\delta_h$  is enhanced in value and the critical  $\Delta'$  for instability increases, which is favorable. Although we cannot overlay the results of Fig. 4 of Drake-Antonsen (Fig. 4.6) on top of our analytical or numerical plots for  $\Delta'_e$  without specifying values for  $\gamma_r/\omega_A$  and  $\beta_t = (\omega_s/\omega_A)^2$ , we can state that this indicates that compressibility effects are able to stabilize the resistive ballooning mode in the first ideally stable region, at least for  $\alpha_c$  values not too close to the ideal threshold, where the ideal ballooning mode dominates and  $\Delta'_e$  is singular.

#### 4.6 CONCLUSIONS

We have investigated the effect of highly energetic particles on the stability of resistive ballooning modes. First, the driving energy parameter  $\Delta'$  obtained from the ideal solution was obtained numerically. Then, we obtained the dispersion relation by matching the ideal solution to the intermediate resistive region to the deeply resistive region.

In the ideal ballooning low-beta first stability region ( $\alpha_c < \alpha_{c, I}$ ), the value of  $\Delta'$ , the parameter that controls the strength of the resistive growth rate at a given value of  $\alpha_c$ , tends to decrease somewhat as  $\alpha_h$  is increased. In the ideally unstable region  $\alpha_{c, I} < \alpha_c < \alpha_{c, II}$  above the first stability threshold  $\alpha_{c, I}$  and below the second stability threshold  $\alpha_{c, II}$ , the presence of highly energetic particles definitely improves the stability of the ideal ballooning mode, converting it from unstable to stable for sufficiently large  $\alpha_h$ . In this region,  $\Delta'$  decreases favorably with  $\alpha_h$ .

The high-beta second ideal stability region ( $\alpha_c > \alpha_{c, II}$ ) is more complicated. The Mercier coefficients tend to acquire large

variation with  $\alpha_c$  in this region, especially the coefficient of the "small" solution. Finally, there is a value of  $\alpha_c$  in this second ideal stability region for which  $\Delta'$  for both even and odd mode becomes singular. This value of  $\alpha_c$  can be analytically determined. It corresponds to the situation of marginal stability in the Mercier sense, for which the large and small solutions are degenerate. This feature has been previously pointed out by Newcomb.<sup>42</sup>

From the dispersion relation, we find that the hot particles contribute an effective curvature that is favorable; this tends to raise the  $\Delta'$  threshold value. At the same time, they tend to reduce the actual value of  $\Delta'$ . Thus, their compressional effects indicate the possibility of stabilizing the resistive ballooning mode in the first ideally stable region, at least away from the ideal stability threshold.

Inasmuch as it neglected the resonant response of the energetic particles in order to focus on their nonresonant effects, this analysis is complimentary to the recent study of resistive ballooning stability by Biglari and Chen,<sup>34</sup> in which only the resonant hot particle behavior was retained, in a very low limit.

## CHAPTER V

### SUMMARY AND DISCUSSION

The results of the work presented here have already been summarized at the end of Chapters II, III and IV. Here we will attempt to provide an overview and then discuss some implications.

In order to give some perspective on how this work fits into the grand scheme, we refer to the rather heuristic cartoon shown in Fig. 5.1. The abscissa in this plot is the energy of the hot species,  $T_h$ . Very energetic particles are nonresonant with the MHD ballooning modes:  $\omega_{dh}/\omega \gg 1$ , where  $\bar{\omega}_{dh}$  is their magnetic drift frequency and  $\omega$  is the mode frequency. Moderately energetic particles do interact with the background plasma resonantly. Low energy particles ( $\omega_{dh}/\omega \ll 1$ ), on the other hand, can be described by ordinary fluid or kinetic theory and hence are not of interest here. The ordinate in this diagram represents the resistivity  $\eta$ , or the inverse of the magnetic Reynold's number  $S_M = \tau_r / \tau_A = \omega_A / \nu_r \gg 1$  where  $\nu_r = (nq/r)^2 (c^2 \eta / 4\pi)$ . Depending on whether the mode frequency is larger than comparable to, or smaller than, the resistive frequency  $\omega_R$  defined by

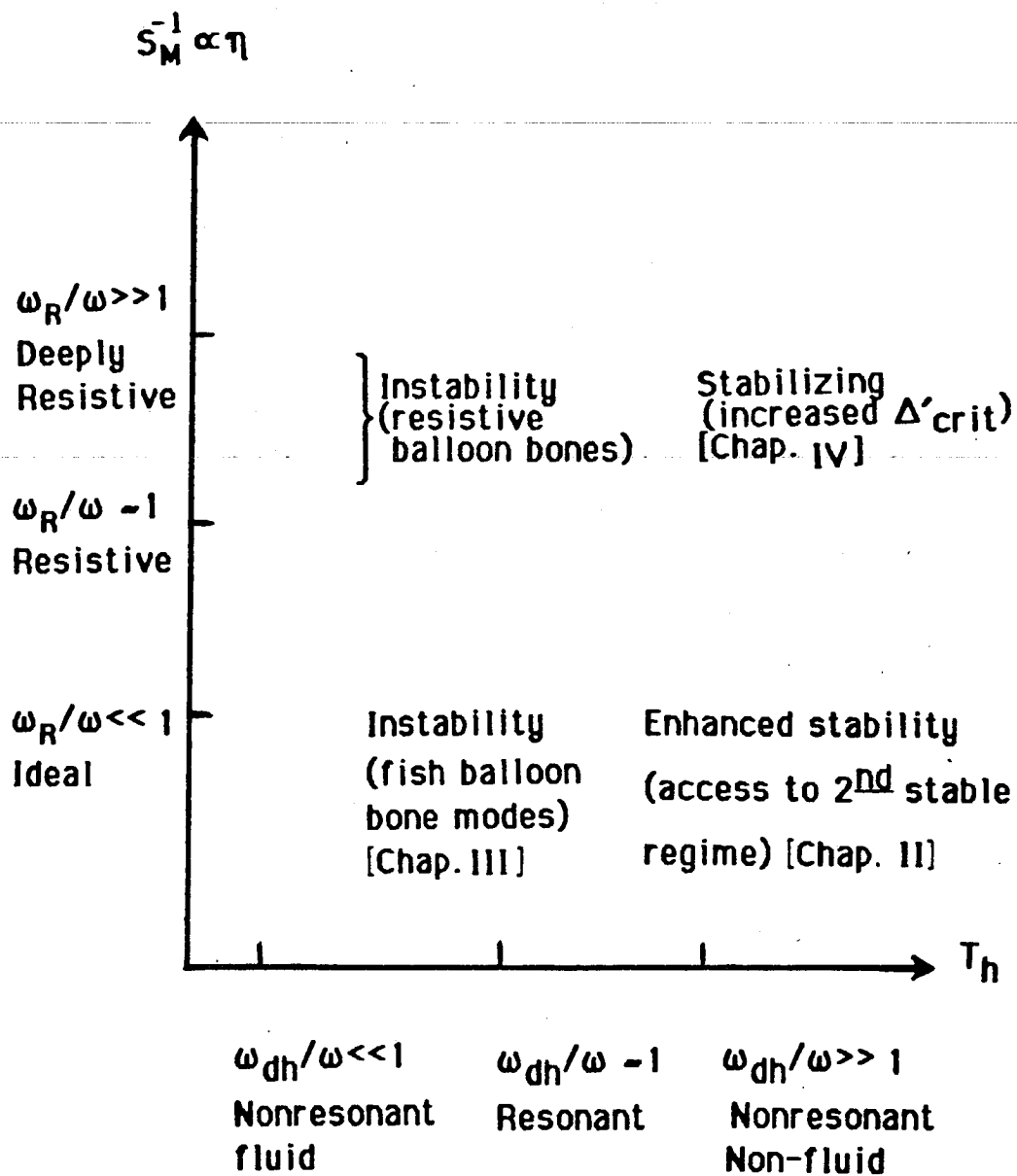


Fig. 5.1 Regimes for various theoretical descriptions

$\omega_R/\omega_A = (n^2 q^2 S^2/S_M)^{1/3} \ll 1$ , we pass from the ideal (collisionless) regime to the resistive regime to the deeply resistive regime.

As is indicated in Fig. 5.1, the work presented in Chap. II dealt with the highly energetic regime of nonresonant non-fluid-like hot particles and their effects on ideal ballooning modes. The work of Chap. III extended that theory to the resonant domain. Interestingly, one finds that in the nonresonant domain, if ideal modes are unstable, then sufficiently large  $\alpha_h$  can lead to stability. On the other hand, for the resonant domain, when the ideal ballooning mode is stable and  $\alpha_h$  is above a threshold, there results instability. These features can be seen in numerically obtained plots<sup>24,32,58</sup> of the growth rate versus, for example,  $\alpha_h$ : when  $T_h$  is large, the two  $\alpha_h$  limits are separated and there is a stability window between them, whereas for smaller  $T_h$ , the two limits cross over each other and the ballooning modes passes continuously from MHD ( $\omega/\omega_{dh} \ll 1$ ) instability to kinetic trapped particle-induced ( $\omega/\omega_{dh} \simeq 1$ ) instability.

The work presented in Chap. IV described the effect of nonresonant hot particles on resistive ballooning modes. Both the resistive and the deeply resistive regimes were involved, because the



effective curvature contributed by the hot particles was taken to be small on the order of the sonic compression and cross-field transport effects. If the energetic particle effect were ordered to larger, then the assumption of incompressibility would be valid and only the resistive regime would need to be considered. We found that the compressible resistive modes are somewhat stabilized by a nonresonant energetic species, in that the threshold  $\Delta'$  value is increased while the actual  $\Delta'$  value is lowered, although near the ideal marginal stability boundary this mechanism becomes ineffective. We did not examine the effect of resonant hot particles on resistive ballooning modes since this problem has recently been studied by Biglari and Chen,<sup>34</sup> who obtained the resistive version of the balloon mode instability.

From the stability point of view, it would clearly be desirable to operate in the nonresonant, highly energetic particle regime. The theoretical results of instability with resonant particles seem to be confirmed by the PDX observations of beam ion-excited fishbone precursor oscillations. The prediction of enhanced stability with nonresonant particles, however, has not yet been tested experimentally. Such a test would require a device that is capable of exploring high-beta second stability. One such device is the PBX tokamak<sup>59</sup> at Princeton, which is using indented bean-shaped cross

sections to attain high beta. Another might be the proposed SRX ("Second Regime Experiment") tokamak at Columbia University, which has been designed with large aspect ratio and with electron cyclotron wave heating to create a population of super-energetic electrons. Some combination of the hot particles and bean shaping schemes — *e.g.*, the use of a modest indentation to establish an improved equilibrium that would require fewer hot particles to gain access to second stability — is also a possibility to be looked into.

There are also technological requirements that would have to be considered. It has been pointed out earlier, in Chap. II, that satisfying the nonresonance condition requires rather high energies, typically in the few MeV range. Even when such energetic particles can be created, there is the question of power balance. For example, it has been estimated<sup>60</sup> that the proposed SRX experiment would require an input power of approximately 400 kW in order to balance the energy lost by hot electrons slowing down by collisions with background electrons. Moreover, with super hot electrons created by ECH, there could also be energy lost by synchrotron radiation, as well as very high-frequency instabilities (*e.g.*, whistlers or modes at the electron cyclotron frequency) on the hot electrons themselves.

There has been other recent work related to enhanced stability with nonresonant energetic particles. Several studies<sup>61,62,63</sup> have pursued the global (as opposed to single flux surface) stability of tokamaks, as numerically computed with a two-dimensional, high beta, finite aspect ratio, anisotropic equilibrium. Also, the power needed to dynamically evolve a stable equilibrium into the second stability regime, with access provided by energetic particles, has been computed with a model ballooning transport formalism.<sup>64</sup>

However, the resonantly unstable ballooning modes that can be excited by trapped hot particles remain a significant concern for tokamak operation. These modes can occur even if the ideal mode is stable; their growth rates can be comparable to MHD growth rates; and a sizeable fraction of beam-injected hot ions can be lost as a result of these resonant instabilities. In Fig. 5.2 we sketch the approximate instability boundaries, which we earlier found in Sec. 3.6 to be  $\alpha_h \gtrsim \text{Max} \{ M_e (2S/\pi), (\omega_{dh}/\omega_A) (4/\pi^3) \}$ . The quantity  $M_e$  is an indicator of ideal stability: for core plasma pressure less than the ideal threshold (*i.e.*,  $\alpha_c < \alpha_{c, \text{crit}}$ ),  $M_e$  is positive and the ballooning mode is ideally stable. However, the resonant branch can be unstable above the threshold boundary for  $\alpha_h$ .

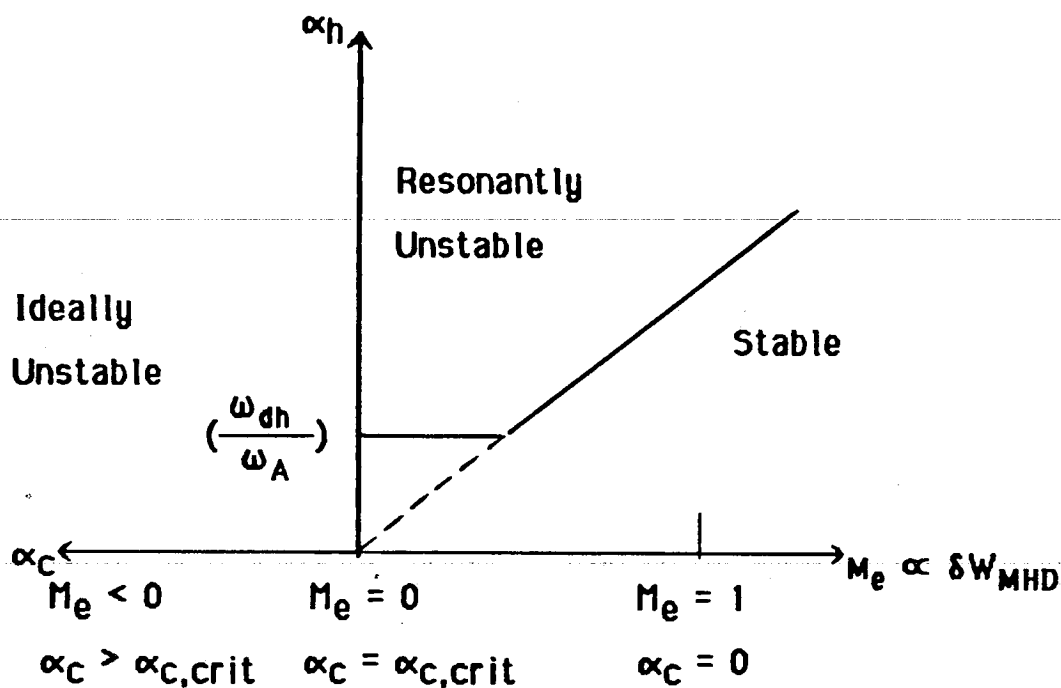


Fig. 5.2 Simple sketch of stability boundaries for resonant and nonresonant ballooning modes.

Several ways to suppress or avoid the resonant instability can be mentioned, some of which are suggested by Fig. 5.2. One approach is to raise the the value of  $\omega_{dh}/\omega_A$ , which is equivalent to increasing the energy of the hot species. Numerical studies<sup>(1)</sup> have found that  $\omega_{dh}/\omega_A \gtrsim 1$  is required to open up a stable regime, which could possibly lead to second stable operation. Our theory described in Chap. III is limited in its validity to  $\omega_{dh}/\omega_A \ll 1$ . A more recent

theoretical treatment<sup>28</sup> that investigates modes with  $\omega \sim \omega_{dh} \sim \omega_A$  has found that energetic particles lead to an unstable discrete Alfvén gap mode, whose growth rate decreases as the ratio  $\omega_{dh}/\omega_A$  is increased. Another approach to raising the threshold for the resonant mode is to stay well below ideal marginal stability so that  $M_e$  is positive and finite.

Yet another idea is to use a "sloshing" distribution of energetic particles, so called by analogy with the ion distributions created in mirror experiments<sup>48</sup> by off-angle neutral beam injection so as to be primarily located in regions of good curvature near the mirror throats. In mirrors, these sloshing particles are used to control MHD stability, since their average magnetic drift is reversed by pressure weighting. In a tokamak with hot particles whose pressure profile peaks toward the small-major-radius side, the resonant mode will be damped, rather than growing. A possible scenario that has been suggested<sup>65</sup> on how to avoid the deleterious effects of resonantly excited MHD instabilities involves programming electron cyclotron heating to have its resonant heating surface be initially located on the small-major-radius side of the torus as the power is being turned up. Moderately energetic electrons with average drift reversal could be created, which, although resonant, are not

unstable. Then, at higher power, the ECH resonant surface could be shifted to the outer side to produce the high temperature, nonresonant, non-drift-reversed electrons desired for stabilization purposes. A recent examination<sup>58</sup> of sloshing energetic particles has found, however, that drift reversal leads to other types of instability.

Finally, an almost trivial suggestion to avoid the resonant instabilities is to use nearly parallel injection for neutral beam heating. This minimizes the trapped fraction of the injected hot ions, which are responsible for the nonadiabatic resonant response. Of course, controlling the direction is not an available option when the energetic particles are the 3.5 MeV alpha particles that are produced isotropically in an ignited fusion plasma. A recent study<sup>30</sup> for TFTR parameters has found that the presence of alpha particles can also lead to resonantly unstable ballooning modes.

Incidentally, energetic particles can also affect the stability of MHD modes higher in frequency than ballooning and kink modes. For example, recent studies<sup>66,67,68</sup> have shown that alpha particles with super Alfvénic parallel velocities can destabilize the global Alfvén waves.

The study of energetic particles, therefore, is of broad interest, whether these particles are intentionally created or occur

as a by-product of auxiliary heating or as the direct product of ignition. As far as the stability of ballooning modes is concerned, we have attempted to show that the presence of energetic particles offers promise in one regime, but could lead to problems in another regime. Ultimately, the nonlinear behavior of the unstable modes and their consequences for transport remain to be explored.

## APPENDIX A

### COEFFICIENTS OF THE DRIFT NONREVERSAL CONDITION

The non-drift reversal condition given in Eq. (2.56), can be written as

$$\int_{-\theta_0}^{\theta_0} \frac{d\theta}{\sqrt{\cos\theta - \cos\theta_0}} \left\{ \cos\theta + h(\theta) \sin\theta - \frac{(\alpha_h + \alpha_c)}{2q^2} \right\} > 0 \quad (\text{A.1})$$

where

$$\alpha_h = \alpha_{h0} \left[ A + \eta (\cos\theta - \cos\theta_0) \right]$$

$$h(\theta) = S(\theta - \theta_k) - \alpha_c (\sin\theta - \sin\theta_k) - \frac{\alpha_{h0}}{2} \left[ g(\theta) - g(\theta_k) \right]$$

The contribution from terms odd in  $\theta$  is zero, so that the inequality (A.1) becomes:

$$\int_0^{\theta_0} \frac{d\theta \cos\theta}{\sqrt{\cos\theta - \cos\theta_0}} + \int_0^{\theta_0} \frac{d\theta \left[ S\theta - \alpha_c \sin\theta \right] \sin\theta}{\sqrt{\cos\theta - \cos\theta_0}}$$



$$\begin{aligned}
& - \left[ \frac{\alpha_{ho}}{2} \right] \int_0^{\theta_0} \frac{d\theta g(\theta) \sin\theta}{\sqrt{\cos\theta - \cos\theta_0}} - \left[ \frac{\alpha_c}{2q^2} \right] \int_0^{\theta_0} \frac{d\theta}{\sqrt{\cos\theta - \cos\theta_0}} \\
& - \left[ \frac{\alpha_{ho}}{2q^2} \right] \int_0^{\theta_0} d\theta \frac{[A + \eta(\cos\theta - \cos\theta_0)]}{\sqrt{\cos\theta - \cos\theta_0}} > 0 \quad (A.2)
\end{aligned}$$

In Eq. (A.2) we now split  $g$  in two parts, using Eq. (2.39) and obtain

$$\begin{aligned}
& \left[ \frac{\alpha_{ho}}{2} \right] \left\{ A \left[ \left( \frac{1}{q^2} \right) \int_0^{\theta_0} \frac{d\theta}{\sqrt{\cos\theta - \cos\theta_0}} + \int_0^{\theta_0} \frac{d\theta g_{sq}(\theta) \sin\theta}{\sqrt{\cos\theta - \cos\theta_0}} \right] \right. \\
& \left. + \eta \left[ \frac{1}{q^2} \int_0^{\theta_0} d\theta \sqrt{\cos\theta - \cos\theta_0} + \int_0^{\theta_0} \frac{d\theta g_{sm}(\theta) \sin\theta}{\sqrt{\cos\theta - \cos\theta_0}} \right] \right\} \\
& + \frac{\alpha_c}{2q^2} \int_0^{\theta_0} \frac{d\theta}{\sqrt{\cos\theta - \cos\theta_0}}
\end{aligned}$$

$$+ \alpha_c \int_0^{\theta_0} \frac{d\theta \sin^2 \theta}{\sqrt{\cos \theta - \cos \theta_0}} < S \int_0^{\theta_0} \frac{d\theta \theta \sin \theta}{\sqrt{\cos \theta - \cos \theta_0}} + \int_0^{\theta_0} \frac{d\theta \cos \theta}{\sqrt{\cos \theta - \cos \theta_0}}$$

Now we rewrite this inequality using the expressions for  $g_{sq}$  and  $g_{sm}$  given in Eqs. (2.40) and (2.41):

$$\begin{aligned} & \left[ \frac{\alpha_{h_0}}{2} \right] \left\{ A \left[ \frac{l_1}{q^2} + l_5 - \frac{(t_0 + \cos \theta_0)}{\pi} l_3 \right] \right. \\ & \left. + \eta \left[ \frac{l_2}{q^2} + \frac{l_6}{4} - l_5 \cos \theta_0 + Y l_3 \right] \right\} \\ & + \alpha_c \left\{ \left[ \frac{1}{2q^2} \right] l_1 + l_5 \right\} < S l_3 + l_4 \end{aligned} \quad (A.3)$$

Here we have defined

$$t_0 = \sin \theta_0 - \theta_0 \cos \theta_0$$

and

$$\begin{aligned} Y = & \cos^2 \theta_0 - \left[ \frac{1}{4} \right] \cos(2\theta_0) - \left[ \frac{1}{8\pi} \right] \left[ \sin(2\theta_0) - 2\theta_0 \cos(2\theta_0) \right] \\ & + \frac{t_0}{\pi} \cos \theta_0 \end{aligned}$$

Note that

$$I_1 = \int_0^{\theta_0} \frac{d\theta}{\sqrt{\cos\theta - \cos\theta_0}} = \sqrt{2} \int_0^{\pi/2} \frac{d\phi}{\sqrt{1 - k^2 \sin^2 \phi}} = \sqrt{2} K(k)$$

Where,  $K$  is the complete elliptic integral of the first kind and  $k = \sin(\theta_0/2)$ .

$$I_2 = \int_0^{\theta_0} d\theta \sqrt{\cos\theta - \cos\theta_0} = 2\sqrt{2} \left\{ (k^2 - 1) K(k) + E(k) \right\}.$$

where  $E$  is the complete elliptic integral of the second kind. Also we compute

$$I_3 = \int_0^{\theta_0} \frac{d\theta \theta \sin\theta}{\sqrt{\cos\theta - \cos\theta_0}} = 4\sqrt{2} \left\{ (k^2 - 1) K + E \right\}$$

$$I_4 = \int_0^{\theta_0} \frac{d\theta \cos\theta}{\sqrt{\cos\theta - \cos\theta_0}} = \sqrt{2} (2E - K)$$

$$I_5 = \int_0^{\theta_0} \frac{d\theta \sin^2 \theta}{\sqrt{\cos\theta - \cos\theta_0}} = 4\sqrt{2} (E - U)$$

We recall that,  $H = (\theta_0 - |\theta - 2\pi n|)$  is the Heaviside step function, and the equations above are written for  $\theta$  in the interval  $(2\pi n - \pi, 2\pi n + \pi)$ ;  $\tilde{P}_{\perp h} = 0$  outside the trapped particle interval, and its value inside depends on which interval is being considered, so that

$$\int_{(n)} = \int_{2\pi n - \theta_0}^{2\pi n + \theta_0}$$

We want to derive the asymptotic (i.e., large  $\theta$ ) form of the above equations, where resistive effects will come into play. The maximal ordering is to take

$$\frac{v_{\perp}}{\gamma} \sim O(Z^{-2}) \quad \frac{v_{\perp} \omega_s^2}{\gamma \omega_A^2} \sim O(Z^{-2})$$

$$\frac{\gamma^2}{\omega_A^2} \sim O(Z^{-2}) \quad \left[ \frac{\omega_s}{\gamma} \right]^2 \sim O(Z^{-2})$$

where  $Z = S \theta \gg 1$  (and  $S \sim O(1)$  is presumed.)

Note that  $1+h^2 = (1+A^2) - 2Z A + Z^2$  where  $A(\theta) = \alpha_c \sin\theta + (\alpha_h/2)$

$g(\tilde{\theta})$ ; also,  $D(\theta) = F(\theta) + S\theta \sin\theta$ , where  $F(\theta) = \cos\theta - A(\theta) \sin\theta$ .

Expand the four field quantities as follows:

$$\tilde{\Phi}(\theta) = \Phi_0(\tilde{\theta}, Z) + \Phi_1(\tilde{\theta}, Z) + \Phi_2(\tilde{\theta}, Z) + \dots$$

$$\tilde{\Psi}(\theta) = \Psi_0(\tilde{\theta}, Z) + \Psi_1(\tilde{\theta}, Z) + \Psi_2(\tilde{\theta}, Z) + \dots$$

$$\tilde{P}_c(\theta) = P_{c0}(\tilde{\theta}, Z) + P_{c1}(\tilde{\theta}, Z) + P_{c2}(\tilde{\theta}, Z) + \dots$$

$$\tilde{P}_{jh}(\theta) = P_{h0}(\tilde{\theta}, Z) + P_{h1}(\tilde{\theta}, Z) + P_{h2}(\tilde{\theta}, Z) + \dots$$

Here,  $P_{c1}/P_{c0} \sim O(Z^{-1}) < 1$ ; also, the  $\theta$  dependence is now decomposed into the rapid variation with the periodic variable  $\tilde{\theta} = \theta \bmod 2\pi$  and the slow variation with  $Z = S\theta$ .

### Lowest order

We proceed to write the lowest order in  $1/Z$  of each equation. [note that the lowest order of Eq. (B.1) and (B.4) is ostensibly  $O(Z^0) = O(1)$ , whereas the lowest order of Eqs. (B.2) and (B.3) is  $O(Z^2)$ ; however, we treat these all simultaneously.]

$$\left[ 1 + \left[ \frac{v_1}{\gamma} \right] Z^2 \right] \frac{\partial \Psi_0}{\partial \tilde{\theta}} = \frac{\partial \Phi_0}{\partial \tilde{\theta}} \quad \Rightarrow \quad \Phi_0 = \Phi_0(Z)$$

$$\frac{\partial}{\partial \tilde{\theta}} Z^2 \frac{\partial}{\partial \tilde{\theta}} \Psi_0 = 0 \quad \Rightarrow \quad \Psi_0 = \Psi_0(Z)$$

$$\left[ \frac{\omega_S}{\gamma} \right]^2 \frac{\partial^2}{\partial \tilde{\theta}^2} (P_{c0} - \Psi_0) = 0 \quad \Rightarrow \quad P_{c0} = P_{c0}(Z)$$

We treat the integral equation as follows:

$$\begin{aligned}
 \int_{(n)} d\theta \left[ D(\theta)\Psi + \frac{\alpha_c}{2q^2} (P_c - \Psi) \right] &= \int_{-\theta_0}^{\theta_0} d\tilde{\theta} \left[ D(\tilde{\theta}) + Z_n \sin\tilde{\theta} \right] \times \\
 &\left[ 1 + S \tilde{\theta} \frac{\partial}{\partial Z_n} + \frac{1}{2} S^2 \tilde{\theta}^2 \frac{\partial^2}{\partial Z_n^2} + \dots \right] \Psi(\tilde{\theta}, Z_n) \\
 &+ \int_{-\theta_0}^{\theta_0} d\tilde{\theta} \frac{\alpha_c}{2q^2} \left[ 1 + S \tilde{\theta} \frac{\partial}{\partial Z_n} + \frac{1}{2} S^2 \tilde{\theta}^2 \frac{\partial^2}{\partial Z_n^2} \right] \left[ P_c(\tilde{\theta}, Z_n) - \Psi(\tilde{\theta}, Z_n) \right] \\
 &= I \Psi_0(Z_n) + Z_n \frac{d\Psi_0}{dZ_n} J + Z_n \beta(Z) + \frac{\alpha_c \theta_0}{q^2} \left[ P_{c0}(Z_n) - \Psi_0(Z_n) \right] + O(Z_n^2)
 \end{aligned}$$

Note that the  $O(Z_n^{-1})$  terms cancel by parity arguments, here we have defined

$$I = \int_{-\theta_0}^{\theta_0} d\tilde{\theta} D(\tilde{\theta})$$

$$J = \int_{-\theta_0}^{\theta_0} d\tilde{\theta} S \tilde{\theta} \sin\tilde{\theta}$$

$$\beta(Z) = \int_{-\theta_0}^{\theta_0} d\tilde{\theta} \sin\tilde{\theta} \Psi_1(\tilde{\theta}, Z) .$$

Also define

$$\lambda_0(Z) = i\Psi_0(Z) + jZ \frac{d\Psi_0}{dZ} + Z\beta(Z) + \frac{\alpha_c \theta_0}{q^2} \left[ P_{co}(Z) - \Psi_0(Z) \right] .$$

Then we find

$$\int_{(n)} d\theta \left[ D(\theta)\tilde{\Psi} + \frac{\alpha_c}{2q^2} (P_c - \tilde{\Psi}) \right] \cong \left[ 1 - s\tilde{\theta} \frac{\partial}{\partial Z} \right] \lambda_0 + o(Z^{-2})$$

Therefore, to lowest order,

$$P_{ho}(Z) = H \left[ \Psi_0(Z) - \frac{\lambda_0(Z)}{\Delta} \right] \Rightarrow P_{ho} = P_{ho}(Z)$$

where

$$\Delta = \int_{-\theta_0}^{\theta_0} d\tilde{\theta} \left[ D(\tilde{\theta}) - \frac{\alpha_c}{2q^2} \right] .$$

The next higher order equations are the following:

$$\left[ 1 + \frac{v_{||}}{\gamma} Z^2 \right] \left[ \frac{\partial \Psi_1}{\partial \tilde{\theta}} + s \frac{\partial \Psi_0}{\partial Z} \right] = \frac{\partial \Phi_1}{\partial \tilde{\theta}} + s \frac{\partial \Phi_0}{\partial Z}$$

$$Z^2 \frac{\partial^2}{\partial \theta^2} \Psi_1 + Z \sin \theta \left[ \alpha_c P_{c0} + \frac{\alpha_h}{2} P_{h0} \right] = 0$$

$$\left[ \frac{\omega_s}{\gamma} \right]^2 + \frac{\partial^2}{\partial \theta^2} (P_{c1} - \Psi_1) + \left[ \frac{2\Gamma_s P_c}{R P'_c} \right] Z \sin \theta \Phi_0 + \left[ \frac{\omega_s}{\omega_A} \right]^2 \left[ \frac{P_{\perp h}}{P'_c} \right] \times$$

$$\left[ \frac{P_{\perp h} H}{R P'_{\perp h}} \right] Z \sin \theta \Phi_0 = 0$$

$$P_{h1} = H \left[ \Psi_1 + \frac{S\tilde{\theta}}{\Delta} \frac{d\lambda_0}{dz} \right]$$

The equation for  $\Psi_1$  is an integral equation:

$$\frac{\partial^2}{\partial \theta^2} \Psi_1(\tilde{\theta}, Z) + \frac{\sin \theta}{Z} \left\{ \alpha_c P_{c0}(Z) + \frac{\alpha_h}{2} H \left[ \Psi_0(Z) - \frac{\lambda_0(Z)}{\Delta} \right] \right\} = 0$$

Its solution is

$$\Psi_1(\tilde{\theta}, Z) = \alpha_c \sin \tilde{\theta} \left[ \frac{P_{c0}(Z)}{Z} \right] + \frac{\alpha_c}{2} g(\tilde{\theta}) \left[ \frac{\Psi_0}{Z} - \frac{\lambda_0}{\Delta \cdot Z} \right]$$

By definition, we have

$$\beta(Z) = \int_{-\theta_0}^{\theta_0} d\tilde{\theta} \sin \tilde{\theta} \left\{ \alpha_c \sin \tilde{\theta} \left[ \frac{P_{c0}}{Z} \right] + \frac{\alpha_h}{2} g(\tilde{\theta}) \left[ \frac{\Psi_0}{Z} - \frac{1}{\Delta} \frac{\Psi_0}{Z} \right] \right\}$$



$$\left. - \frac{J}{\Delta} \frac{d\Psi_0}{dZ} - \frac{\beta(Z)}{\Delta} - \frac{\alpha_c \theta_0}{\Delta q^2} \left[ \frac{P_{c0} - \Psi_0}{Z} \right] \right\} .$$

$$= \frac{\alpha_c M \left[ \frac{P_{c0}}{Z} \right] + \frac{\alpha_h}{2} L \left[ \left( 1 - \frac{1}{\Delta} \right) \frac{\Psi_0}{Z} - \frac{J}{\Delta} \frac{d\Psi_0}{dZ} - \frac{\alpha_c \theta_0}{q^2 \Delta} \left[ \frac{P_{c0} - \Psi_0}{Z} \right] \right]}{1 + \frac{\alpha_h}{2} L \left[ \frac{1}{\Delta} \right]}$$

where

$$M = \int_{-\theta_0}^{\theta_0} d\tilde{\theta} \sin^2 \tilde{\theta}$$

$$L = \int_{-\theta_0}^{\theta_0} d\tilde{\theta} g(\tilde{\theta}) \sin \tilde{\theta}$$

The equation for  $P_{c1}$  can be solved in terms of  $\Psi_1$  as

$$\left[ \frac{\omega_S}{\gamma} \right]^2 (P_{c1} - \Psi_1) = \left[ \frac{2\Gamma_S P_c}{R P_c'} \right] Z \sin \theta \Phi_0(Z)$$

$$+ \left[ \frac{\omega_S}{\omega_A} \right]^2 \left[ \frac{P_{1h}}{P_c'} \right] \left[ \frac{P_{1h}}{R P_{1h}'} \right] Z g(\tilde{\theta}) \Phi_0(Z)$$

The Equation for relating  $\Psi_1$  and  $\Phi_1$  may be left as an equation for

$\Phi_1$ :

$$\frac{\partial \phi_1}{\partial \tilde{\theta}} = \left[ 1 + \frac{v_1}{\gamma} z^2 \right] \left[ \frac{\partial \psi_1}{\partial \tilde{\theta}} + s \frac{\partial \psi_0}{\partial z} \right] - s \frac{\partial \phi_0}{\partial z}$$

or we can solve it as

$$\phi_1 \left[ 1 + \frac{v_1}{\gamma} z^2 \right] \left[ \psi_1 + s \tilde{\theta} \frac{\partial \psi_0}{\partial z} \right] - s \tilde{\theta} \frac{\partial \phi_0}{\partial z}$$

Note that averaging these "next order" equations produces no new information, except for the preceding equation, yields

$$\left[ 1 + \frac{v_1}{\gamma} z^2 \right] \frac{d\psi_0}{dz} = \frac{d\phi_0}{dz} .$$

The last order equations that we need to consider are as follows:

$$\left[ 1 + \frac{v_1}{\gamma} z^2 \right] \left[ \frac{\partial \psi_2}{\partial \theta} + s \frac{\partial \psi_1}{\partial z} \right] - \frac{v_1}{\gamma} (2zA) \left[ \frac{\partial \psi_1}{\partial \theta} + s \frac{\partial \psi_0}{\partial z} \right]$$

$$= \frac{\partial \phi_2}{\partial \theta} + s \frac{\partial \phi_1}{\partial z}$$

$$\frac{\partial}{\partial \theta} \left[ z^2 \left[ \frac{\partial \psi_2}{\partial \theta} + s \frac{\partial \psi_1}{\partial z} \right] - 2zA \left[ \frac{\partial \psi_1}{\partial \theta} + s \frac{\partial \psi_0}{\partial z} \right] \right]$$

$$+ s \frac{\partial}{\partial z} \left[ z^2 \left[ \frac{\partial \psi_1}{\partial \theta} + s \frac{\partial \psi_0}{\partial z} \right] \right]$$

$$-\frac{\gamma^2}{\omega_A^2} Z^2 \phi_0 + F \left[ \alpha_c P_{c0} + \frac{\alpha_h}{2} P_{c0} \right] + Z \sin \theta \left[ \alpha_c P_{c1} + \frac{\alpha_h}{2} P_{h1} \right] = 0$$

$$\left[ 1 + \frac{v_{\perp}}{\gamma} \frac{\omega_s^2}{\omega_A^2} Z^2 \right] P_{c0} = \left[ \frac{\omega_s}{\gamma} \right]^2 \left[ \frac{\gamma^2}{\partial \theta^2} (P_{c2} - \Psi_2) + 2S \frac{\partial^2}{\partial \theta \partial Z} (P_{c1} - \Psi_1) \right.$$

$$\left. + S^2 \frac{\partial^2}{\partial Z^2} (P_{c0} - \Psi_0) \right]$$

$$+ \phi_0 + \left[ \frac{2\Gamma_c P_c}{R P'_c} \right] \left[ F \phi_0 + Z \sin \theta \phi_1 \right] - \left[ \frac{\omega_s}{\omega_A} \right]^2 \left[ \frac{P'_{\perp h}}{P'_c} \right] \left[ P_{h0} - \phi_0 \right.$$

$$\left. - \left[ \frac{P_{\perp h} H}{R P'_{\perp h}} \right] \left[ F \phi_0 + Z \sin \theta \phi_1 \right] \right]$$

$$P_{h2} = H \left\{ \Psi_2 - O(Z^{-2}) \text{ terms} \right\}.$$

We proceed to average these equations over  $\tilde{\theta}$ .

$$S^2 \frac{d}{dZ} \left[ Z^2 \frac{d\Psi_0}{dZ} \right] - \frac{\gamma^2}{\omega_A^2} Z^2 \phi_0 + \alpha_c P_{c0} \langle F \rangle_{2\pi} + \frac{\alpha_h}{2} \langle F P_{h0} \rangle_{2\pi}$$

$$+ \alpha_c Z \langle \sin \theta P_{c1} \rangle_{2\pi} + \frac{\alpha_h}{2} Z \langle \sin \theta P_{h1} \rangle_{2\pi} = 0$$

$$\left[ 1 + \left[ \frac{v_{\perp}}{\gamma} \frac{\omega_s^2}{\omega_A^2} \right] Z^2 \right] P_{c0} = \left[ \frac{\omega_s}{\gamma} \right]^2 S^2 \frac{d^2}{dZ^2} (P_{c0} - \Psi_0) + \phi_0$$

$$+ \left[ \frac{2\Gamma_s P_c}{R P'_c} \right] \left[ \phi_0 \langle F \rangle_{2\pi} + Z \langle \sin \theta \phi_1 \rangle_{2\pi} \right]$$

$$- \left[ \frac{\omega_s}{\omega_A} \right]^2 \left[ \frac{P_{\perp h}}{P'_c} \right] \left[ \langle P_{h0} \rangle_{2\pi} - \Phi_0 - \left[ \frac{P_{\perp h}}{R P'_{\perp h}} \right] \left\{ \Phi_0 \langle F \rangle_{tr} + Z \langle \sin \theta \Phi_1 \rangle_{tr} \right\} \right]$$

We do not need  $P_{h2}$ ; we do need the previous order equation

$$\left[ 1 + \left[ \frac{\nu_1}{\gamma} \right] Z^2 \right] \frac{d\psi_0}{dZ} = \frac{d\Phi_0}{dZ} .$$

We need to calculate the following averages:

$$\langle F \rangle_{2\pi} = -\frac{1}{2} \left[ \alpha_c + \frac{\alpha_h M}{2\pi} \right]$$

$$\langle F P_{h0} \rangle_{2\pi} = \left[ \psi_0 - \frac{\lambda_0}{\Delta} \right] \langle F \rangle_{tr}$$

$$\langle F \rangle_{tr} = \frac{1}{2\pi} (I-J)$$

$$\langle \sin \theta P_{c1} \rangle_{2\pi} = \left[ \frac{\gamma}{\omega_s} \right]^2 \left[ \frac{2\Gamma_s P_c}{R P'_c} \right] Z \Phi_0 \langle \sin^2 \theta \rangle_{2\pi}$$

$$+ \left[ \frac{\gamma}{\omega_s} \right]^2 \left[ \frac{\omega_s}{\omega_A} \right]^2 \left[ \frac{P_{\perp h}}{P'_c} \right] \left[ \frac{P_{\perp h}}{R P'_{\perp h}} \right] Z \Phi_0 \langle \sin \theta g(\tilde{\theta}) \rangle_{2\pi}$$

$$+ \langle \sin \theta \Psi_1 \rangle_{2\pi}$$

$$\langle \sin^2 \theta \rangle_{2\pi} = \frac{1}{2}$$

$$\langle \sin \theta g(\tilde{\theta}) \rangle_{2\pi} = \frac{M}{2\pi}$$

$$\langle \sin \theta \Psi_1 \rangle_{2\pi} = \alpha_c \left[ \frac{P_{c0}}{Z} \right] \langle \sin^2 \theta \rangle_{2\pi} + \frac{\alpha_h}{2} \left[ \frac{\Psi_0}{Z} - \frac{\lambda_0}{Z\Delta} \right] \langle \sin \theta g(\tilde{\theta}) \rangle_{2\pi}$$

$$\langle \sin \theta P_{h1} \rangle_{2\pi} = \langle \sin \theta \Psi_1 \rangle_{1r} + \frac{1}{\Delta} \frac{d\lambda_0}{dZ} \langle \sin \theta S \tilde{\theta} \rangle_{1r}$$

$$\langle \sin \theta \Psi_1 \rangle_{1r} = \alpha_c \left[ \frac{P_{c0}}{Z} \right] \langle \sin^2 \theta \rangle_{1r} + \frac{\alpha_h}{2} \left[ \frac{\Psi_0}{Z} - \frac{\lambda_0}{\Delta Z} \right] \langle \sin \theta g(\tilde{\theta}) \rangle_{1r}$$

$$\langle \sin^2 \theta \rangle_{1r} = \frac{1}{2\pi} \left[ \theta_0 - \frac{1}{2} \sin(2\theta_0) \right] = \frac{M}{2\pi}$$

$$\langle \sin \theta g(\tilde{\theta}) \rangle_{1r} = \frac{L}{2\pi}$$

$$\langle S \tilde{\theta} \sin \theta \rangle_{1r} = \frac{J}{2\pi}$$

Also recall that

$$1 = J + 2 \sin \theta_0 - \alpha_c M - \frac{\alpha_h}{2} L$$

Thus, the vorticity equation becomes

$$S^2 \frac{d}{dZ} \left[ Z^2 \frac{d\Phi_0}{dZ} \right] - \left[ \frac{\gamma^2}{\omega_A^2} \right] Z^2 \Phi_0 + \alpha_c P_{c0} \left[ -\frac{1}{2} \right] \left[ \alpha_c + \frac{\alpha_h M}{2\pi} \right]$$

$$\begin{aligned}
& + \frac{\alpha_h}{2} \left[ \Psi_0 - \frac{\lambda_0}{\Delta} \right] \left[ \frac{1-J}{2\pi} \right] \\
& + \alpha_c Z \left[ \left[ \frac{\gamma}{\omega_s} \right]^2 \left[ \frac{2\Gamma_s P_c}{R P_c'} \right] Z \Phi_0 \left( \frac{1}{2} \right) + \left[ \frac{\gamma}{\omega_A} \right]^2 \left[ \frac{P_{\mu h}}{P_c'} \right] \times \right. \\
& \left. \left[ \frac{P_{\mu h}}{R P_{\mu h}'} \right] Z \Phi_0 \left[ \frac{M}{2\pi} \right] + \alpha_c \left[ \frac{P_{c0}}{Z} \right] \left( \frac{1}{2} \right) \right. \\
& \left. + \frac{\alpha_h}{2} \left[ \frac{\Psi_0}{Z} - \frac{\lambda_0}{Z\Delta} \right] \frac{M}{2\pi} \right] + \frac{\alpha_h}{2} Z \left[ \alpha_c \left[ \frac{P_{c0}}{Z} \right] \langle \sin^2 \theta \rangle_{tr} \right. \\
& \left. + \frac{\alpha_h}{2} \left[ \frac{\Psi_0}{Z} - \frac{\lambda_0}{\Delta Z} \right] \frac{L}{2\pi} + \frac{1}{\Delta} \frac{d\lambda_0}{dZ} \left[ \frac{J}{2\pi} \right] \right] = 0 .
\end{aligned}$$

or

$$\begin{aligned}
& S^2 \frac{d}{dZ} \left[ Z^2 \frac{d\Psi_0}{dZ} \right] - \left[ \frac{\gamma}{\omega_A} \right]^2 Z^2 \Phi_0 + Z^2 \Phi_0 \alpha_c \left[ \frac{\gamma}{\omega_s} \right]^2 \left[ \left[ \frac{\Gamma_s P_c}{R P_c'} \right] \right. \\
& \left. + \left[ \frac{\omega_s}{\omega_A} \right]^2 \left[ \frac{P_{\mu h}}{P_c'} \right] \left[ \frac{P_{\mu h}}{R P_{\mu h}'} \right] \frac{M}{2\pi} \right] \\
& + \frac{1}{2\pi} \sin \theta_0 \alpha_h \left[ \Psi_0 - \frac{\lambda_0}{\Delta} \right] + \frac{\alpha_h}{4\pi} \frac{J}{\Delta} Z \frac{d\lambda_0}{dZ} = 0
\end{aligned}$$

The last two terms of this expression can be written as

$$\begin{aligned}
t &= \frac{\alpha_h}{4\pi} \left\{ 2 \sin\theta_0 \Psi_0 - \frac{2\sin\theta_0}{\Delta} \lambda_0 + \frac{J}{\Delta} Z \frac{d\lambda_0}{dZ} \right\} \\
&= \frac{\alpha_h}{4\pi} \left\{ 2\sin\theta_0 \Psi_0 - \frac{2\sin\theta_0}{\Delta} \left[ 1 \Psi_0 + JZ \frac{d\Psi_0}{dZ} + \frac{\alpha_c \theta_0}{q^2} (P_{\infty} - \Psi_0) \right] \right. \\
&\quad \left. + \alpha_c M P_{\infty} + \frac{\alpha_h}{2} L \frac{\left\{ \left[ 1 - \frac{1}{\Delta} \right] \Psi_0 - \frac{J}{\Delta} Z \frac{d\Psi_0}{dZ} - \frac{\alpha_c \theta_0}{q^2 \Delta} (P_{\infty} - \Psi_0) \right\}}{1 + (\alpha_h L / 2\pi)} \right. \\
&\quad \left. + \frac{J}{\Delta} Z \frac{d}{dZ} \left[ 1 \Psi_0 + JZ \frac{d\Psi_0}{dZ} + \frac{\alpha_c \theta_0}{q^2} (P_{\infty} - \Psi_0) \right] \right. \\
&\quad \left. + \frac{\alpha_c M P_{\infty} + \frac{\alpha_h}{2} L \left\{ \left[ 1 - \frac{1}{\Delta} \right] \Psi_0 - \frac{J}{\Delta} Z \frac{d\Psi_0}{dZ} - \frac{\alpha_c \theta_0}{q^2 \Delta} (P_{\infty} - \Psi_0) \right\}}{1 + \frac{\alpha_h L}{2\pi}} \right\}
\end{aligned}$$

We write

$$Z\beta = \beta_1 \Psi_0 + \beta_2 Z \frac{d\Psi_0}{dZ} + \beta_3 P_{\infty}$$

where

$$\beta_1 = \frac{\frac{\alpha_h}{2} L \left[ \left[ 1 - \frac{1}{\Delta} \right] + \frac{\alpha_c \theta_0}{q^2 \Delta} \right]}{1 + \frac{\alpha_h L}{2\Delta}}$$

$$\beta_2 = \frac{-\frac{\alpha_h}{2} L \left[ \frac{J}{\Delta} \right]}{1 + \frac{\alpha_h L}{2\Delta}}$$

$$\beta_3 = \frac{\alpha_c M - \frac{\alpha_h}{2} L \left[ \frac{\alpha_c \theta_0}{q^2 \Delta} \right]}{1 + \frac{\alpha_h L}{2\Delta}}$$

This gives

$$t = \frac{\alpha_h}{4\pi} \left\{ \frac{2\sin\theta_0}{\left[ \Delta + \frac{\alpha_h L}{2} \right]} \Psi_0 \left[ (\Delta-1) \left[ 1 + \frac{\alpha_h L}{2\Delta} \right] + \frac{\alpha_c \theta_0}{q^2} \left[ 1 + \frac{\alpha_h L}{2\Delta} \right] \right. \right. \\ \left. \left. - \frac{\alpha_h}{2} L \left[ \left[ 1 - \frac{1}{\Delta} \right] + \frac{\alpha_c \theta_0}{\Delta q^2} \right] \right] \right\} \\ + \frac{2 \frac{d\Psi_0}{dz}}{\left[ \Delta + \frac{\alpha_h L}{2} \right]} \left[ -2\sin\theta_0 \left[ 1 + \frac{\alpha_h L}{2\Delta} \right] (J + \beta_2) + J \left[ 1 + \frac{\alpha_h L}{2\Delta} \right] \times \right. \\ \left. \left[ 1 + \beta_1 - \frac{\alpha_c \theta_0}{q^2} \right] \right]$$



$$\begin{aligned}
& + \frac{J}{\Delta} (J + \beta_2) Z \frac{d}{dZ} \left[ Z \frac{d\Psi_0}{dZ} \right] - \frac{2\sin\theta_0}{\Delta} \left[ \frac{\alpha_c \theta_0}{q^2} + \beta_3 \right] P_{c0} \\
& \left. + \frac{J}{\Delta} \left[ \frac{\alpha_c \theta_0}{q^2} + \beta_3 \right] Z \frac{dP_{c0}}{dZ} \right\}
\end{aligned}$$

Thus, finally the vorticity equation becomes

$$\begin{aligned}
& S^2 \frac{d}{dZ} \left[ Z^2 \left\{ 1 + \frac{\left[ \frac{\alpha_h}{4\pi S^2} \right] J^2}{\left[ \Delta + \frac{\alpha_h}{2} L \right]} \right\} \frac{d\Psi_0}{dZ} \right] - \left[ \frac{\gamma}{\omega_A} \right]^2 Z^2 \phi_0 \\
& + Z^2 \phi_0 \alpha_c \left[ \frac{\gamma}{\omega_s} \right]^2 \left[ \left[ \frac{\Gamma_s P_c}{R P'_c} \right] \right. \\
& \left. + \left[ \frac{\omega_s}{\omega_A} \right]^2 \left[ \frac{P'_{\perp h}}{P'_c} \right] \left[ \frac{P_{\perp h}}{R P'_{\perp h}} \right] \frac{M}{2\pi} \right] \\
& - \left[ \frac{\alpha_h}{2\pi} \right] \frac{\sin \theta_0 \left[ \alpha_c M + \frac{\alpha_c \theta_0}{q^2} \right]}{\left[ \Delta + \frac{\alpha_h}{2} L \right]} \Psi_0
\end{aligned}$$

$$+ \left[ \frac{\alpha_h}{4\pi} \right] \frac{\left[ \alpha_c M + \alpha_c \frac{\theta_0}{q^2} \right]}{\left[ \Delta + \frac{\alpha_h}{2} L \right]} \left[ JZ \frac{d}{dZ} (P_{c0} - \Psi_0) \right] = 0$$

Now we examine the  $P_{c0}$  equation:

$$\langle F \rangle_{2\pi} = -\frac{1}{2} \left[ \alpha_c + \frac{\alpha_h M}{2\pi} \right]$$

$$\langle \sin\theta \Phi_0 \rangle_{2\pi} = \langle \cos\theta \left[ \left( 1 + \frac{v_{\perp} Z^2}{\gamma} \right) \left( \frac{\partial \Psi_1}{\partial \theta} + S \frac{\partial \Psi_0}{\partial Z} \right) - S \frac{\partial \Phi_0}{\partial Z} \right] \rangle_{2\pi}$$

$$= \left[ 1 + \frac{v_{\perp} Z^2}{\gamma} \right] \left[ \alpha_c \left[ \frac{P_{c0}}{Z} \right] \frac{1}{2} + \frac{\alpha_h}{2} \left[ \frac{\Psi_0}{Z} - \frac{\lambda_0}{\Delta Z} \right] \frac{M}{2\pi} \right]$$

$$\langle P_{h0} \rangle_{2\pi} = \frac{\theta_0}{\pi} \left[ \Psi_0 - \frac{\lambda_0}{\Delta} \right]$$

$$\langle \sin\theta \Phi_1 \rangle_{1r} = \left[ 1 + \frac{v_{\perp} Z^2}{\gamma} \right] \left[ \alpha_c \left[ \frac{P_{c0}}{Z} \right] \frac{M}{2\pi} + \frac{\alpha_h}{2} \left[ \frac{\Psi_0}{Z} - \frac{\lambda_0}{Z\Delta} \right] \frac{L}{2\pi} \right.$$

$$\left. + \frac{d\Psi_0}{dZ} \frac{J}{2\pi} \right] - \frac{d\Phi_0}{dZ} \frac{J}{2\pi}$$

Therefore, we obtain

$$\left[ 1 + \left[ \frac{v_{\perp} \omega_s^2}{\gamma \omega_A^2} \right] Z^2 \right] P_{c0} = \left[ \frac{\omega_s}{\gamma} \right]^2 S^2 \frac{d^2}{dZ^2} (P_{c0} - \Psi_0) + \Phi_0$$

$$\begin{aligned}
& + \left[ \frac{2\Gamma_s \rho_c}{R P'_c} \right] \left[ -\frac{\Phi_0}{2} \left[ \alpha_c + \frac{\alpha_h M}{2\pi} \right] + Z \left[ 1 + \frac{v_1 Z}{\gamma} \right] \left\{ \frac{\alpha_h}{2} \left[ \frac{P_{c0}}{Z} \right] \right. \right. \\
& \quad \left. \left. + \frac{\alpha_h}{2} \left[ \frac{\Psi_0}{Z} - \frac{\lambda_0}{Z\Delta} \right] \frac{M}{2\pi} \right\} \right] \\
& - \left[ \frac{\omega_s}{\omega_A} \right]^2 \left[ \frac{P'_{1h}}{P'_c} \right] \left[ \frac{\theta_0}{\pi} \left[ \Psi_0 - \frac{\lambda_0}{\Delta} \right] - \Phi_0 \right. \\
& - \left. \left[ \frac{P'_{1h}}{R P'_{1h}} \right] \left\{ \Phi_0 \left[ \frac{1-J}{2\pi} \right] + Z \left[ 1 + \frac{v_1 Z^2}{\gamma} \right] \left\{ \alpha_c \left[ \frac{P_{c0}}{Z} \right] \frac{M}{2\pi} + \frac{J}{2\pi} \frac{d\Psi_0}{dZ} \right. \right. \right. \\
& \quad \left. \left. + \frac{\alpha_h}{2} \left[ \frac{\Psi_0}{Z} - \frac{\lambda_0}{\Delta Z} \right] \frac{L}{2\pi} \right\} - \frac{J}{2\pi} \frac{d\Phi_0}{dZ} \right\} \right]
\end{aligned}$$

Consider how rewrite the following :

$$\begin{aligned}
t_1 = & -\frac{1}{2} \left[ \alpha_c + \frac{\alpha_h M}{2\pi} \right] \Phi_0 + \left[ 1 + \frac{v_1 Z^2}{\gamma} \right] \left\{ \frac{\alpha_c}{2} + P_{c0} \right. \\
& \left. + \frac{\alpha_h}{2} \left\{ \frac{1}{\Psi_0 + JZ \frac{d\Psi_0}{dZ}} \right. \right. \\
& \quad \left. \left. \Psi_0 - \frac{\lambda_0}{\Delta} \right\} \right\}
\end{aligned}$$

$$\left. \frac{\frac{\alpha_c \theta_0}{q^2} (P_{c0} - \psi_0) + \beta_1 \psi_0 + \beta_2 z \frac{d\psi_0}{dz} + \beta_3 P_{c0}}{\Delta} \right\} \frac{M}{2\pi} \left. \right\}$$

$$= -\frac{1}{2} \left[ \alpha_c + \frac{\alpha_h M}{2\pi} \right] \phi_0 + \left[ 1 + \frac{v_1 z^2}{\gamma} \right] \left\{ P_{c0} \left[ \frac{\alpha_c}{2} - \frac{M \left[ \alpha_c M + \frac{\alpha_c \theta_0}{q^2} \right]}{\left[ \Delta + \frac{\alpha_h}{2} L \right]} \right] \right\}$$

$$\left. - \frac{\alpha_h M J}{4\pi \left[ \Delta + \frac{\alpha_h}{2} L \right]} z \frac{d\psi_0}{dz} \right\}$$

$$t_2 = \frac{\theta_0}{\pi} \left[ \psi_0 - \frac{\lambda_0}{\Delta} \right] - \phi_0 = -\frac{\theta_0}{\pi} \left\{ z \frac{d\psi_0}{dz} \left[ \frac{J}{\Delta + \frac{\alpha_h}{2} L} \right] \right\}$$

$$\left. + P_{c0} \left[ \frac{\alpha_c M + \frac{\alpha_c \theta_0}{q^2}}{\Delta + \frac{\alpha_h}{2} M} \right] \right\} - \phi_0$$

$$t_3 = \phi_0 \left[ \frac{1-J}{2\pi} \right] + \left[ 1 + \frac{v_1 z^2}{\gamma} \right] \left\{ \alpha_c P_{c0} \left[ \frac{M}{2\pi} \right] + \frac{J}{2\pi} z \frac{d\psi_0}{dz} \right\}$$

$$-\frac{\alpha_h}{2} \left[ \frac{L}{2\pi} \right] \left[ z \frac{d\Psi_0}{dz} \left[ \frac{J}{\Delta + \frac{\alpha_h}{2} L} \right] + P_{c0} \left[ \frac{\alpha_c M + \frac{\alpha_c \theta_0}{q^2}}{\Delta + \frac{\alpha_h}{2} L} \right] \right] \left. \right\}$$

$$-\frac{J}{2\pi} z \frac{d\Phi_0}{dz}$$

$$= \Phi_0 \left[ \frac{1-J}{2\pi} \right] + \left[ 1 + \frac{v_{\perp} z^2}{\gamma} \right] \times$$

$$\left\{ \frac{P_{c0} \left[ \alpha_c \Delta \left[ \frac{M}{2\pi} \right] - \frac{\alpha_c \alpha_h \theta_0 L}{4\pi q^2} \right] + \frac{J}{2\pi} z \frac{d\Psi_0}{dz} \Delta}{\Delta + \frac{\alpha_h}{2} L} \right\}$$

$$-\frac{J}{2\pi} z \frac{d\Phi_0}{dz}$$

This gives

$$\left[ 1 + \left[ \frac{v_{\perp} \omega_s^2}{\gamma \omega_A^2} \right] z^2 \right] P_{c0} = \left[ \frac{\omega_s}{\gamma} \right]^2 S^2 \frac{d^2}{dz^2} (P_{c0} - \Psi_0) + \Phi_0$$

$$+ \frac{2\Gamma_s \rho_c}{R P_c} \left\{ -\frac{1}{2} \left[ \alpha_c + \frac{\alpha_h M}{2\pi} \right] \Phi_0 + \left[ 1 + \frac{v_{\perp} z^2}{\gamma^2} \right] \left\{ P_{c0} \left[ \frac{1}{2} \alpha_c \right. \right. \right.$$

$$\left. \left. \left. \frac{M \left[ \alpha_c M + \frac{\alpha_c \theta_0}{q^2} \right]}{2\pi \left[ \Delta + \frac{\alpha_h}{2} L \right]} \right] - \frac{\alpha_h M J Z}{4\pi \left[ \Delta + \frac{\alpha_h}{2} L \right]} \frac{d\psi_0}{dZ} \right\} \right\}$$

$$+ \left[ \frac{\omega_s}{\omega_A} \right]^2 \left[ \frac{P_{\perp h}}{P_c} \right] \left\{ \frac{\theta_0}{\pi} \left[ Z \frac{d\psi_0}{dZ} \left[ \frac{J}{\Delta + \frac{\alpha_h}{2} L} \right] \right. \right.$$

$$\left. \left. + P_{c0} \left[ \frac{\alpha_c M + \frac{\alpha_c \theta_0}{q^2}}{\Delta + \frac{\alpha_h}{2} L} \right] \right] + \phi_0 \right.$$

$$\left. + \left[ \frac{P_{\perp h}}{R P_{\perp h}} \right] \left[ \phi_0 \left[ \frac{1-J}{2\pi} \right] + \left[ 1 + \frac{v_{\perp} Z^2}{\gamma} \right] \times \right. \right.$$

$$\left. \left. \left[ \frac{P_{c0} \left[ \alpha_c \Delta \frac{M}{2\pi} - \frac{\alpha_c \alpha_h \theta_0 L}{4\pi q^2} \right] + \frac{J}{2\pi} Z \frac{d\psi_0}{dZ} \Delta}{\Delta + \frac{\alpha_h}{2} L} \right] \right. \right.$$

$$\left. \left. - \frac{J}{2\pi} Z \frac{d\phi_0}{dZ} \right] \right\} \right\}$$

At this point, we note that  $(\omega_s/\omega_A)^2 = 4\pi \Gamma_s P_c/B^2 \ll 1$  by our assumption of low beta; also

$$\frac{P_{th}}{P_c} \sim O(1) \quad , \quad \text{but} \quad \frac{P_c}{RP_c} \sim \frac{\Delta_r}{R} \ll \frac{a}{R} \ll 1$$

Therefore, we drop these small terms in the core plasma pressure equation:

$$\left[ 1 + \frac{v_\perp \omega_s^2}{\gamma \omega_A^2} Z^2 \right] P_{co} = \left[ \frac{\omega_s}{\gamma} \right]^2 S^2 \frac{d^2}{dZ^2} (P_{co} - \Psi_0) + \Phi_0 \quad (B.5)$$

$$\frac{d}{dZ} \left\{ \left[ 1 + \frac{\alpha_h J^2/4\pi S^2}{\left[ \Delta + \frac{\alpha_h}{2} \right]} \right] Z^2 \frac{d\Psi_0}{dZ^2} \right\} - \left[ \frac{\gamma}{S\omega_A} \right]^2 Z^2 \Phi_0$$

$$- \left[ \frac{\alpha_h}{2\pi S^2} \right] \frac{\sin \theta_0 \left[ \alpha_c M + \frac{\alpha_c \theta_0}{q^2} \right]}{\Delta + \frac{\alpha_h}{2} L} \Psi_0$$

$$- \left[ \frac{\alpha_h}{4\pi} \right] \frac{\left[ \alpha_c M + \frac{\alpha_c \theta_0}{q^2} \right]}{S^2 \left[ \Delta + \frac{\alpha_h}{2} L \right]} \left[ 2 \sin \theta_0 - JZ \frac{d}{dZ} \right] (P_{co} - \Psi_0) = 0 \quad (B.6)$$

$$\left[ 1 + \frac{v_i Z^2}{\gamma} \right] \frac{d\Psi_0}{dZ} = \frac{d\Phi_0}{dZ}$$

We note that,

$$\left[ \frac{\alpha_h}{2\pi S^2} \right] \frac{\sin\theta_0 \left[ \alpha_c M + \frac{\alpha_c \theta_0}{q^2} \right] \left[ \Delta + \frac{\alpha_h}{2} L \right]}{\left[ \Delta + \frac{\alpha_h}{2} L \right] \left[ \Delta + \frac{\alpha_h}{2} L + \frac{\alpha_h J^2}{4\pi S^2} \right]} = \mu (\mu + 1),$$

Where  $\mu$  is the ideal Mercier exponent.



## REFERENCES

1. B. Coppi, A. Ferreira, J. W. -K. Mark, and J. J. Ramos, Nucl. Fusion **19**, 715 (1979).
2. J. M. Greene and M. S. Chance, Nucl. Fusion **21**, 453 (1981).
3. M. S. Chance, S. C. Jardin, and T. H. Stix, Phys. Rev. Lett. **51**, 1963 (1983).
4. J. Manickam, R. C. Grimm, and M. Okabayashi, Phys. Rev. Lett. **51**, 1959 (1983)
5. McGuirre, R. Goldston, M. Bell, M. Bitter, K. Bol, K. Brau, D. Buchenauer, T. Crowley, S. Davis, F. Dylla, H. Eubank, H. Fishman, R. Fonck, B. Grek, R. Grimm, R. Hawryluk, H. Hsuan, R. Hulse, R. Izzo, R. Kaita, S. Kaye, H. Kugel, D. Johnson, J. Manickam, D. Manos, D. Mansfield, E. Mazzucato, R. McCann, D. McCune, D. Monticello, R. Motley, D. Mueller, K. Oasa, M. Okabayashi, K. Owens, W. Park, M. Reusch, N. Sauthoff, G. Schmidt, S. Sesnic, J. Stachan, C. Surko, R. Slusher, H. Takahashi, F. Tenney, P. Thomas, H. Towner, J. Valley, and R. White, Phys. Rev. Lett. **50**, 891(893).
6. N. C. Christofilis, in Proceedings of the Second United Nations International Conference on the peaceful Uses of Atomic Energy, Geneva, 1958 (United Nations, Geneva, Switzerland, 1958), Vol. **32**, p.279.

7. R. N. Sudan and E. Ott, Phys. Rev. Lett. **33** 355 (1974).
8. H. H. Fleischmann, Ann. N. Y. Acad. Sci. **251**, 472 (1975).
9. B. H. Quon, R. A. Dandl, W. DiVergilio, G. E. Guest, L. L. Lao, N. H. Lazar, T. K. Samec, and R. F. Wuerker, Phys. Fluids **28**, 1503(1985).
10. R. A. Dandl, H. O. Eason, G. E. Guest, C. L. Hedrick, H. Ikegami, and D. B. Nelson, Plasma physics and Controlled Nuclear Fusion Research (International Atomic Energy Agency, Vienna, 1975), Vol. II, p. 141.
11. M. N. Rosenbluth, S. T. Tsai, J. W. Van Dam, and M. G. Enquist, Phys. Rev. Lett. **51**, 1967(1983).
12. T. M. Antonsen, Jr., Y. C. Lee, H. L. Berk, M. N. Rosenbluth, and J. W. Van Dam, Phys. Fluids **26**, 3580 (1983).
13. D. B. Nelson and C. L. Hedrick, Nucl. Fusion **19**, 283 (1979).
14. J. W. Van Dam, M. N. Rosenbluth, and Y. C. Lee, Phys. Fluids **25**, 1349 (1982).
15. T. M. Antonsen and Y. C. Lee, in Proceedings of 2nd Workshop on Hot Electron Ring Physics (Oak Ridge National Laboratory, Oak Ridge, 1981) Conf. 811203, p.191.
16. D. E. Baldwin and H. L. Berk, Phys. Fluids, **26**, 3595(1983).
17. H. L. Berk and Y. Z. Zhang, Institute for Fusion Studies Report ISFR No. 199 (1985).
18. D. A. Spong, private communication

19. J. W. Van Dam, in Proceeding of Mirror-Based and Field-Reversed Approaches to Magnetic Fusion Workshop , Italy, 1984  
Vol. 1, p. 239.
20. M. S. Chance, R. L. Dewar, E. A. Frieman, A. H. Glasser, J. M. Greene, R. C. Grimm, S. C. Jardin, J. L. Johnson, Manickman, M. Okbayashi, A. M. M. Todd, Plasma Physics and Controlled Fusion Research (International Atomic Energy Agency, Vienna 1978)  
Vol. 1, p. 677.
21. J. W. Van Dam and Y. C. Lee, in Proceedings of EBT Ring Workshop (Oak Ridge National Laboratory, Oak Ridge, 1979), Conf. 791288, P. 471
22. D. B. Nelson, *Phys. Fluids* **23**, 1850(1980).
23. M. N. Rosenbluth, *Phys. Rev. Lett.* **46**, 1525(1981).
24. J. W. Connor, R. J. Hastie, T. J. Martin, and M. F. Turner, in Proc. of The 3rd Joint Varenna-Grenoble International Symp. on Heating in Toroidal Systems (Comission of the European Communities, Brussels,1982), Vol. 1, p. 65.
25. L. Chen, R. B. White, and M.N. Rosenbluth, *Phys. Rev. Lett.* **52**, 1122 (1984).
26. R. B. White, L. Chen, F. Romanelli, and R. Hay, *Phys. Fluids* **28**, 278 (1985).
27. J. Weiland and L. Chen, *Phys. Fluids* **28**, 1359 (1985).

28. J. W. Van Dam and M. N. Rosenbluth, 1985 Annual Controlled Fusion Theory Meeting (April 14, Madison, WI). Paper 1C6.
29. L. Chen, R. B. White, C. Z. Cheng, F. Romanelli, J. Weiland, R. Hay, J. W. Van Dam, D. C. Barnes, M. N. Rosenbluth, And S. T. Tsai, in Proceedings of Plasma Physics and Controlled Fusion Research (International Atomic Energy Agency, Vienna, 1985), Vol. II, p. 59.
30. D. A. Spong, D. J. Sigmar, W. A. Cooper, D. E. Hastings, and K. T. Tsang, *Phy. Fluids* **28**, 2494 (1985).
31. D. A. Spong, D. E. Hastings, D. J. Sigmar, W. A. Cooper, Oak Ridge National Laboratory Report No. ORNL/TM-9688(1985)
32. G. Rewold and W. M. Tang, *Nucl. Fusion* **24**, 1573 (1984).
33. H. Biglari and L. Chen, *Phys. Fluids* **29**, 1760 (1986).
34. H. Biglari and L. Chen, Princeton Plasma Physics Laboratory Report PPPL No. 2303 (1986).
35. P. J. Catto, R. J. Hastie, and J. W. Connor, *Plasma Phys. Controlled Fusion* **27**, 307 (1985).
36. B. Coppi and F. Porcelli, Massachusetts Institute of Technology Report PTP-85/13 (1985).
37. Y. C. Lee and J. W. Van Dam , in Proceedings of the Finite Beta Theory Workshop Varenna , Italy , edited by W. Sadowski and B. Coppi (U. S. Department of Energy, Washington , D. C., 1979) , p. 55 .

38. T. M. Antonsen and Y. C. Lee , Phys. Fluids **25** , 132 (1982) .
39. T. M. Antonsen, B. Lane, and J. J. Ramos, Phys. fluids **24**, 1465 (1981) .
40. H. Grad , Phys. Fluids **10** , 137 (1967) .
41. W. A. Newcomb , J. Plasma Physics **26** , 529 (1981) .
42. W. A. Newcomb , Annals of Phys. **10** , 232 (1960) .
43. J. P. Freidberg , Reviews of Modern Phys. **54** , 801 (1982) .
44. M. N. Rosenbluth in Magnetohydrodynamic Stability and Thermonuclear Containment, Pag. 206 . Edited by A. Jeffrey and T. Taniuti . Academic Press. 1966 .
45. W. V. Lovitt, Linear Integral Equations., Dover Publications Inc. New York,1950.
46. X. Llobet, H. L. Berk and, M. N. Rosenbluth, Bull. Am. Phys. Soc. **30**, 1427 (1985).
47. J. Manickam, K. Mc Guirre, and A. E. Miller. 1984 Annual Controlled Fusion Theory Meeting. Paper 2R22.
48. F. Hinton and M. N. Rosenbluth, Nucl. Fusion **22**, 12 (1982).
49. Research and Education Association. Advanced Methods for solving differential equations . 1982 .
50. C. Mercier, in Plasma Physics and Controlled Nuclear Fusion Research (International Atomic Energy Agency, Vienna, 1979), Vol. I, p. 701.

51. J. W. Connor, R. J. Hastie and J. B. Taylor, Proc. R. Soc. Lond. A. **365**, 1(1979).
52. N. A. Krall and A. W. Trivelpiece, Principles of Plasma Physics, (McGraw-Hill Book Company, St. Louis, 1973).
53. S.T. Tsai and S. G. Guo, private communication (1986)
54. J. F. Drake and T. M. Antonsen , Phys. Fluids **28** , 544 (1985) .
55. H. R. Strauss , Phys. Fluids **24**, 2004 (1981).
56. A. H. Glasser, J. M. Green , and J. L. Johnson , Phys. Fluids **18**, 875 (1975).
57. M. Abramowitz and I. A. Stegun, Handbook of Mathematical functions (National Bureau of Standar, Washington D. C, 1970).
58. D. P. Stotler, Ph. D. thesis, University of Texas at Austin, Institute for Fusion Studies Report IFSR No. 238 .
59. K. Bol et al., Princceton Plasma Physiscs Laboratory Report PPPL No. 2032 (1983).
60. A. Bhattacharjee, private communication.
61. D. Barnes, Bull. Am. Phys. Soc. **28**,1137 (1983).
62. H. Naito, "Energetic Particle Stabilization of Ballooning Modes in Finite Aspect Ratio Tokamaks," presented at U. S.- Japan JIFT workshop on Advanced Concepts for Macroscopic Stability in Axisymmetric Systems (Nagoya, Sept. 9-13,1985).

63. R. L. Miller, private communication.
64. G. Y. Fu, private communication.
65. L. Chen, private communication.
66. Y. M. Li, Ph. D. thesis, University of Texas at Austin, Fusion Research Center Report FRCR No. 271 .
67. Y. M. Li, S. Mahajan, and D. W. Ross, Fusion Research Center Report FRCR No. 276 .
68. G. Y. Fu, private communication.

## VITA

Nicolas Dominguez Vergara was born on January 30, 1955 in San Miguel Totolapan Guerrero, Mexico, the son of Felipe Dominguez and Josefa Vergara. In 1973 he obtained his High School diploma from the National Autonomous University of Mexico (UNAM). In 1977 he received the degree of Bachelor of Science in Physics (UNAM) and in 1980 he was granted the degree of Master of Science in Nuclear Physics (UNAM). He was a fellow of the Program for the Formation of Academic Personnel of UNAM from 1978 to 1980. At the same time he was a Teaching Assistant at UNAM. In January 1981, he entered the Graduate School of the University of Texas at Austin. From 1981 to 1984 he was fellow of the Mexican National Council for Science and Technology (CONACYT) at the University of Texas at Austin. On August 20, 1982 he married Hortensia Pérez Vivian. He has been employed by the Institute for Fusion Studies since 1984.

Permanent Address: Amado Nervo 151  
Col. Sta. Ma. La Ribera  
Mexico 4, D. F. c.p. 06400  
MEXICO

This Dissertation was typed by Hortensia Pérez Vivian